Influence of Acid Mine Drainage on the soils of Nababeep, Namaqualand with reference to soil chemistry, minerals and metal mobility

Ian Heinrich Smuts
B. Ing (Stellenbosch)

A thesis submitted in partial fulfillment of the
requirements for the degree of
Master of Science (Agriculture)

Department of Soil Science
Stellenbosch University

Supervisor: Dr Catherine E. Clarke
Co-supervisor: Dr Ailsa G. Hardie

March 2015

Declaration

I, the undersigned, hereby declare that the work contained in this thesis is my own original work and that I have not previously in its entirety or in part submitted it at any university for a degree.

Ian Heinrich Smuts

15 December 2014

Abstract

The Okiep copper district in the north-western corner of South Africa is a region that has been mined for over 150 years. Most mining operations have ceased, but years of mining has left the area scattered with abandoned mining sites. Acids (as used in ore processing) together with acid mine drainage generated from tailings exposure, collectively referred to as AMD hereafter, are a contamination risk to water resources and the biodiversity of this arid area.

This study focused on an abandoned copper processing pond located close to the town of Nababeep. The leaching pond is unlined and has been excavated in the shallow colluvial soils. The natural soils of the area are shallow (60 cm) (WRB – Arenosol; SA – Oakleaf). Formations of corroded granite-gneiss boulders are an indication of the corrosiveness of the AMD collecting in the pond. The AMD was collected from the pond in the dry season at its most concentrated form and the AMD had exceptionally high concentrations of Al (26.9 g/l), Fe (42.9 g/l), Mg (20.5 g/l), Cu (3.8 g/l) and Mn (3.4 g/l). Melanterite ($FeSO_4 \cdot 7H_2O$), a soluble ferrous compound, was found to play an important role in the immediate release of Fe and sulfates.

The pristine soils have a sandy texture (2–5.2 %clay). The minerals detected in the clay phase include illite, kaolinite, montmorillonite and quarts. Pristine soils show some degree of contamination with low pH (4.38–4.77) and high Cu and sulfate contents. Soils located in the processing pond, which have been exposed to AMD for an extended period of time, showed poorly crystalline phases to be present (indicated by a broadening of the XRD peaks for clay minerals). Saturation indices (SI) were determined for saturated paste extracts of the pond soils and the obtained SI values support the notion of dissolution of silicate clays, as the obtained SI values ranged between –1.3 and –11.77 for illite and –4.76 to 0.58 for kaolinite. Jarosite, a new phase, formed in the contaminated soil and is a sink for K.

Long term weathering experiments of pristine soils exposed to AMD indicated that clay minerals are significantly weathered and altered, which was identified by observing the broadening of the clay XRD peaks. Fourier transform infrared (FTIR) spectra were generated by scanning clay samples of the weathered soil. Amorphous phases were confirmed by structured water bands with wavenumber values of 3700 and 3300 cm^{-1} for acid treated soil. Micrographs showed a more amorphous and corroded morphology in the acid treated soil.

Metal retention experiments were conducted by exposing the pristine soil to AMD repeatedly. Iron was the predominant metal attenuated in the soil. Metals such as Al, Mn, Na, K, Ca and Co were released by the soil into solution. Removal of Si is associated with the dissolution of clay minerals. The pristine soil shows limited capacity to neutralize acidity and low capacity to retain metals when leached with AMD.

Metals were predominantly extracted in the water soluble phase of the long term weathering treatments. Aluminium was the most mobile fraction, being extracted predominantly from the water soluble fraction (2035 mg/kg). Exchangeable and acid soluble fractions did not retain significant quantities of metals. In the soil from the processing pond, the reducible fraction had a high concentration of reducible Fe (21175 mg/kg) and Si (3070 mg/kg). The reducible fraction also had the highest concentration of Cr (15.85 mg/kg), Cu (41.53 mg/kg), Pb (8.0 mg/kg) and Zn (10.65 mg/kg)

compared to the other fractions of this soil. For the control experiment, the concentration of Cu (77.3 mg/kg), Pb (10.8 mg/kg) and Zn (24.1 mg/kg) were higher than contaminated soil yet lower for Cr (6.05 mg/kg). From these experiments, it can be concluded that the pristine soils studied have a limited ability to retain heavy metals in the non-bioavailable fraction, and, due to the nature of AMD, they are not effective in retaining metals sufficiently.

The findings of this study suggest that the capacity of these pristine soils to buffer pH and retain metals is greatly limited. This could be as a result of (1) the low clay content, (2) the low concentration of secondary carbonates and (3) the low pH of the soil. The leaching of AMD from the pond is thus not regulated by the soils and poses a risk for nearby water resources.

Uittreksel

Die Okiep Koper Distrik, geleë in die noord-westelike hoek van Suid-Afrika, is ‘n streek waar mynbou al vir meer as 150 jaar plaasvind. Die meeste mynbou aktiwiteite is gestaak, maar jare van mynbou het die streek nagelaat met verskeie verlate mynbouterreine. Sure, wat in die prosessering van erts gebruik word, en suurmynwater wat gegenereer word uit die mynuitskot (gesamentlik verwys na as suurmynwater) is ‘n besoedelingsrisiko vir waterbronne en biodiversiteit in hierdie dorre area.

Die studie fokus op ‘n verlate koper prosesserings aanleg naby die dorpie Nababeep. Die logingsdam is nie geseël nie en is uitgegrawe in vlak, kolluviale grond. Die natuurlike gronde van hierdie area is vlak (60 cm) (WRB – Arenosol; SA – Oakleaf). Formasies van weggevrete graniet-gneis rotse in die opgaardam is ‘n aanduiding van die bytende potensiaal van hierdie suurmynwater. Suurmynwater was versamel in die dam gedurendie die droë seisoen in die mees gekonsentreerde vorm. Die suurmynwater het besonderse hoë konsentrasies van Al (26.9 g/l), Fe (42.9 g/l), Mg (20.5 g/l), Cu (3.8 g/l) en Mn (3.4 g/l). Melanteriet ($FeSO_4 \cdot 7H_2O$) is ‘n ysterhoudende verbinding en, alhoewel dit oplosbaar is, speel dit ‘n belangrike rol in die onmiddelike vrylating van Fe en sulfate.

Die onversteurde grond het ‘n sand tekstuur (2–5.2 % klei). Die minerale wat in die klei fraksie ge-identifiseer is sluit illiet, kaoliniet, montmorilloniet en kwarts in. Die ongerepte gronde dui egter op ‘n mate van besoedeling deurdat dit ‘n lae pH (4.38–4.77) enhoë Cu en sulfaat inhoud het. Die grond wat geleë is naby die prosesseringsaanleg en ook blootgestel is aan suurmynwater vir ‘n verlengde tyd, dui daarop dat swak kristallyne fases teenwoordig is in die grond. Dit word bevestig deur ‘n verbreding van die XRD pieke van kleiminerale. Versadiging indekse (VI), wat bepaal is in versadigde grondekstraksies van die damgrond, ondersteun die oplossing van die silikaatkleie en word gereflekteer deur VI waardes wissel tussen –1.3 en –11.77 vir illiet en –4.76 tot 0.58 vir kaoliniet. Jarosiet is ‘n nuwe fase wat gevorm het in die besoedelde grond en is ‘n sink vir K.

Langtermyn verweringseksperimente wat gedoen is deur die onversteurde grond bloot te stel aan suurmynwater wys beduidende verwering en verandering van klei-minerale deur verbreding van die XRD pieke. Fourier transform infrarooi (FTIR) spektra is op kleimonsters van die verweerde grond gegenereer. Amorfe fases is bevestig deur gestruktureerde waterbindings met frekwensies tussen 3700 en 3300 cm^{-1} vir suurbehandelde grond.

Metaal-vasleggings eksperimente is uitgevoer deur herhaaldelik die onversteurde grond aan die suurmynwater bloot te stel. Yster is die metaal wat hoofsaaklik in die grond vasgehou is. Metale soos Al, Mn, Na, K, Ca en Co was vrygestel in oplossing deur die grond. Die vrylating van Si deur die grond word geassosiëer met die oplossing van kleiminerale. Die onversteurde grond toon beperkte vermoë om suur te neutraliseer en metale te bind in die grond wanneer dit met suurmynwater geloog word.

Metale was hoofsaaklik ge-ekstraëer in die wateroplosbare fase vir die langtermyn verweringsbehandelings. Aluminium was die mees mobiele fraksie wat ontrek is van die water oplosbare fraksie (2035 mg/kg). Uituilbare en suuroplosbare fraksies het nie ‘n groot hoeveelheid metale vasgehou nie. Gronde wat versamel is naby die prosesseringsdam het die hoë konsentrasies vanFe (21175 mg/kg) en Si (3070 mg/kg) in die gereduseerde fraksie gehad. Die reduserende fraksie het ook die hoogste

konsentrasie van Cr (15.85 mg/kg), Cu (41.53 mg/kg), Pb (8.0 mg/kg) en Zn (10.65 mg/kg) gehad in vergelyking met ander fraksies in die grond. Vir die beheer eksperiment was die konsentrasie van Cu (77.3 mg/kg), Pb (10.8 mg/kg) en Zn (24.1 mg/kg) hoër as in die besoedelde grond en laer vir Cr (6.05 mg/kg). Dus kan daar van hierdie eksperimente afgelei word dat die onversteurde grond beperkte kapasiteit het om swaar metale in grond vas te hou in die nie-biobeskikbare fraksie. As gevolg van die aard van die suurmynwater, is die grond nie voldoende om die metale effektief in grond te behou nie.

Die bevindinge van hierdie studie dui daarop dat die kapasiteit van die ongerepte grond om pH te buffer en metale in grond te behou baie beperk is. Dit kan toegeskryf word aan die lae kleiinhoud, lae konsentrasie van sekondêre karbonate en die lae pH van die grond. Die loging van suurmynwater van die logingsdam is dus nie gereguleer deur die gronde nie en stel die naasliggende waterbronne in gevaar.

Acknowledgements

I firstly want to thank Jesus Christ my Lord and savior for the strength through this period.

A special thanks to my supervisor Dr. Cathy Clarke for her assistance, guidance and patience during this project, who took me in from another field of study and accommodated me. I am also grateful for my co-supervisor, Dr Ailsa Hardie, for her advice and open door for input into the study.

I would like to express gratitude to my financial sponsors, the NRF (grant number 80400), Inkaba ye Africa and the Ericson trust that made this study possible

I would also like to offer sincere thanks to the following people and institutions:

At the Department of soil Science the lecturers, technical staff and colleagues: Makhosazana Sika, Ilana van der Ham, Ignacio Ros Mesa, Cou Pienaar, Jacques Smit, Naude Smith, Nina Swiegelaar, Michael Esmeraldo, Marilee Carstens, Abie Voster, Hennie Bekker, Luan le Roux, Charlo Scheepers, Glen Cooper, Matt Gordon, Delphine Gordon, Dr. Andre Rozanov, Dr. Eduard Hoffman, Dr. Willem de Clercq, Mr Jan Lambrechts and a special thanks to Adrian Adams for technical advice and proofreading;

Dr Paul Verhoeven for assistance with FTIR at the Department of Chemistry and Polymer Science and for making the facility available to me.

All assistance at CAF especially Riana Rossouw at the ICP facility and Madeleine Frazenburg and Donavon Lombard at the SEM facility for accurate and prompt analysis.

To Remy Bucher and Zakhele Khumalo at the XRD facility at iThemba Labs for numerous analyses and assistance and professional help.

Mr Basie Fourie at the Okiep Copper Company for valuable knowledge about mining in the study area and transparency regarding issues and challenges they face.

The South African Weather Service for climatic data.

I would finally like to thank my family and friends for their support and encouragement.

Table of Contents

List of Figures

List of Tables

Symbols and Abbreviations Used

AMD	Acid Mine Drainage
Å	Ångström, 1Å = 1 × 10^{-10} m = 0.1 nm
CEC	Cation exchange capacity
cm	Centimetre
cm^{-1}	Inverse centimetres
DI	Deionized
*E*h	Redox potential
eq/l	Equivalents per litre, equivalent to N
et al.	"Et alii" (and others)
FTIR	Fourier transform infrared
g	Gram
g/l	Gram per litre
IC	Ion chromatography
ICP-AES	Inductively coupled plasma – atomic emission spectrometry
kg	Kilogram
kV	Kilovolt
l	Litre
LOD	Limit of detection
mamsl	Metres above mean sea level
m	Metre
µm	Micrometre
mg/kg	Milligram per kilogram
mg/l	Milligram per litre
mm	Millimetre
M	Molar, equivalent to mol/l
mM	Millimolar, equivalent to mmol/l
mol	Mole
nA	Nano-Ampere
nm	Nanometre
N	Normal, equivalent to eq/l
pH	"Power of hydrogen" – a logarithmic scale of measuring acidity/alkalinity
SEM	Scanning electron microscope
SI	Saturation Index
WRB	World Reference Base
XRD	X-ray diffraction
XRF	X-ray fluorescence

Introduction

Acid mine drainage (AMD) is the acidic metalliferous solution emanating from metal- and coal-mines. The generation of AMD is associated with the oxidation of sulfide minerals, especially pyrite (FeS_2). Mining processes expose the ore rock to atmospheric conditions where the combination of moisture, oxygen and microbes accelerate the oxidation of sulfide minerals. A very small fraction of ore is actually extracted for economic use. During the extraction process, several tons of gangue mineral material called tailings, which contains residual sulfide minerals and possesses a high surface area, are generated. This very fine material is usually stored in what is known as tailings dams, which are vast constructions that are highly exposed to the atmosphere. This exposure, along with the increased reactive surface area of the fine material, further enhances the oxidation of residual sulfide minerals and the subsequent release of the AMD into the environment from these tailings dams. The generation of AMD from processed tailings is a process that continues for many years, often long after the closure of the mine(s) which produced the tailings. The oxidation of these sulfide minerals also release the metals contained within them in a soluble form. The high mobility of these metals in an acid medium such as AMD makes them prone to dispersion and diffusion, away from their source into surrounding aquatic systems, such as streams and rivers, where they have detrimental effects on aquatic ecosystems. Heavy metals are toxic and harmful to fauna and flora. In addition to this generation of acidity from mine tailings, some processing techniques used during mining involve the addition of acids in order to leach metals into solution. When these processing techniques are not conducted in a confined environment, process acids (usually sulfuric acid) contribute further to the acidity of the already acidic leachate generated from tailings oxidation. In this study, the term AMD is therefore used to represent both the acidic drainage emanating from oxidation of sulfide minerals as well as the contribution from sulfuric acid added during ore processing techniques.

Located on the west coast of South Africa is the region called Namaqualand, which is well known for its mining heritage. This is an arid region in the Northern Cape province of South Africa. Within the Namaqualand region is the Okiep Copper District where copper was discovered in 1685 (Cairncross, 2004). Mining was significantly inhibited by both the harsh conditions and the distance from the then Cape colony, and commercial mining only commenced in 1852. This initiated mining activity near the towns of Springbok, Nababeep, Okiep, Concordia and Carolusberg, which continued for over a century. Today, major mining has ceased, with only isolated operations of ore processing still occurring. The extended period of mining has left the area with numerous remnants of the years of exploitation. In an unpublished document of the Okiep Copper Company, 41 different mining sites are listed in the region. The list includes mines, tailings heaps, smelter sites and treatment plants, sites which all require rehabilitation. The mining practices used in the area at the time were in use long before the drafting and subsequent enforcement of any environmental protection legislation, which is mandatory practice today. This resulted in poor to non-existent pollution prevention strategies being employed, for example, the use of unlined tailings dams and ore processing plants, and today these sites serve as point sources of contamination. Soil contamination is evident in many of the derelict mining areas, with Cu concentrations as high as 14% having been observed in some soils (Clarke et al., 2014).

The area is arid and receives 50–250 mm of rainfall per annum (Desmet, 2007). The aridity of the area adds an important dimension to the hydrological flow of contaminants in that conditions are highly evaporative. Evaporation leads to the concentration of contaminated solutions. Soluble metal salts precipitate out of solution, but heavy rainfall events can cause mobilization and dissemination of the salts and metals into the environment. The soil is a major pathway between the point source of contamination and the groundwater receptor and it is therefore important to understand the potential of the soils to buffer and attenuate metals in contaminated waters. Soils in this arid region are poorly developed and shallow, and thus their metal retention capacity is likely to be limited. The area has no surface water supplies, and therefore the area relies predominantly on its groundwater supply (Pieterson et al., 2009). In a report by the Water Research Commission of South Africa, Pieterson et al. (2009) stated that the projected water demand would not meet the available yield. The protection of water resources is therefore of utmost importance, since local communities, especially in rural areas, are dependent on these groundwater resources.

Very little work has been conducted on the impact that Cu mining activities have had on the soil and water systems of the Namaqualand region. A geo-environmental assessment was conducted by Hohne & Hansen (2008) to specifically investigate the environmental impact of mining activities at the major Cu mining locations. In this report it is recommended that further work has to be conducted on the soil and water conditions to assess the mobility of metals. Contaminant transport in arid systems is poorly understood, as the effects are not always immediately evident. However, once contamination has commenced, these contamination sources can continue to have a detrimental effect on the surrounding environment for thousands of years (Kempton & Atkins, 2000). This could mean that the severity of the problem may be somewhat misjudged, and that the pollution of the mining sites has not yet been experienced in its full capacity, with the full extent of the detrimental effects on the environment not accurately predicted.

Protecting the environment from pollution is important especially in sensitive ecosystems with high biodiversity. Namaqualand falls under the Greater Cape Floral Kingdom and is one of only two desert regions recognized as a global biodiversity hotspot. The specific region of Namaqualand falls under a subdivision of the Succulent Karoo which contains about 3500 species of flora, of which 25% are endemic (Desmet, 2007). The flora of the area is a significant tourist attraction, especially during spring when the area boasts a spectacular scene of blooming flowers. Therefore, understanding the impact of AMD on the soil is also important from an ecological perspective.

In this study, a derelict ore processing pond located near the town of Nababeep was investigated. The site was not fenced or barricaded and thus was easily accessible it. The site is situated north of the town where Cu was mined. Very little information is available on how the ore was treated and processed in the pond. It is suspected that the site of investigation was a copper leach plant as it has terraces interconnected with pipes. This means that although the ore contains pyrite and other sulfide minerals, further acid would have been added to solubilize the metals. This enhances the threat to the environment and the spreading of the toxicity further into soils and water sources of the area. It is unclear when operations ceased at the processing pond, but anecdotal reports suggest it was in 1972. The contamination footprint of the pond is large and metals are accumulating upslope from an

ephemeral stream. This stream runs through the town and is a water source for local livestock. The site is also not fenced and the public has direct access to the pond. The location itself is wasteland and no vegetation is present in the contaminated region.

The overall aim of this study is to investigate the impact AMD has on soil mineralogy and metal mobility in order to determine the role that the Nababeep soils play in buffering additions of acidity and metals to the environment. To achieve the overall aim the following objectives are outlined:

1. Characterize the effects of long term exposure of the soils to acid mine drainage by comparing the chemical and mineralogical composition of contaminated soils to nearby pristine soils.
2. Assess the changes that occur in mineralogy and mineral equilibria when pristine soils come in contact with AMD.
3. Evaluate the soil's capacity to buffer the acidity of the AMD and attenuate metals to prevent further leaching into the environment
4. Determine the mobility and bioavailability of the metals in the soils that have been exposed to AMD for an extended period.

The structure of this thesis is arranged to determine each of the above objectives systematically. The first chapter, provides a physical and historical background into the area and reviews the latest literature on the mechanisms of AMD generation. This chapter also characterizes the physical, mineralogical and chemical composition of soils directly in contact with AMD, as well as nearby pristine soils.

The second chapter is an investigation into the weathering effect that AMD has on the soil. This was achieved by conducting laboratory weathering experiments over an 8 month period after which the mineralogical and chemical compositions of the soils were assessed.

In the third chapter, the mobility of the metals associated with AMD, are evaluated. The objective is to assess the capacity of the pristine soil to buffer pH and attenuate metals upon being contaminated with AMD. The partitioning of metals in the soil was investigated by sequential extraction to determine mobile and bioavailable fractions of these metals in the soils exposed to AMD for an extended period of time.

Chapter 1. Characterization of Soils and Acid Mine Drainage

1. Introduction

This study focuses on a site that shows clear signs of contamination from a tailings pond located close the town of Nababeep in the Namaqualand region of South Africa. In this chapter the aim will be to firstly characterize AMD collected at the tailings pond. Secondly, the natural soils in close proximity to the leaching pond that has been contaminated with the AMD will be characterized. This will be done with focus on soil chemistry and mineralogy. To assess the change or influence of the AMD, pristine soils from the same area will characterized in a similar fashion. The Namaqualand region has a long mining history and this makes it a unique site to investigate. Background information on the physical setting, climate, vegetation, geology and history of the area will be provided next, followed by a review on the formation of AMD.

1.1. Background information

1.1.1. Location and Physical Setting

The Namaqualand region is located along the north-west coast of South Africa (Figure 1.1). The region is bounded by the Atlantic Ocean in the west and the plains of the Bushmanland in the east, which forms the western plateau of the subcontinent (< 900 mamsl). In the west, there is a strip of coastal plain which is comprised of marine sands (< 300 mamsl) and moving eastwards these sandy plains give way to the western escarpment of South Africa, which is formed by the Kamiesberg mountain range. The Kamiesberg range is composed of granite gneiss rock formations. An undulating landscape forms the intermediate region from the foothills of the Kamiesberge to the interior. The east to west distance of Namaqualand is less than 300 km. To the south the sandy plains transition into a plain covered with gravel or pebbles which is known as the Knersvlakte. The Knersvlakte forms the southern boundary of the Namaqualand region which is also the border between the igneous rock formations of Namaqualand and the sedimentary shale and sandstones of the Cape Fold Mountains (Desmet, 2007). The Olifants River defines this southern border whilst the northern border stretches to the Orange River, which runs through the region known as the Richtersveld. The Orange River also forms the border between South Africa and Namibia.

There is a wide variety of soil types found in Namaqualand. In the northern part, gypsic and petrogypsic soils occur, while aeolian sands are located closest to the coast. The coastal sands are grey while sands further inland are red, with an intermediate zone of yellow sands occurring in between. In the higher relief areas of the interior, lithosols and shallow red soils on duric horizons are found. In the south, a wide variety of soil types are found which are influenced by other parent materials such as dolerite and alluvial deposits. A complete overview of the soils of the Namaqualand region is given by Francis et al. (2007). Heuweltjies (hillocks) are common in all regions of Namaqualand.

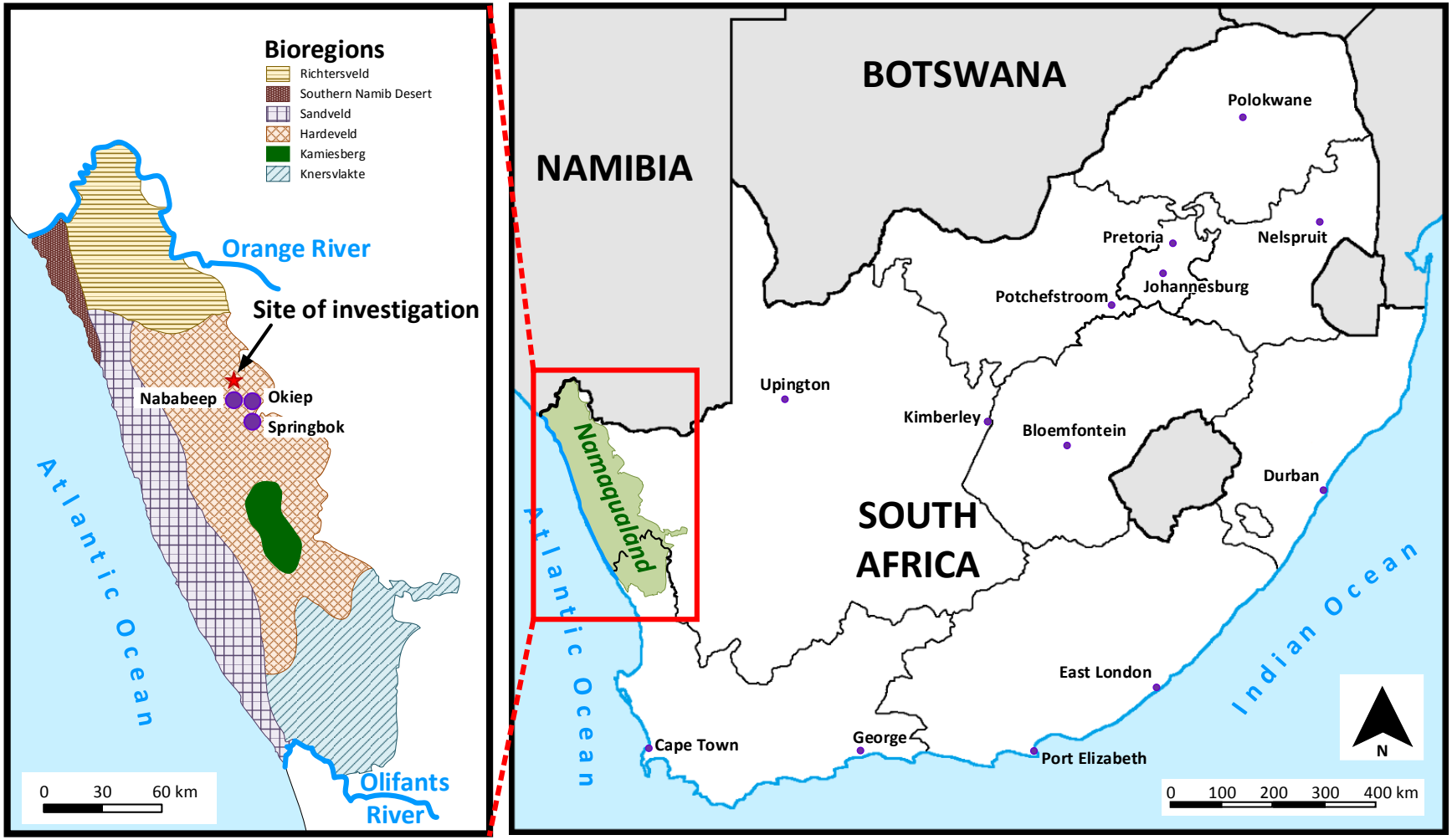

Figure 1.1: Map of South Africa indicating the extent of the Namaqualand region. Inset shows the bioregions of Namaqualand (modified from Cowling et al. (1999)) as well as the location of the study site and nearby towns.

The specific study site is located approximately 5 km north of the town of Nababeep (Figure 1.1) in a valley that runs in a north-south direction. The elevation is approximately 770 mamsl and the closest distance to the coast is 73 km. It is therefore situated not quite in the interior, but in the undulating intermediate region of the Kamiesberg. The soils found in this area are shallow red sands, which are derived from the granite gneiss (Clifford & Barton, 2012).

1.1.2. Climate and Vegetation

The Namaqualand region is arid with predominantly winter rainfall at the coast and summer rainfall in the interior (Desmet, 2007). Rainfall steadily increases towards the inland areas, ranging from 50–70 mm per annum at the coast to 150–300 mm per annum upon moving further inland (Kelso & Vogel, 2007; and authors therein). Aside from this east-west rainfall gradient, a gradual decrease in rainfall from south to north is also observed in the area (Desmet, 2007).

Climatic data specific to the study site is provided by weather station located in the town of Springbok, situated approximately 13 km south east of Nababeep. The average monthly maximum and minimum temperatures, recorded between the years 1990 and 2014, are provided in Figure 1.2. The warmest month of the year is February, which has an average maximum monthly temperature of 30°C. The coolest month is August, with an average monthly minimum temperature of 7.8°C. Rainfall data was recorded in same time period as the temperature data and is provided in Figure 1.3. The highest annual precipitation occurs in the months of May, June, July and August, typically coinciding with austral winter. The average annual rainfall for the study area is 228.2 mm per annum. Older data for the town of Okiep, situated close to the sampling site (approximately 10 km East), was obtained from the Department of Water Affairs and Sanitation. The monthly precipitation of Okiep is depicted in Figure 1.3. This rainfall data for Okiep was recorded from 1957 to 1985 and although the rainfall is on average lower, the same pattern as described before for Springbok is observed. The average annual rainfall for Okiep recorded during this period (1957–1985) was 167 mm per annum. An annual evaporation rate of 2879 mm per annum was measured in Okiep. This high evaporation rate, which greatly exceeds the precipitation, highlights both the aridity and water scarcity of the area.

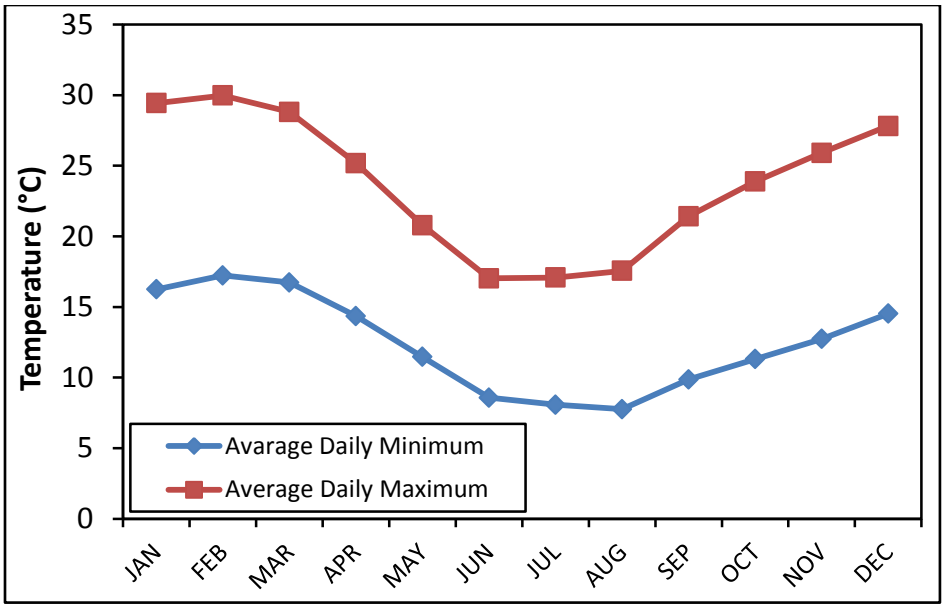

Figure 1.2: Average maximum and minimum Monthly Temperatures in Springbok

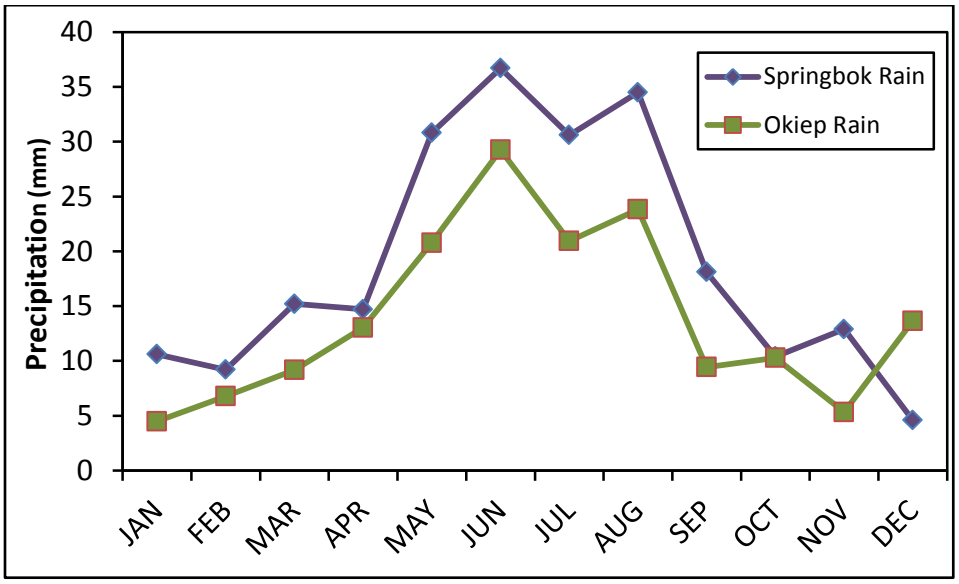

Figure 1.3: Average Monthly Precipitation for the towns of Springbok and Okiep

Desmet (2007) reports that the succulent Karoo biome, into which Namaqualand falls, is part of the Cape Floral Kingdom and has recently been added to this unique area of plant diversity. This area is now termed the Greater Cape Floral Kingdom, and is one of only two desert regions recognized for its biodiversity. Namaqualand constitutes one quarter of the Succulent Karoo biome and contains 3500 species of plants, of which 25% are endemic to this region only (Desmet, 2007). The Namaqualand region is divided into 7 bioregions (Figure 1.1). The location where this study will be conducted is situated in the Kamiesberg bioregion. According to the South African National Biodiversity Institute

(SANBI) the study area falls under the Namaqualand Klipkoppe Shrubland vegetation group, which again falls under the Namaqualand Hardeveld (Mucina et al., 2006). This specific vegetation type consists of small- to dwarf-size shrubs with either ericoid or succulent leaves. Succulents are found within the cracks occurring, whilst 1–3m tall non-succulent shrubs are found at the bottom of steep rock sheets where water from runoff collects.

1.1.3. Geology

The geology of the Nababeep region is comprised of granite gneiss. Reid & Barton (1983) characterized the geology of the whole Namaqualand into different domains and suites. The area of investigation falls under the Okiep domain which is then further classified into the syn-tectonic Little Namaqualand suite. The dominant rock forming minerals present in this suite are primarily feldspars, biotite and hornblende.

The copper ore found in the Okiep Copper district occurs mostly in the Koperberg suite. The Koperberg suite consists of basic to intermediate rocks which intrude into the granitic gneisses that dominate the Namaqualand region. These host rocks for the copper ore consist of jotunite, anorthosite, biotite diorite as well as hypersthenic rocks that range from leuconorite to hypersthenite (Clifford & Barton, 2012). Kisters et al. (1996), and authors therein, describe these intrusions as small and irregular, dyke-, sill- or plug-like basic formations in which Cu has mineralized.

The predominant Cu minerals that occur in the ore body are chalcopyrite ($CuFeS_2$), bornite (Cu_5FeS_4), chalcocite (Cu_2S), malachite $[Cu_2CO_3(OH)_2]$ and magnetite (Fe_3O_4) (Personal communication, Mr Basie Fourie, chief executive officer (CEO) of the O'kiep Copper Company). Cairncross (2004) also describes an ore that was collected at the mines near Okiep and Nababeep which contains chalcopyrite ($CuFeS_2$), chalcocite (Cu_2S), fluorite (CaF_2), calcite ($CaCO_3$) and gypsum ($CaSO_4 \cdot 2H_2O$).

1.1.4. Historical background

Copper was discovered by Dutch colonials in 1685 in the Northern Cape province of South Africa during an expedition led by Simon van der Stel. They discovered deposits of malachite (Miller, 1995) in an area located near the present-day towns of Okiep and Springbok. After this discovery, little development took place, mostly because of the remoteness and harsh conditions of the area and for many years the area was only prospected and explored (Cairncross, 2004).

The beginning of commercial mining in the area only commenced once The South African Mining Company started mining operations in 1846 (Smalberger, 1975). In 1852, a company called Phillips and King purchased the farm upon which the town of Springbok is located today. Phillips and King owned the Spektakel, Nababeep and Okiep mines which were later taken over by the Cape Copper Company. Another company called Namaqua Copper Company had mining operations at Concordia, an area north east of Okiep. In 1919, the Cape Copper Company ceased their operations in the area due to the post First World War economic slump. In 1939, the Okiep Copper Company (est. 1937) acquired the sites of both Cape Copper Company and later that of Namaqua Copper Company. Development throughout the 20th century took place at many mining sites in the area. Namaqua Copper Company commissioned a flotation plant, and material that could not be smelted or treaded by flotation was leached from the tailings dumps (Cairncross, 2004; and authors therein). During the 20th century, 27 mines were operated

until the last mine (Carolusberg) closed down in 1998. At that time the Okiep Copper Company was managed by Goldfields of South Africa and then bought out by Metorex.

Currently, most of the mines are inactive with unlined mine dumps and slimes dams remaining as evidence of many years of exploitation. However, the advantage of such abandonment is that the impact of long-term exposure of the environment to acid mine drainage (AMD) can be investigated. Little is known about the history of the town of Nababeep where the site of investigation is located. This is because the town was controlled by the mine and consequently all documented history was destroyed when the South African Copper Company ceased operations and the Okiep Copper Company took over on May 29, 1937 (Smalberger, 1975). This lack of information makes the management of the contaminated areas difficult, and, as a result, simplistic remediation techniques are applied, such as liming for example (Personal communication, Mr Basie Fourie, CEO of the O'kiep Copper Company). The sites are still managed by Okiep Copper Company, who have an interest in barricading the contaminated sites in order to prevent people and livestock from being exposed to contamination. Many of the sites are in close proximity to villages and one of the problems faced is theft of the fences. The specific site of investigation is located approximately 5 km from the town of Nababeep, and has no barrier preventing outsiders from reaching and being exposed to the contamination source.

Lastly, it is important to mention that at the investigation site, the mineralogy of the Cu ore is such that it contains pyrite, which acts as a source of sulfuric acid generation. Another source of acid is as a result of the introduction of sulfuric acid to the ore in order to leach the metals out for extraction purposes. This older mining practice was also carried out in the district (Cairncross, 2004), of which the contaminated site of investigation could be a possible example. Sampling was conducted downslope from the site, which was terraced and interconnected by overflow pipes.

1.1.5. Review on the generation of Acid Mine Drainage (AMD)

Acid mine drainage (AMD) is a term used to describe the discharge water that emanates from abandoned mining sites, which is both highly acidic (very low pH) and contains high concentrations of heavy metals and toxic elements. Upon release into the surrounding environment, these acidic, metal-laden waters causes an instant threat to biota and ecological balance. They also result in contamination of surface and groundwater, as well as soils (Peppas et al., 2000).

The occurrence of AMD is associated with the presence of sulfide (S^{2-}, S^{-})-bearing minerals in potentially both ore and mine tailings exposed to oxygen and water. The oxidation of sulfide minerals leads to the formation of acidic sulfate (SO_4^{2-})-rich drainage. There are several reactions by which the acidity is generated. The presence of particular metals at particular concentrations will depend on the type and amount of sulfide mineral oxidized. The key components necessary for the formation of AMD are the sulfide minerals, water or atmospheric humidity and an oxidant such as oxygen (O_2). The generation of acid sulfate waters is a process that occurs naturally, but mining operations can significantly enhance this process due to the increased exposure of the sulfides to the atmosphere through mining activities (Akcil & Koldas, 2006). Exposure is further increased during the crushing of ore rock into fine particles, a process necessary for the extraction of valuable metals from the ore. As these minerals are crushed, reactive sites such as grain edges and corners, defects, solid and liquid inclusion pits, as well as

cleavages and fractures, are created and subsequently exposed, and it is on these reactive sites where oxidation is most focused (Mckibben & Barnh, 1986). The source of AMD is not solely due to processed rock dumps, flotation tailings dams and concentrate stockpiles, but underground and open pit mining works also contribute to AMD generation.

As mentioned, the origin of AMD is the oxidation of sulfide minerals, the most common of which is pyrite (FeS_2). Table 1.1 indicates the names and formulae of the minerals associated with AMD (Gray, 1997). Pyrite is found in coal fields and is also associated with many other ores including those of Zn, Pb, As, U, Au and Ag.

Table 1.1: Minerals associated with the generation of AMD (adapted from Gray (1997)).

Mineral	Composition
Arsenopyrite	$FeS_2{\cdot}FeAs$
Bornite	$CuFeS_4$
Chalcocite	Cu_2S
Chalcopyrite	$CuFeS_2$
Covellite	CuS
Galena	PbS
Millerite	NiS
Molybdenite	MoS_2
Pyrite	FeS_2
Pyrrhhdite	$Fe_{11}S_{12}$
Spharerite	ZnS

The reaction by which pyrite is oxidized was investigated by Singer & Stumm (1970) and is given in reaction 1:

$$FeS_{2(S)} + \frac{7}{2}O_2 + H_2O \rightarrow 2SO_4^{2-} + Fe^{2+} + 2H^+ \qquad (1)$$

The buffering capacity of the waste rock is usually not sufficient to neutralize the acid (Tutu et al., 2008). The Fe(II) can be further oxidized to Fe(III) through reaction 2:

$$Fe^{2+} + \frac{1}{4}O_2 + H^+ \rightarrow Fe^{3+} + \frac{1}{2}H_2O \qquad (2)$$

The Fe(III) can then further oxidize pyrite as described by reaction 3:

$$FeS_{2(S)} + 14Fe^{3+} + 8H_2O \rightarrow 15\,Fe^{2+} + 2SO_4^{2-} + 16H^+ \qquad (3)$$

The stability of Fe(III) depends on the pH. According to Tutu et al. (2008), the Fe(III) remains in solution at pH lower than 3.5, but at higher pH values the Fe(III) precipitates as $Fe(OH)_3$ through hydrolysis, as shown in Reaction 4:

$$Fe^{3+} + 3H_2O \rightarrow Fe(OH)_{3(S)} + 3H^+ \quad (4)$$

This reaction is described by Stumm & Morgan (1996). The specific hydrolysis given in reaction 4, is however only one hydrolysis reaction and many other species can form depending on the conditions - for example partially hydrolyzed Fe(III). Each reaction has its own equilibrium constant. Furthermore it has been reported that the precipitation of $Fe(OH)_3$ acts as a buffer to keep the pH between 2.5 and 3.5 (España et al., 2005). This phenomenon has two opposing effects. The first effect is that the acidity increases the mobility and toxicity of the metals whilst the second is that the precipitation of $Fe(OH)_3$ results in co-precipitation and adsorption of the metals in solution. Tutu et al. (2008) state that the second precipitation effect is more prevalent. Mcgregor et al. (1998) found that metals such as Ni, Co, Cu, Cd and Zn co-precipitated out with goethite, a ferric (oxy)-hydroxide, which forms as per reaction 5:

$$xFe^{3+} + (1-x)M^{2+} + 2H_2O \rightarrow \alpha Fe_xM_{(1-x)}OOH_{(S)} + H^+ \quad (5)$$

In summary, the reactions that govern AMD are sometimes given in stepwise succession, where step one is the pyrite reaction with oxygen and water (reaction 1), and step two is the oxidation of Fe(II) to Fe(III), step three involves the hydrolysis reactions given in reactions 4 and 5 and step four is the additional oxidation of pyrite by Fe(III). Reactions 3, 4 and 5 all contribute to the acidity of the system.

The reactions above are balanced but they do not have molecular mechanistic or kinetic meaning. The rates of these reactions have been investigated by authors such as Singer & Stumm (1970), who found that reaction 2 is the rate-limiting step in abiotic conditions. In these systems, however bacteria play a major role in the acceleration of acid generation, by catalyzing the reactions that generate AMD. The presence of the bacterium, *Thiobacillus ferrooxidans* has been commonly suggested to accelerate the acid generation significantly. This was investigated by Fowler et al. (1999), who found that bacteria increased the pH at the surface of the pyrite, which resulted in higher leaching rates. Schrenk et al. (1998), and references therein, investigated pyrite oxidation by another acidophilic bacterium, namely *Leptospirillum ferrooxidans*. *L. ferrooxxidans* exists in environments with a lower pH while *T. ferrooxidans* are found to exist in peripheral slime-based communities with a pH higher than 1.3 and temperatures lower than 30°C. It is also reported that *T. ferrooxidans* affects the precipitation of ferric iron but neither species, *T. ferrooxidans nor L. ferrooxidans*, play a role in direct catalysis at low pH values at Iron Mountain, California. In the same study, species of domains Eukarya and Archaea were also found in extreme acidic conditions that could contribute to AMD generation. A new species of Archaea of the order *Thermoplasmales*, was investigated by Edwards et al. (2000) that grows at pH values of 0.5 and temperatures of 40°C. This species oxidizes iron and is thought to impact iron and sulfur cycles substantially (Edwards et al., 2000).

Johnson (1998) reports of fungi, yeasts and protozoa that exists at lower pH levels although these are not the optimum conditions for growth of these organisms, unlike organisms such as acidophiles that have an optimum growth rate at pH lower than 3. Due to the complexities of microbial interactions, the contribution of specific microorganisms to AMD remains somewhat controversial. Most reports, however, agree that microbial interactions significantly increase the rate of AMD formation, up to 10^6 times relative to abiotic-only systems.

1.1.6. Secondary minerals associated with AMD

Secondary minerals formed from AMD are dominated by Fe as this is the cation that has the highest concentration in most cases. The cause of precipitation of these secondary minerals is listed by Alpers et al. (1994) and includes evaporation, oxidation, reduction, dilution, mixing and neutralization. Extensive research has been conducted on secondary minerals forming from acid mine waters (e.g. Nordstrom, 1982; Blowes et al., 1991; Bigham & Murad, 1996; Bigham et al., 1996; Yu, 1996; España et al., 2006; and more). Secondary minerals play an important role in the recycling of metals and acidity in surficial environments (Hammarstrom & Smith, 2002).

One of the most common groups of these secondary minerals is ochre deposits. In the context of AMD, this refers to iron reprecipitating from solution. Some authors list this only as iron oxyhydroxide minerals (Hammarstrom & Smith, 2002). In an extensive description of these minerals, Bigham & Murad (1997) list the most common minerals in ochre deposits as goethite (α-FeOOH), ferrihydrite, schwertmannite and jarosite. The colours of these minerals are very distinct yellow to reddish brown. Ferrihydrite and schwertmannite are poorly crystalline minerals while jarosite is highly crystalline. Goethite does exist as a well crystalline material in nature, although specimens that form in AMD are short rod like particles (Brady et al., 1986).

Yu (1996) investigated Fe and Al mineral phases precipitating from acid mine waters by simulating equilibrium with the MINTEQA2 computer program, which suggested that ferrihydrite, $FeOHSO_4$, gibbsite ($Al(OH)_3$) and $AlOHSO_4$ should precipitate. However, experimental results indicated that only ferrihydrate and $Al_4(OH)_{10}SO_4$ could be recognized as precipitates at the bottom of the streams and mine drainage channels. The conclusion was made that the lack of $FeOHSO_4$ and $AlOHSO_4$ formation occurred because the formation of these minerals are kinetically inhibited and that mineral phases forming from the solutions cannot be predicted by equilibrium calculations but rather by identification of the actual phases present.

The fact that AMD solutions are often close to saturation with respect to a number of phases makes the solutions difficult to analyze. The solutions are mostly filtered through a 0.45 µm filter. A concern that was investigated since 1840 (Mill, 1980) is the presence of colloidal material (particles with diameter < 0.45 µm) that can pass through a 0.45 µm filter along with the filtered solution, but is not actually part of the true solution and rather part of particulate matter. Yu et al. (1999) similarly address the same issue with a 0.45 µm filter, but then express concerns over using smaller filters (0.2 µm or 0.1 µm) in that it may lead to an underestimation of iron when it precipitates from solution. Yu et al. (1999) made the conclusion that filtering with 0.45 µm filters causes insignificant overestimation relative to the dissolved iron concentration.

2. Materials and Methods

2.1. Sampling

The site chosen for the study is an abandoned ore processing site located 5km to the north of Nababeep (Figure 1.4). The processing site is situated close to a stream feeding to Nababeep River. Although no information was available about the type of ore or ore processing that took place at the site, information from Mr Fourie suggests sulfuric acid heap leaching processes were used to extract Cu from the ore. This leaching pond is unlined and unfenced. Iron plates were then placed in the impregnated solutions for Cu-plating. Four main sampling locations were chosen for the purpose of the study (Figure 1.4). These locations were strategically chosen to represent the various extents of contamination by AMD. The sample locations are all situated within the same terrain unit, namely, a colluvial toeslope. The first site (Nb1) is in the AMD pond which was covered with a silt layer of gangue material saturated with water. This appeared to be the base of a leaching pond and the terraces that were interconnected can be observed in the lighter region in Figure 1.4, which possesses no observable vegetation. The sampling was conducted in May 2013, before the onset of the rainy season. This means that sampling was conducted when conditions were at their most dry and that the water in the pond was at its most concentrated in terms of its chemistry. At the time of sampling, a salt crust had formed above the gangue material and no free water was visible in the lower pond. The AMD was sampled by digging pits in the gangue material, thereby allowing the solution in equilibrium with the gangue material to seep into these pits. The AMD was collected in both Nalgene® and glass bottles. During sampling, green crystals were observed at the base of the gangue-silt material. These crystals formed a hardpan layer at approximately 25 cm beneath the surface.

The other sampling sites are situated progressively further away from the pond. The second (Nb2) and third (Nb3) sites are natural soils that are contaminated with AMD and would be saturated with contaminated water at the height of the rainy season. Between Nb2 and Nb3, a sample of disintegrated granite-gneiss, which had been exposed to AMD, was sampled. The fourth site (Nb4) is a pristine soil site located approximately 700 m north of the first sampling site on the same terrain unit (Figure 1.5).

The soil at site Nb4 was classified according to the South African Soil Classification (Soil Classification Working Group, 1991). Three main horizons (top to bottom) were identified as the A, B1 and B2 horizons, which overlie the solid granite bedrock. For Nb2 and Nb3, soil sampling was conducted at different depths where clear morphological differences were observed (Table 1.2). All the samples were bagged in soft polyethylene (PE) bags which were sealed in in an attempt to maintain the soil equilibrium conditions at the time of sampling.

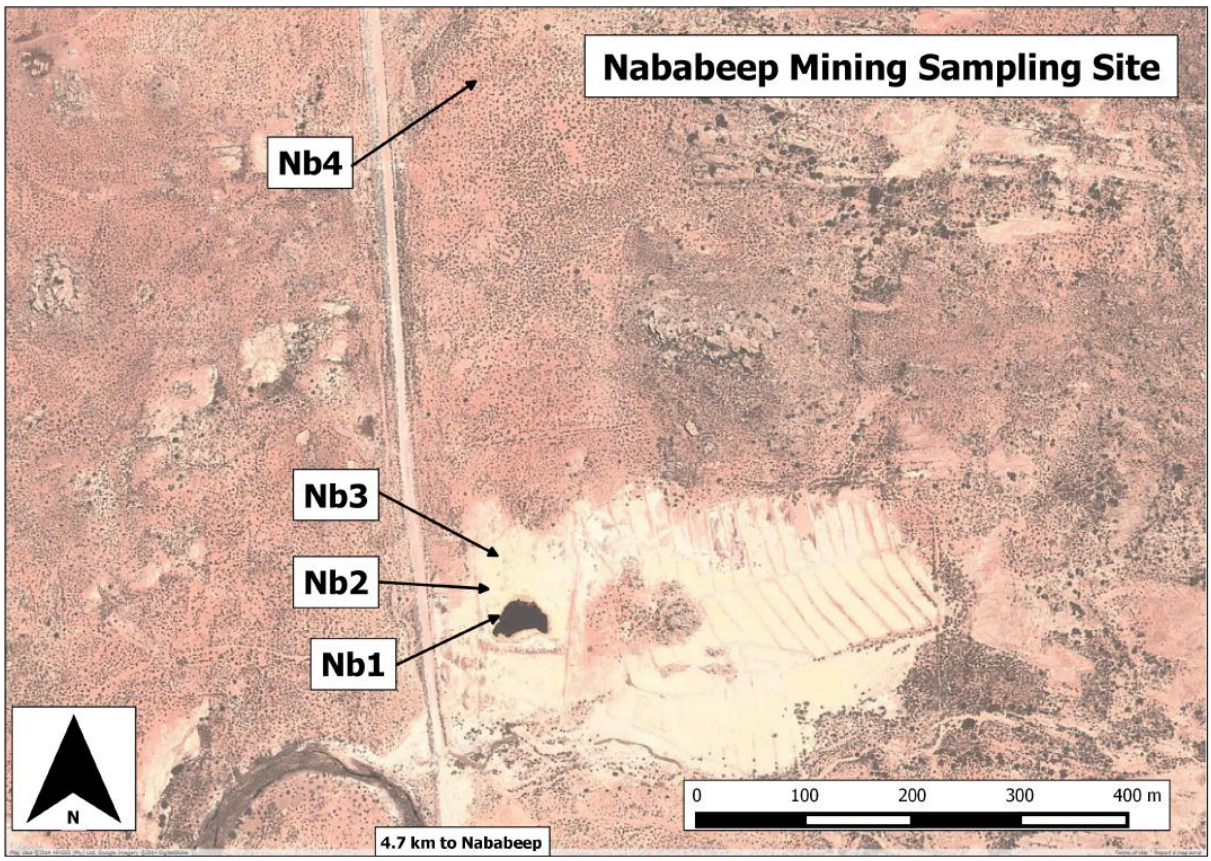

Figure 1.4: Aerial view of the sampling location which comprises 4 sampling sites.

Figure 1.5: Pristine soil sampling pit located at sampling site Nb4.

Table 1.2: List of samples according to location and horizon sampled.

Sampling site/Profile	Horizon
Nb1	AMD Pond
Nb2	Crust
	0-3 cm
	3-20 cm
	20-40 cm
	40-50 cm
Nb3	Crust
	1-15 cm
	15-30 cm
Nb4	A
(Pristine soil)	B1
	B2

2.2. Characterization of Soil Solutions and AMD

In order to determine the equilibrium conditions in the soil solution, a saturated paste extraction was conducted on the soils as described by Whitney (2011). In order to preserve chemical equilibria, the soil was not dried or sieved prior the extraction. The pH and electrical conductivity (EC) was measured in the paste using a Metrohm 827 pH lab pH meter and a Jenway 4510 Conductivity Meter, respectively. Redox potential of extracted solutions was measured by a Metrohm 744 pH meter with a Pt Ag/AgCl electrode. The values were adjusted to the Standard Hydrogen Electrode (SHE) as described by Nordstrom & Wilde (2005). The extracted solution was also analyzed for metals and sulfur by inductively coupled plasma-atomic emission spectrometry (ICP-AES) using a Thermo ICAP ICP-AES. The instrument was calibrated every day with multi-element, NIST traceable standards and verified through analysis of a separate set of NIST standards. The standards are verified after every twelfth analysis in order to verify calibration integrity and monitor drift. Dissolved silica was analyzed colorimetrically with the blue ammonium molybdate ($(NH_4)_6Mo_7O_{24}\cdot 4H_2O$) method. For the pristine soils, anion concentrations were determined by ion chromatography (IC) (Dionex®).

Three samples of AMD were collected from the AMD pond (Nb1) and analyzed. Prior to analysis, the AMD samples were filtered through 0.45 µm nylon syringe filters and then diluted with nitric acid adjusted water (pH ~ 2) to prevent precipitation of Fe-phases. Diluted samples were analyzed for major metals (ICP-AES) and dissolved silica (colorimetric). Due to the excessively high sulfate concentrations, IC analysis required extremely high dilution ratios and yielded unsatisfactory results with large anion – cation balance errors. Therefore, sulfur was determined by ICP-AES and converted to the equivalent concentration of sulfate with the assumption that all the sulfur measured in the samples is in the form of sulfate. Two additional techniques were used to determine sulfate concentrations. The first is a gravimetric $BaCl_2$ test which is based on the fact that $BaSO_4$ is virtually insoluble in water. Briefly, an excess amount of $BaCl_2$ is added to a known volume of AMD and the precipitate is then collected and

the remaining solution removed. The precipitate is then dried and weighed. The second method used is a turbidimetric method used to test the sulfates in solution with the Spectroquant® Sulfate Cell test. Although the gravimetric and the turbidimetric methods yielded higher SO_4^{2-} concentrations, the ICP-AES method resulted in the best anion-cation balance in all replicates and was thus deemed to be the most accurate.

The pH and electrical conductivity (EC) were determined with a standard 10 g soil to 25 g of distilled water ratio. The pH was also determined by a 1:2.5 soil to 1 M KCl solution.

Equilibrium modeling of both the soil solutions and AMD was conducted using the PHREEQC software package (version 2.17.1.4468 by the United States Geological Survey).

2.3. Mineralogical and chemical characterization

The mineralogy of the collected soil samples was characterized using X-ray diffraction (XRD) analysis and Fourier transform infrared (FTIR) spectroscopy. For the separation of the clay fraction prior to analysis by XRD and FTIR, the clay fraction was first dispersed with NaOH in a manner similar to the method used by Norrish & Tiller (1976). Firstly, the bulk soil was air dried and sieved through a 2 mm sieve and the <2 mm fraction was used. Approximately 100 g of sieved soil was placed in a 250 ml bottle. Thereafter, distilled water was added to produce a liquid slurry. To this slurry, 1 M NaOH was added in order to raise the pH. Sodium carbonate (Na_2CO_3) was then added to raise the pH to a final value of 9.5. This slurry was then shaken for 3 to 4 hours.

After shaking, the slurry was transferred to large 3 l jar, which was filled with distilled water to form a suspension. This suspension was stirred thoroughly and was allowed to stand for 16 hours. Thereafter, the uppermost part of the suspension was siphoned off to a depth of 10 cm. A single performance of this procedure was found to be sufficient for separating the clay fraction in the pristine soils. With the contaminated soils, however, the ionic strengths of the solutions were too high and this procedure had to be repeated in order to obtain dispersion of the clay. The siphoned-off part of the suspension was settled out (via flocculation) by lowering its pH to between 5 and 7 with the addition of 1 M HCl. Magnesium chloride ($MgCl_2$) was added to enhance flocculation. Once the clay suspension had settled out, the clear supernatant above the clay slurry was siphoned off and discarded. The remaining slurry was then split into two equal parts.

The first half of the suspension was saturated with 0.5 M $MgCl_2$ while the second half was saturated with 1M KCl to promote Mg and K saturation respectively. The slurries were shaken by hand and centrifuged. The supernatant was discarded and the respective samples were again treated with 0.5 M $MgCl_2$ and 0.5 M KCl and centrifuged. Once the supernatant was discarded, the excess salt was removed by the addition of a 1:1 methanol-water mixture to each sample, after which they were shaken and re-centrifuged.

The slurries were poured into dialysis tubing and put into a dialysis bath of distilled water. The water was replaced at frequent intervals until the water bath tested free of chlorides (upon addition of 0.1 M $AgNO_3$). Thereafter, the clays were dried in evaporation basins and then mortared to fine powders. The powders were analyzed by XRD analysis. For those clays where a 14 Å peak was observed on their

diffractograms, those clays had to be tested for montmorillonite by saturation with ethylene glycol (EG). Mosser-Ruck et al. (2005) report that the procedures for saturation with EG should be standardized since there are many reports using different procedures. Liquid EG solvation was performed in this study by adding EG onto dry samples until the clay formed a paste. The samples were solvated at room temperature (25 ˚C) for 24 hours and thereafter the powder was analyzed.

The clay powders were analyzed at iThemba Labs, Somerset West, South Africa. The X-ray diffractometer was a Bruker AXS (Germany) with Cu-K-alpha radiation (1.5406 Å) and a LynxEye detector. The measurements were conducted with a tube voltage of 40kV, a tube current of 40mA, and a step size of 0.027 degrees in the 2 theta range. The angle ranges was 3–50 degrees 2θ.

Infrared spectra (IR) were generated using a Thermo Nicolet Nexus™ FTIR spectrophotometer. The air-dry clay fraction was used and discs were pressed using spectrographic grade KBr. The KBr was dried overnight at 100 °C. A 1% w/w KBr disc was made by weighing 2 mg of sample and 200 mg of KBr. The two components were mixed by mortar and pestle until uniform colour appeared. A 13 mm pellet was then pressed at 5–8 tons of pressure with a hydraulic press. A blank KBr pellet was also pressed for background spectra. The spectra were generated between wavenumbers of 4000 and 400 cm^{-1} with 128 co-added scans per run at a resolution of 4 cm^{-1} and analyzed with Omnic™ 8.1 software suite.

The total elemental composition of the soils (<2 mm) was determined by X-ray fluorescence (XRF) spectrometry, using a handheld Niton® XL3t GOLDD™++ analyzer by Thermo Scientific.

2.4. Textural Analysis

The soils were all sieved with a 2 mm sieve and the fraction remaining on the sieve was weighed to determine the percentage of coarse fragments. Sand grades were determined through sieving while silt and clay fractions were determined on the pristine soils with the pipette method as described by the Soil Classification Working Group (1991).

3. Results and Discussion

3.1. Field observations in parent material

The leaching pond showed extreme evidence of rock weathering. For example, the boulders within the area of the pond had mushroom (Figure 1.6a) or column (Figure 1.6b) forms as a result of the aggressive weathering caused by the AMD. A sample of this weathered granite was milled and analyzed by XRD to determine the phases present (see Figure D2 in Appendix D for the XRD pattern of this weathered granite). The main phases identified were quarts, microcline, albite and jarosite. The absence of amphibole and biotite, both of which are common components of the granite-gneiss, suggests that these minerals have been weathered away, which is a reasonable deduction, considering their high susceptibility to weathering relative to the other phases present such as quarts for example (Goldich, 1938).

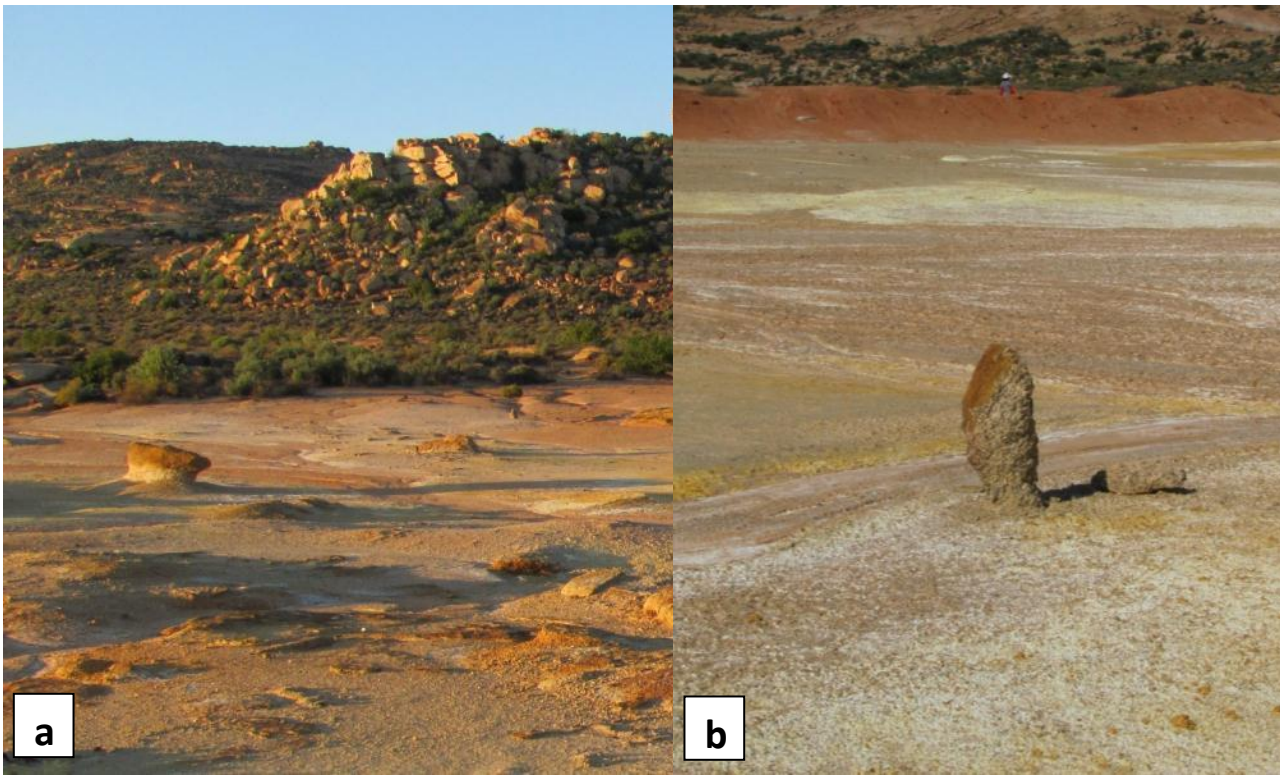

Figure 1.6: Photos of leaching pond with clear evidence of deterioration of granite rock formations in the form of (a) mushroom and (b) column forms.

3.2. Characterization of AMD

The concentrations of the various species in the sampled AMD, are provided in Table 1.3. A pH of 1.5 and an average EC of 24.2 mS/cm was measured. Exceptionally high metal concentrations were measured for Al (26.9 g/l), Cu (3.8 g/l), Fe (42.9 g/l), Mg (20.5 g/l) and Mn (3.45 g/l). Other notably high metal concentrations were Ca (230 mg/l), Ni (340 mg/l) and Zn (1688 mg/l). To put these values into context, they can be compared to a set of published guidelines for aquatic systems, which indicates what the maximum and/or target concentrations for these different chemical species should be in a particular context. Examples of these guidelines include drinking water, water suitable for industrial usage, domestic usage, and recreational usage as well as for pristine waters to maintain pristine aquatic ecosystems. In South Africa, the Department of Water Affairs and Forestry (now Department of Water Affairs and Sanitation) published a series of these guidelines for different industries, as well as aquatic and marine environments in 1996. The target water quality range (TWQR) for Cu in very hard waters should be 1.4 µg/L (Department of Water Affairs and Forestry, 1996) and thus in the sampled AMD is over 2.7 million times higher than the TWQR. The TWQR for Al for waters with pH lower than 6.5 is 5 µg/L and therefore the Al concentration in the sampled AMD is over 5.3 million times higher than the TWQR. Although these standards are for pristine aquatic ecosystems, the comparisons illustrate the unusually high concentrations of metals present in the AMD.

Cobalt, Na, K and Pb showed very high standard deviations. In the case of monovalent cations it could be matrix interferences. Low concentrations of monovalent cations are difficult to determine accurately

with ICP in the presence of higher valency cations at high concentrations. The percentage cation/anion balance error calculated by PHREEQC is 16% in favor of the cations and is attributed to this complexity of analyzing the solution.

Table 1.3: Elemental analysis and selected chemical parameters for AMD collected in leaching pond.

Element/Parameter	Concentration/Parameter value	Standard Deviation [a] (mg/L)
pH	1.5	n.d.
EC (mS/cm)	24.4	n.d.
Eh (mV)	652	n.d.
Al (mg/L)	26897	1517
B (mg/L)	24.12	0.64
Ba (mg/L)	0.50	0.55
Ca (mg/L)	230	15.34
Cd (mg/L)	1.53	0.45
Co (mg/L)	127	15.49
Cr (mg/L)	19.89	0.80
Cu (mg/L)	3819	284
Fe (mg/L)	42923	4357
K (mg/L)	7.86	6.20
Mg (mg/L)	20493	1744
Mn (mg/L)	3448	182
Na (mg/L)	20.25	7.79
Ni (mg/L)	340	43.11
P (mg/L)	52.17	9.35
Pb (mg/L)	5.72	2.09
Si (mg/L)	16.57	2.99
Sr (mg/L)	0.07	0.01
Zn (mg/L)	1688	132
$[SO_{4(aq)}]_{(total)}$(mg/L)	318353	24475

a. Determined from triplicate samples (n =3)
n.d. = not determined
$[SO_{4(aq)}]_{(total)} = [HSO_4^{1-}{}_{(aq)}] + [SO_4^{2-}{}_{(aq)}] + \Sigma$ of all metal complexes

3.3. PHREEQC Modeling

Once the solution chemistry of the AMD and soil saturated pastes were known, the data was run on a thermodynamic simulation program called PHREEQC to determine which mineral phases were expected to form under these chemical conditions. Using this modeling software, comparisons could be drawn between what the actual and simulated products in equilibrium with the AMD would be.

Modeling aqueous systems with geochemical software requires the selection of a thermodynamic model to characterize the interactions between species in a solvent. España & Ercilla (2008) investigated the

Pitzer ion-interaction theory as well as the ion-association model and the Davies equation, by applying the models to a highly metal-laden AMD solution in equilibrium with melanterite, a case similar to this study. The concentration of iron was 74 g/l, sulfate was 134 g/l and aluminium was 7.5 g/l. It was concluded that although both systems have limitations, the Pitzer approach best described the water-melanterite equilibrium and hence this system was also used for the modeling in this study. It has been reported that the Pitzer specific-ion-interaction can predict the behavior of electrolyte solutions with ionic strengths of up to 6 mol/kg.

Other species that are close to saturation are the sulfate salts, for example $MgSO_4 \cdot 7H_2O$ (epsomite), $MnSO_4$ and $BaSO_4$ (barite).

3.4. Iron and its precipitates

The AMD had very high Fe and Al concentrations (Table 1.3). A green crystal, identified as melanterite by XRD analysis, was found at the base of the pond at Nababeep. This is an emerald green crystal as shown in Figure 1.8. In a study by Valente & Gomes (2009), melanterite was also identified. Melanterite has the chemical formula $FeSO_4 \cdot 7H_2O$, meaning iron is in its ferrous state (Fe^{2+}) in this mineral. Frau (2000) reports that pyrite from the Genna Luas mine in Italy weathers rapidly to melanterite without observing ferric iron oxyhydroxides.

The molality calculated in PHREEQC for Fe(II) was 0.254 mol/kg while the molality for Fe(III) was 0.515 mol/kg, which means two thirds of the solution consists of ferric iron. In Figure 1.7, the saturation indices of selected mineral species that are close to zero or positive, as determined with the Pitzer database in PHREEQC, are given. Most of the saturation indices were less than zero, which indicates unsaturated conditions. The exceptions were hematite and quarts. The saturation indices for the ferrous oxyhydroxides (ferrihydrite and lepidocrocite) are less than zero and would suggest that colloidal particles were not forming, as will be explained later. The melanterite saturation index is –1.14, which indicates that although it is relatively close to saturation, it is dissolving.

Oxidation of pyrite has been investigated by several authors (e.g. Buckley & Woods, 1987; Nesbitt & Muir, 1994; and several others) under varying conditions. As previously discussed for the oxidation of pyrite, the two other main components needed for pyrite oxidation are water and oxygen. The ratio of water to oxygen and the amount of exposure time to water and oxygen not only changes the rate of the oxidation reactions, but also influences the species that will form (Nesbitt & Muir, 1994). Jerz & Rimstidt (2004) found that the oxidation of pyrite in air was more appropriate than aqueous oxidation modeling when pyrite oxidation is modeled in waste dumps. In the latter study it was found that air with a humidity of less than 95% resulted in a ferrous solid phase, either melanterite or szolmonokite ($Fe^{2+}SO_4 \cdot H_2O$), precipitating in cracks and on the pyrite surfaces. Frau (2000) found that melanterite is especially observed during low rainfall periods with high humidity, since melanterite is soluble in water. Humidity prevents melanterite from undergoing dehydration to phases such as rozenite ($FeSO_4.4H_2O$) or szomolnokite which are greenish-white powders. The melanterite samples from Nababeep, when stored in the laboratory, also turned white on their surfaces. This mineral results from the precipitation of ferrous iron and sulfate, which means that a portion of Fe is still reduced while the sulfide has been oxidized to sulfate. The presence of melanterite in the mine tailings in Nababeep, means that iron was

not oxidized. The lack of iron oxidation could be attributed to oxygen depletion deeper within the tailings layer, especially considering that the tailings were saturated with water. The oxidation of Fe^{2+} to Fe^{3+} is favored by increase in pH. At this low pH (1.5) the oxidation is slow and as a result the Fe^{2+} persists. Coupled with that could be the possible presence of microbial species.

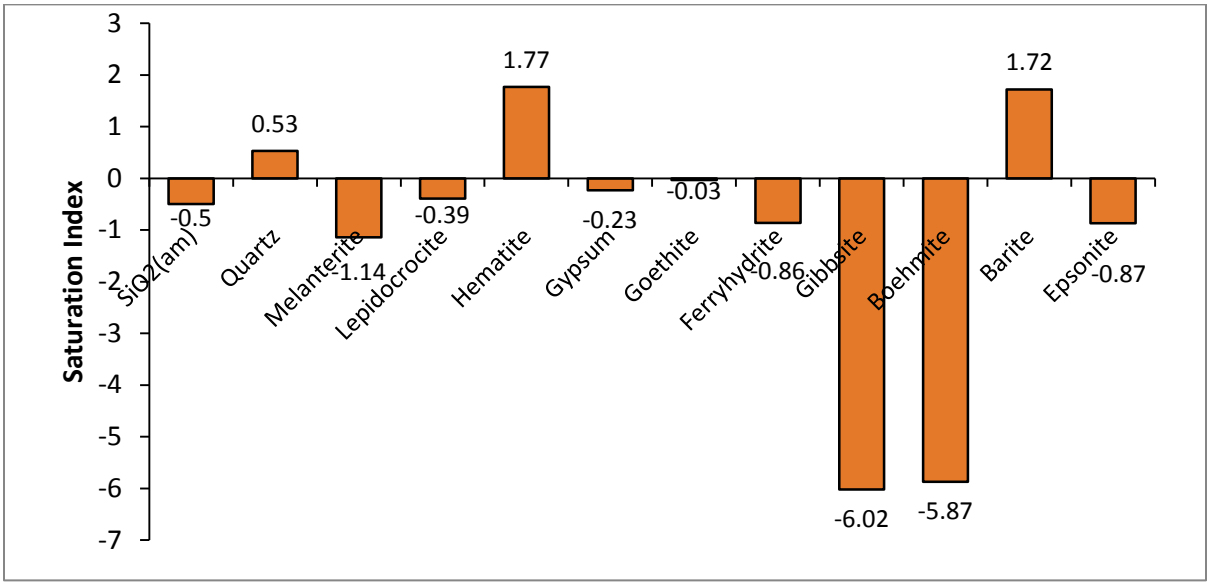

Figure 1.7: Saturation indices for selected species in the sampled AMD.

Figure 1.8: Melanterite sampled at the site near Nababeep.

As explained earlier, certain microbes are specialized to use certain chemical species as electron donors, which might explain the substantial oxidation of sulfur and limited oxidation of Fe.

Melanterite is usually identified by its evanescent efflorescence, but Blowes et al. (1991) reported a discontinuous hardpan layer in tailings at a mine in Quebec, Canada. The nature of the melanterite at the Nababeep site was also more of a deposited hardpan layer in the tailings. Frau (2000) found that the dissolution of melanterite is an acidity-generating process and is a source of Fe(III) for aqueous oxidation of pyrite.

The fact that melanterite was identified in the tailings means that iron is present in its reduced, Fe(II) form. The overall redox potential of a system can give some indication as to how reduced or oxidized a system is. The AMD solution collected for this study had a distinct red-brown color which is usually associated with ferric (Fe^{3+}) iron. The melanterite was, however, observed at the base of the tailings material (approximately 30 cm) beneath the crusted surface where oxygen levels would be lower as it is not exposed to the atmosphere.

When the redox potential of a system is considered, the system is often visually depicted on an Eh-pH diagram, also known as a Pourbaix diagram. These diagrams often make use of the parameter called pe, instead of Eh. These diagrams are usually defined in terms of a single chemical species (e.g. Fe), although many attempts have been made to construct it for several species, for example the Fe-S-K-O-H system, as depicted in Figure 1.9 (used with permission from Bigham et al. (1996)). The system was developed by using activities from previous investigations with specific application to acid sulfate waters. From Figure 1.9 it can be deduced that goethite and jarosite are the main mineral phases regulating the solubility of Fe in AMD with lower pH. The redox potential of the AMD in this study was 651.5mV (pe = 11) with a pH of 1.5, and this is indicated with a red star in the dissolved species stability field on the pe-pH diagram (Figure 1.9). At this position in the diagram, all the species are in the dissolved form but close to the jarosite and goethite phase. This is expected as the AMD was in a stable solution. From this figure, some predictions can be made when the system is diluted. This might shift the position of the star to the right and lead to precipitation of either goethite or jarosite. If the solution is further oxidized, jarosite will precipitate.

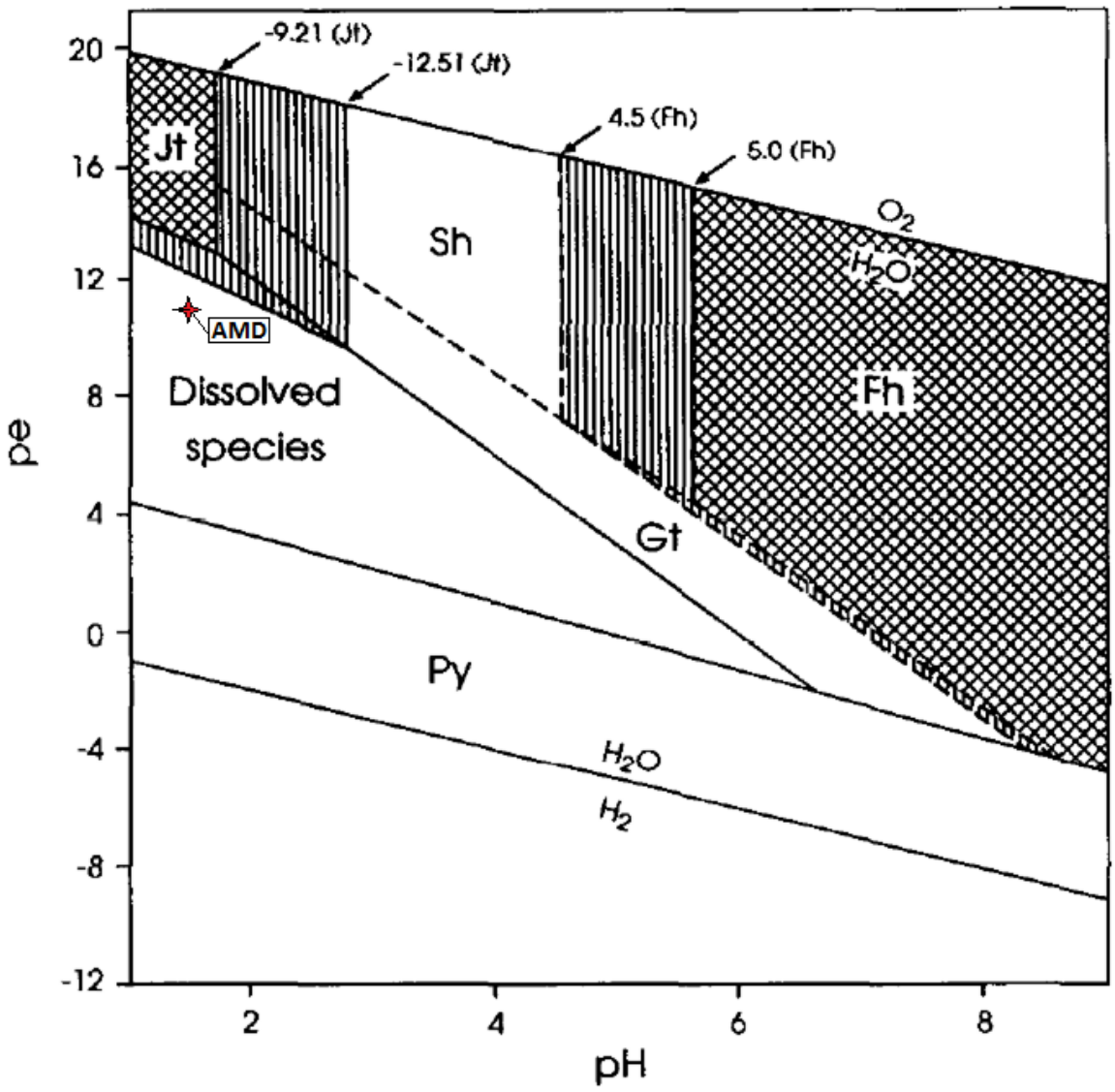

Figure 1.9: A pe-pH diagram for the Fe-S-K-O-H system at 25 °C, where pe = Eh(mV)/59.2. Total log activities of Fe^{2+}= 3.47; Fe^{3+} = 3.36 or 2.27; SO_4^{2-} = 2.32, K^+ = 3.78 and log K_{SO} values for solid phases are as given previously in paper. Jt = K-jarosite, Sh = schwertmannite, Fh = ferrihydrite, Gt = goethite, Py = pyrite. Line equations are Gt (pe = 17.9 – 3pH); Jt (pe = 16.21 – 2 pH); Fh (pe = 21.50 – 3 pH); Sh (pe = 19.22 – 2.6 pH), and Py (pe = 5.39 – 1.14 pH). Fields of metastability are indicated by dashed lines. Single-hatched areas demonstrate expansion of the K-jarosite and ferrihydrite fields if lower log K_{SO} values are selected. Used with permission from Bigham et al. (1996).

Yu (1996) investigated the precipitation of Fe and Al compounds from acid mine waters. In this study, an Eh-pH system was drawn for iron in water (Figure 1.10), but a dashed line is added in the dissolved species stability field of Fe^{2+} which is a stability line for the $FeSO_4^+$ ion at an Eh of approximately 500 mV (pe = 8.45). This is significant, since it would mean that Fe can exist in the oxidized Fe(III) form although a pure Fe-H_2O system pe-pH diagram would suggest that Fe is stable in its reduced, Fe(II) state. Given the high concentration of sulfate in this system, this species of Fe(III) would exist in the AMD. The acidity stabilizes ferrous iron. It is expected that strong solution complexation of ferrous iron with sulfate in

solution will occur resulting in a decrease in the activity of ferrous iron in solution. This will lower its propensity to change phase (oxidize to ferric iron). Again, the conclusion must be made that AMD systems are extremely complex and cannot be regarded or treated in parts, but must be investigated by taking everything into account. Ferrous iron in solution was determined spectrophotometrically by authors such as Frau (2000) using the colorimetric 2,2'-Bipyridine method. The AMD was highly concentrated and possessed a red-brown colour, thus colorimetric analyses were not possible. Diluting the sample with deionized water was not a suitable solution to the issue, as this resulted in precipitation of solid phases, and would also change the system completely in terms of Eh and pH. The colour of the AMD and presence of melanterite suggests that Fe is present in both states concurrently and would be related to Fe-sulfate complexes.

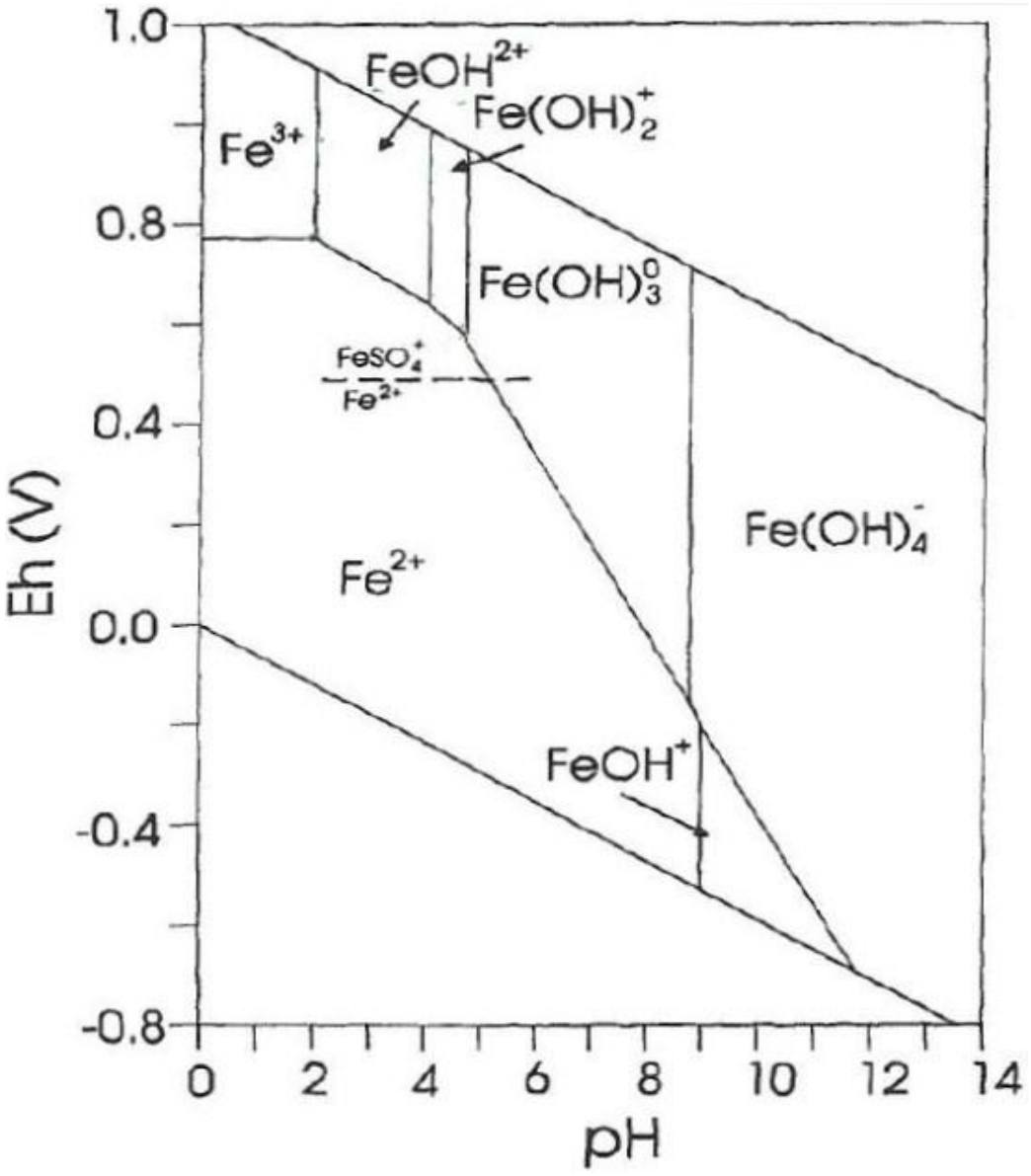

Figure 1.10: An Eh-pH diagram adapted from (Yu, 1996) that shows stability diagram of iron with SO_4^{2-} taken into account.

3.5. Aluminium minerals

Aluminium occurs at extremely high levels in the AMD (Table 1.3). Despite this, minerals such as gibbsite ($Al(OH)_3$) and boehmite (AlO(OH)) had SI values of -6.02 and -5.87, respectively (Figure 1.7) and thus the solution was undersaturated with respect to these minerals. This relates to the low pH of the solution. Aluminium sulfate minerals are likely to be more stable under acid conditions. A change in pH would however change saturation conditions that could lead to Al phases precipitating. With a high Al coupled with high sulfate at low pH it is expected that an Al hydroxysulfate such as basaluminite would precipitate.

3.6. Metal Toxicity

Figure 1.11 depicts the concentrations of Ni, Co, Cu and Zn for this study, as well as the studies by Smith & Williams (2000) and Frau (2000). Note that the *y*-axis scale is logarithmic due to the variance in the concentrations of the different studies. This study had higher concentrations for Ni, Co and Zn with values of 340 mg/l, 127 mg/l and 3819 mg/l respectively and are several orders of magnitude larger than the comparative studies. The zinc concentration in Frau (2000) is however higher than this study with a concentration of 10750 mg/l. The concentration of metals in the AMD is related to the ore from which the AMD is generated. Frau (2000) investigated a mining area of predominantly pyrite-melnikovite with minor amounts of Fe-rich sphalerite (ZnS) to which high zinc concentrations can be attributed. The minerals found in the Nababeep ore were chalcopyrite ($CuFeS_2$), bornite (Cu_5FeS_4), chalcocite (Cu_2S), malachite $Cu_2CO_3(OH)_2$ and magnetite (Fe_3O_4). Copper is therefore the predominant metal of interest at this mine and this is reflected in the mine drainage found and would be the element of concern when the toxicity of the local water sources in the area are evaluated.

The main concern with AMD is the threat that it poses to the environment. This threat is firstly related to the unnaturally very low pH of the leachate, and secondly, the metals that are released into the environment. The discussion of metal toxicity is beyond the scope of this dissertation, although the concentration of dangerous and toxic elements in this AMD should be highlighted. Iron and manganese are not considered highly toxic although they play an important role in the minerals that precipitate from an AMD solution. Toxicity is a complex issue as it is related to both the quantity and how the various living organisms are affected by that metal. Copper and zinc are essential for life, as they are very important in enzymatic reactions (Brewer, 2010), however, when present in quantities that exceed safe levels in water, they can lead to diseases such as Alzheimer's disease. Zinc, which is considered to be relatively non-toxic, has been found to interfere with Cu and Fe utilization in the human body (Fosmire, 1990).

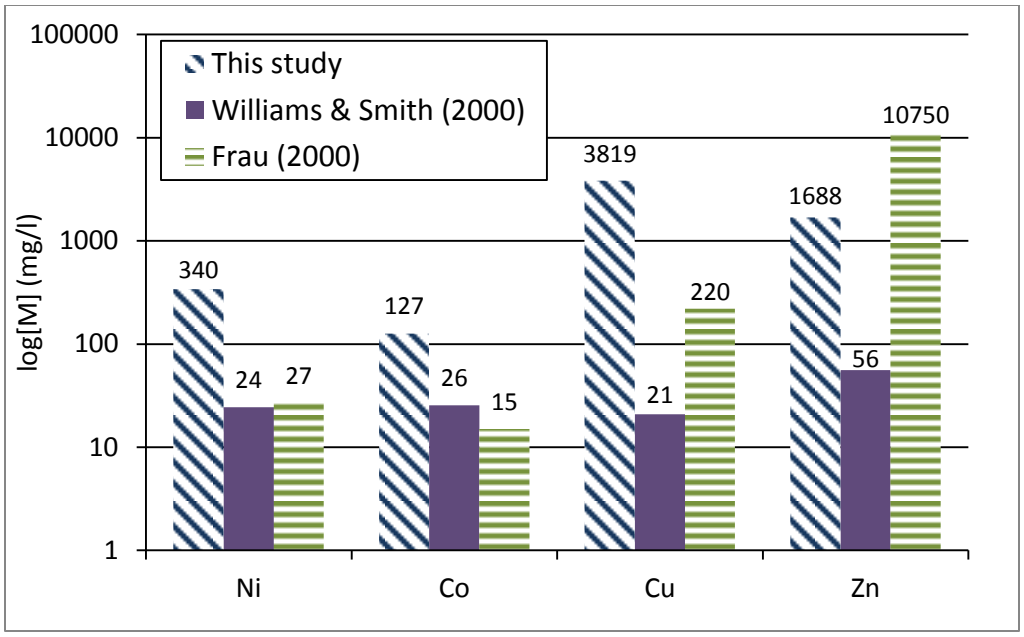

Figure 1.11: Heavy metal concentrations in AMD for this study, along with two comparable previous studies.

3.7. Characterization of pristine soils

3.7.1. Soil Classification and texture analysis

The pristine soil (Nb4) was classified as a Rubic Arenosol (Food and Agricultural Organization of the United Nations, 2014) or an Oakleaf 21/210 (Soil Classification Working Group, 1991) which has formed in granite-gneiss colluvial material (binary profile suspected). The coarse texture of the soil (Table 1.4) is both an indication of the colluvial nature of the material as well as the immaturity of the solum. The soil is relatively shallow with a depth of 60 cm. Three horizons were identified which were an A horizon and a B1 horizon, followed by a B2 horizon which overlies solid granite-gneiss. In the field moist state, the soil had a red appearance and possessed rhodic properties (Food and Agricultural Organization of the United Nations, 2014), but after drying the soil had a more bleached appearance. The Munsell colors in the wet state are 5 YR 4/6, 2.5 YR 4/6 and 2.5 YR 3/6 for horizons A, B1 and B2 respectively. The dry Munsell colors are 7.5 YR 5/6 7.5 YR 4/6 and 5 YR 5/6 for horizons A, B1 and B2 respectively. This bleaching indicates a relatively low Fe content in the soil.

Table 1.4: Texture of pristine soil, with sand, silt and clay percentages.

Horizon	Sand (%)	Silt (%)	Clay (%)
A (0-20 cm)	86.4	11.5	2.10
B1 (20-55 cm)	88.0	8.40	3.60
B2 (55-70 cm)	86.7	8.17	5.10

The percentage coarse fragments for each soil depth are provided in Table 1.5 for Nb2, Nb3 and Nb4, bearing in mind that Nb4 is a pristine soil. It is included in Table 1.5 for comparison with the contaminated soils. The tailings layer found within the Nb2 profile contains 0.56% coarse fragments. It is interesting to note that there are more coarse fragments in the A horizon of the pristine soil than in the

B1 or B2 horizons. A possible explanation might be that the A horizon is colluvium while the lower horizons have been weathered in situ.

Table 1.5: Coarse fragment percentage for sampled soils.

Profile	Horizon	Coarse Fragments (%)
Nb2	Crust	8.71
	0-3 cm	0.56
	3-20 cm	16.1
	20-40 cm	15.9
	40-50cm	41.4
Nb3	Crust	7.75
	1-15cm	8.49
	15-30cm	16.3
Nb4	A	17.7
	B1	7.79
	B2	11.5

3.7.2. Soil Chemistry

Despite the arid climate, the pristine soil has a low pH (Table 1.6). The difference between pH in water and pH in KCl is noteworthy. Given the low clay fraction, exchangeable acidity would be expected to be lower. As shown in Table 1.6, the pH measured in water increases with every horizon from 5.25 to 6.18. The reason for the low pH observed in the pristine soils could be attributed to the acidic granite-gneiss from which these soils are derived, although, even in acidic parent material the aridity of the area would normally result in higher soil pH values. Another possible cause could be a smelter located at the mine (5 km away), which has a chimney. It is possible that emissions from this smelter chimney could have contained sulfur particles, which has led to acidification of the area by atmosphere-soil-water interactions. The electrical conductivity (EC) for the pristine soil is low, with values of 9.58, 7.02 and 6.03 µS/cm for horizons A, B1 and B2 respectively.

Table 1.6: The pH (in deionized water and in 1M KCl) and EC values of the pristine soil (Nb4).

Horizon	pH (H_2O) (1:2.5)	pH (KCl) (1:2.5)	EC (1:2.5 H_2O)
A	5.25	3.78	9.58
B1	5.60	4.02	7.02
B2	6.18	4.21	6.03

The saturated paste extraction data is presented in Table 1.7 for the different depths of the pristine soil (Nb4). The highest concentrations of elements included Al (0.04–0.72 mmol/l), Mg (0.055–0.66 mmol/l) and Si (0.62–0.68 mmol/l) which are all associated with clay minerals and favour the formation of these minerals. The concentration of sulfate ranged from 0.15 to 0.24 mmol/l. The reason for the presence may therefore be attributed to pollution from smelter.

Table 1.7: Concentration of elements, pH and EC of saturated paste extracts for the pristine soil.

Sample	Al	Ca	Co	Cr	Cu	Fe	K	Mg	Mn	Na	Ni	Pb	Si	Zn
	concentration (mmol/l)													
Nb 4 (A)	0.0395	0.1204	0.0002	nd	0.0072	0.0109	0.1188	0.0545	0.0033	0.4142	0.0005	nd	0.6202	0.0028
Nb 4 (B1)	0.0975	0.1402	0.0001	nd	0.0059	0.0593	0.1314	0.1124	0.0066	0.4042	0.0008	nd	0.4707	0.0043
Nb 4 (B2)	0.7235	0.3326	0.0015	nd	0.0408	0.6036	0.1226	0.6587	0.0484	0.4554	0.0044	nd	0.6829	0.0186

nd – not detected

Sample	pH	EC	SO_4^{2-}
		mS/cm	mmol/l
Nb 4 (A)	4.48	0.105	0.1518
Nb 4 (B1)	4.38	0.116	0.1791
Nb 4 (B2)	4.77	0.088	0.2388

3.7.3. Soil Mineralogy

Figure 1.12 depicts the XRD patterns for the clay fractions of the three horizons of the pristine soil. The patterns reflect a similar mineralogy for all three horizons, which is quarts (SiO_2) (4.264 Å), kaolinite [$Al_2Si_2O_5(OH)_4$] (7.128, 4.029 and 3.574 Å) and illite [$KAl_2Si_3AlO_{10}(OH)_2$] (9.97, 4.967 and 2.988 Å). For the A-horizon, a fourth phase was identified which has a d spacing at 14.931 Å. This d-spacing matches the d-spacing for montmorillonite ($MgO{\cdot}Al_2O_3{\cdot}5SiO_2{\cdot}xH_2O$). The intensity of this peak is less than the intensity of the other peaks for the phases such illite or silica. Peak intensity depends on factors such as crystallinity and the concentration of the component which produces the peak in the sample. The d-spacing at 14.932 Å, as shown in Figure 1.13, is attributed to montmorillonite, chlorite or vermiculite (Brindley, 1955). After treatment with Mg, K and ethylene glycol it can be concluded that the mineral is montmorillonite (see Appendix - Appendix D - Supplementary Data relating to Chapter 1).

The concentrations of species within the saturated paste extracts can be used to model the phases that are in equilibrium within the soil plasma conditions.

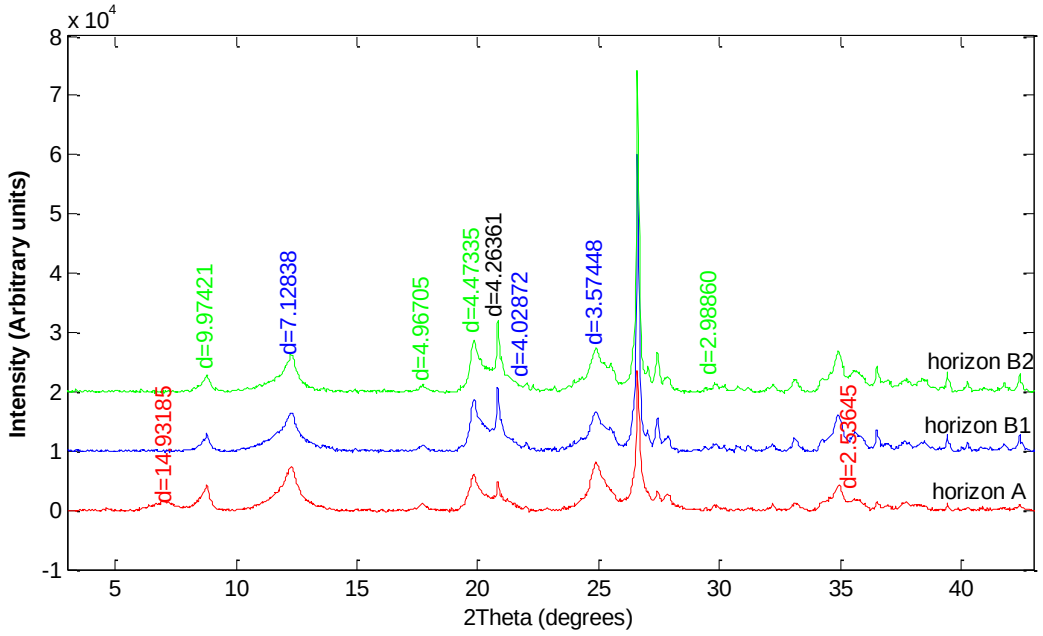

Figure 1.12: XRD patterns for the three horizons of the pristine soil (Nb4).

The saturation indices for some of the common soil minerals are given in Figure 1.13 for soil minerals considered in this study. This was calculated by PHREEQC using the Pitzer database. Kaolinite and illite, which were detected with XRD analysis, are stable phases in the soil solution. Ferric and Al oxides and oxy-hydroxides, such as goethite (FeOOH), gibbsite ($Al(OH)_3$) and hematite (Fe_2O_3), are also stable, as indicated by a positive saturation index. Two different sets of montmorillonite stabilities are calculated in PHREEQC. The first is an Fe-montmorillonite ($Mg_{0.17}Mg_{0.33}Fe_{0.67}Al_{1.01}Si_{3.99}O_{10}(OH)_2{:}5H_2O$) type and the second is a Mg-montmorillonite ($Mg_{0.17}Mg_{0.33}Al_{1.68}Si_{3.99}O_{10}(OH)_2{:}5H_2O$) type. The Fe-montmorillonite has a positive saturation index (SI) for all the horizons while the SI for Mg-montmorillonite is negative for horizons A and B1. It is therefore possible that montmorillonite is forming in the soils, although it was

only detected in the A horizon. The source of Mg in montmorillonite could be attributed to biotite which is a primary mineral found in the granite-gneiss. The fact that montmorillonite was not detected in horizons B1 or B2 could simply be due to the low concentration of this mineral in the fine earth fraction of soil.

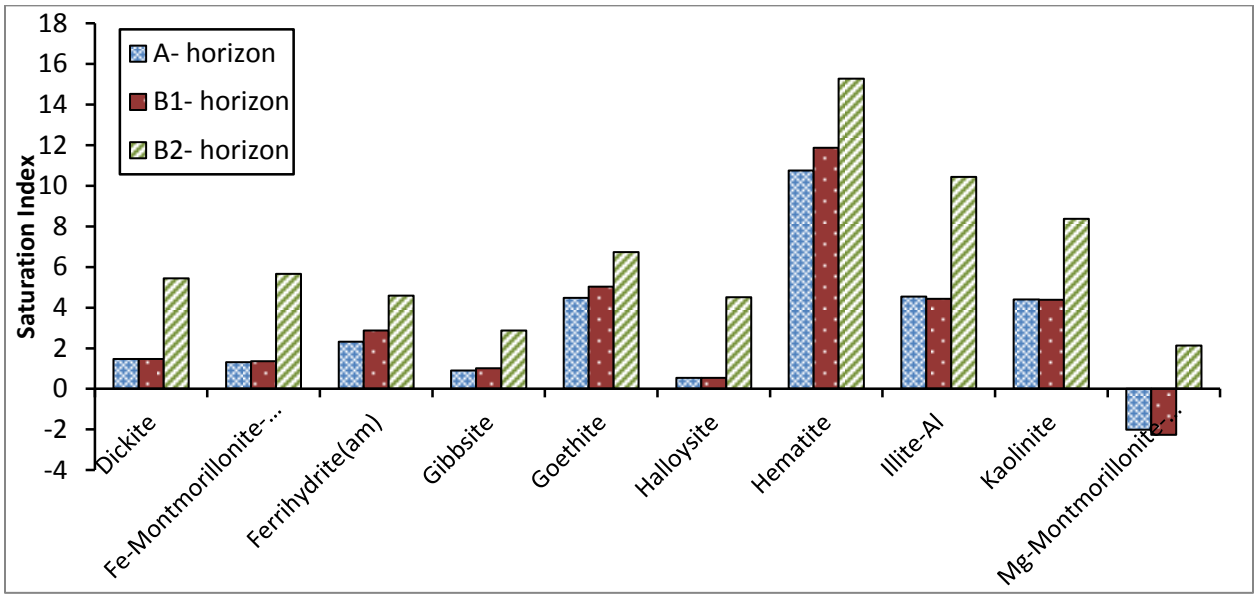

Figure 1.13: Saturation indices of selected minerals for the A, B1 and B2 horizons of the pristine soil (Nb4).

The FTIR spectra obtained for the clay fractions of the pristine soil are depicted in Figure 1.14. Spectra for the three samples are very similar. The one exception is the peaks for the B horizons (B1 and B2) at 1094 cm^{-1}. The peak at 1636 cm^{-1} for the A horizon is also more prominent than that for the other horizons. The peaks at 3695–3696 cm^{-1} can be assigned to OH-stretching of inner-surface hydroxyl groups of kaolinite. The second peak at 3621 cm^{-1} can again be attributed to OH-stretching of inner hydroxyl groups of kaolinite and peak around 912 cm^{-1} would also be OH-deformation of inner kaolinite hydroxyl groups. This band can also be assigned to the AlAlOH bending of illite. Peaks located at 1032 and 1009 cm^{-1} would be assigned to in-plane Si–O stretching of kaolinite. The bands between 780 and 684 cm^{-1} can be related to Si–O vibrations. The peak at 538 cm^{-1} is Si–O–Al out-of-plane bending with Al in tetrahedral sheet, whilst the peak at 470 cm^{-1} would be assigned to Si–O (in-plane) bending and OH-bending, both associated with illite clays (Steudel et al., 2009a).

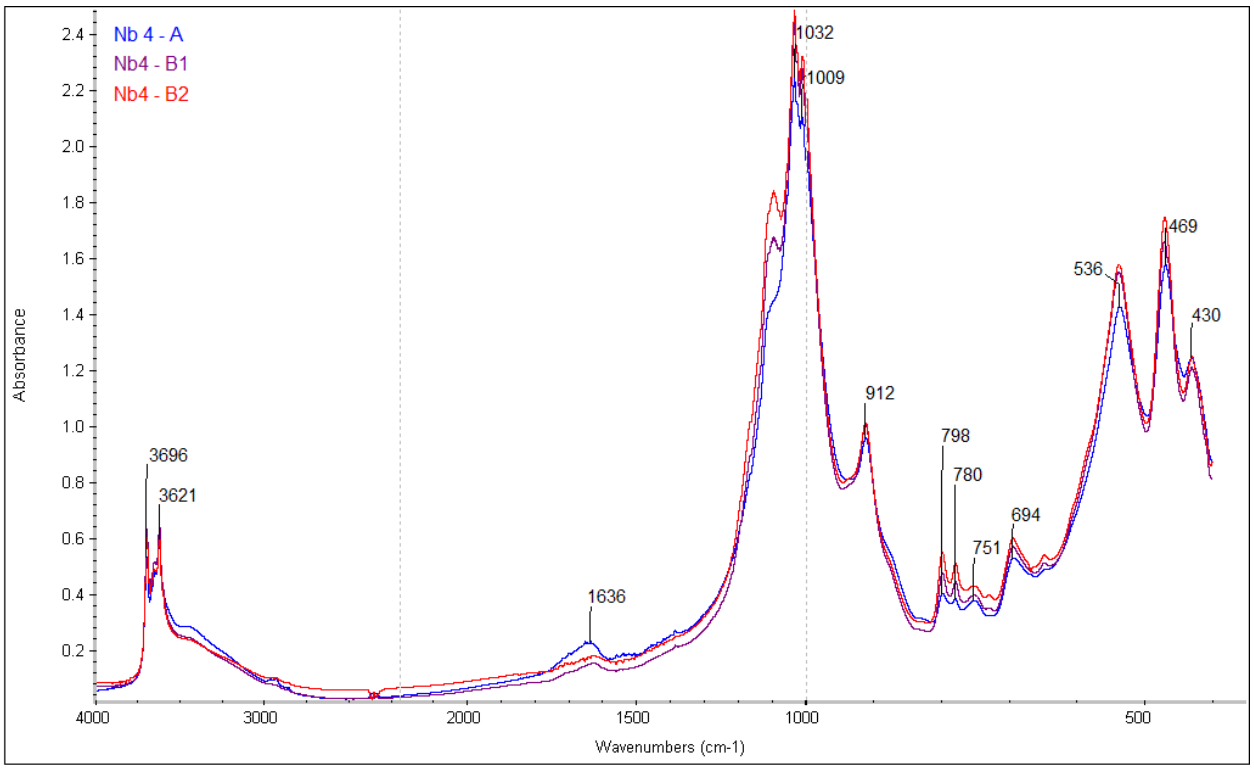

Figure 1.14: FTIR spectra generated for the pristine soil.

3.8. Characterization of contaminated soils

3.8.1. Soil description

Two contaminated natural soils were sampled in close proximity to the tailings dump. Soil samples were collected at different depths as shown in Table 1.5. Both these soils were covered in a crust that formed on the surface and although this is not considered to be a soil horizon, it was analyzed in a similar fashion. The layer in Nb2 directly below the crust is tailings material and had the same silty texture and colour as the mine tailings (Figure 1.15). This layer could have formed by material being washed over the soil when the ponds were in use. This is therefore also not true soil material and the material would classify as artifacts according to the World Reference Base for soil resources (Food and Agricultural Organization of the United Nations, 2014).

Figure 1.15: Soil profile of sampling site Nb2.

3.8.2. Chemical Characterization

From the data in Table 1.8, the EC's of the crusts are, as expected, high with a value of 22.9 mS/cm recorded for Nb2, whilst a lower value of 6.35 mS/cm is recorded for the crust formed on Nb3. An EC of 15.51 mS/cm is measured for the tailings layer formed on Nb2 and this layer has the lowest pH of these samples, measuring 2.76 in water. There is a clear difference in both EC and pH between the natural soil layers in Nb2 (3-20 cm, 20-40 and 40-50 cm) and those of Nb3 (1-15 cm and 15-30 cm), in that the values are less extreme for Nb3 i.e. higher pH and lower EC values than Nb2. Although in both cases it is far above "normal" soil conditions (or those observed in pristine soil). Both Nb2 and Nb3, were classified as a Witbank soil form (Soil Classification Working Group, 1991).

Table 1.8: The soil depths, pH's and EC values of the contaminated soils

Profile	Horizon	pH H_2O (1:2.5)	pH KCl (1:2.5)	EC (mS/cm) (1:2.5)
Nb2	Crust	2.91	2.70	22.9
	0-3 cm	2.76	2.48	15.5
	3-20 cm	2.94	2.76	8.90
	20-40 cm	2.91	2.77	9.79
	40-50 cm	2.84	2.66	11.0
Nb3	Crust	3.42	3.39	6.35
	1-15 cm	3.52	3.37	1.44
	15-30 cm	3.36	3.28	1.31

The saturated paste extraction data is presented in Table 1.9 for the different depths of the two contaminated soils (Nb2 and Nb3). There is an order of magnitude difference between the different soils sampled. One example of this phenomenon is the concentrations of Al in the saturated paste extract for Nb2 (20–40 cm), Nb3 (15–30 cm) and Nb4 (B-horizon), which are at similar depths, which were 860.6 mmol/l, 18.4 mmol/l and 0.097 mmol/l (Table 1.7), respectively. The concentration of Fe is not proportional to that of AMD. The AMD concentration of Fe was 768.6 mmol/l and for Al was 996.9 mmol/l but for Nb2 (40–50 cm) the concentration for Fe and Al were 67.5 mmol/l and 591.4 mmol/l, respectively. Therefore, assuming the source of these metals is from the AMD, there is a ratio change for two cases. Cations with the highest concentrations in the saturated paste extracts were Al and Mg. One source of these cations can be weathering of primary and secondary minerals such as biotite. Thus the lower concentration Fe that exists in the soil solution is attributed to Fe bound in Fe-precipitates. Copper is the heavy metal with the highest concentration in the soil. The concentrations were 23.6 mmol/l in the Nb2 (3–20 cm) soil sample and for Nb3 (1–15 cm), located further away from source, Cu concentration was 0.47 mmol/l. The highest concentration for all species except Na and K is observed for Nb2 (0–3 cm). This layer is the tailings layer wherein primary sulfide minerals such as pyrite occur and metals are readily released into solution as these tailings are oxidized. The low K value would be attributed to formation of jarosite. Arsenate is not given in Table 1.9 as it was not detected in any of the soil solutions. Also the concentration of Pb is low and only observed for Nb2. The difference between the concentrations of the two contaminated soils, Nb2 and Nb3, is attributed to less exposure to AMD for the Nb2 soil located further away from the leaching pond.

Table 1.9: Concentrations of different species, pH and EC measured in saturated paste extracts for contaminated soils.

Sample	Al	Ca	Co	Cr	Cu	Fe	K	Mg	Mn	Na	Ni	Pb	Si	Zn
	concentration (mmol/l)													
Nb 2 (0–3 cm)	1619.26	20.65	2.57	0.42	77.72	117.43	0.97	1007.20	81.11	1.45	6.79	0.05	2.36	34.92
Nb 2 (3–20 cm)	546.67	14.01	0.85	0.14	23.62	29.08	1.01	357.79	27.98	1.49	2.25	0.01	1.42	10.72
Nb 2 (20–40 cm)	860.59	14.78	1.33	0.19	37.33	49.40	2.84	548.04	42.25	1.70	3.51	0.02	1.84	16.78
Nb 2 (40–50 cm)	591.52	14.96	0.94	0.18	26.75	67.54	1.04	390.04	30.74	1.48	2.56	0.02	1.82	13.72
Nb 3 (1–15 cm)	19.79	12.53	0.03	0.00	0.47	0.29	0.76	15.96	1.55	0.79	0.08	nd	1.08	0.44
Nb 3 (15–30 cm)	18.36	15.53	0.0271	0.0008	0.4104	0.0270	0.1966	13.71	1.34	0.8356	0.0786	nd	1.8429	0.4084

nd – not detected

Sample	pH	EC	SO_4^{2-}
		mS/cm	mmol/l
Nb 2 (0-3 cm)	1.74	30.4	1477.00
Nb 2 (3-20 cm)	2.2	34.8	1728.05
Nb 2 (20-40 cm)	2.1	34.5	2475.91
Nb 2 (40-50 cm)	2.23	35.2	1735.85
Nb 3 (1-15 cm)	3.27	5.75	71.11
Nb 3 (15-30 cm)	3.16	5.04	63.03

3.8.3. Soil Mineralogy

The results of the XRD analysis for Nb2 site are depicted in Figure 1.17. The patterns of the 3–20, 20–40 and 40–50 cm horizons are very similar, however there are some differences. The first difference is the absence of the peak at 9.98 Å for the 40–50 cm layer. This peak has been identified as the peak for illite. Another peak representing illite also occurs at 4.47 Å, as indicated in magenta. Kaolinite (d = 7.11 and 3.57 Å) and quarts (d = 4.26 and 3.35 Å, and others) were two other minerals identified in this soil. A new mineral, not previously detected in pristine soil, is jarosite, which has clear and sharp peaks at d = 5.94, 5.67 and 2.97 Å. This is a ferric iron-sulfate mineral with general formula $(K,H_3O)Fe_3(SO_4)_2(OH)_6$ and forms in AMD solutions with low pH (Bigham et al., 1996). Only two minerals were identified from the XRD pattern for the clay sample of the tailings layer (0-3cm), and these were jarosite and quarts. It was extremely difficult to extract clay size particles from this sample since the suspension had a high ionic strength that made particles flocculate and settle rapidly. Secondly, it had a very low percentage clay and the procedure had to be repeated several times to extract enough clay-sized material for analysis.

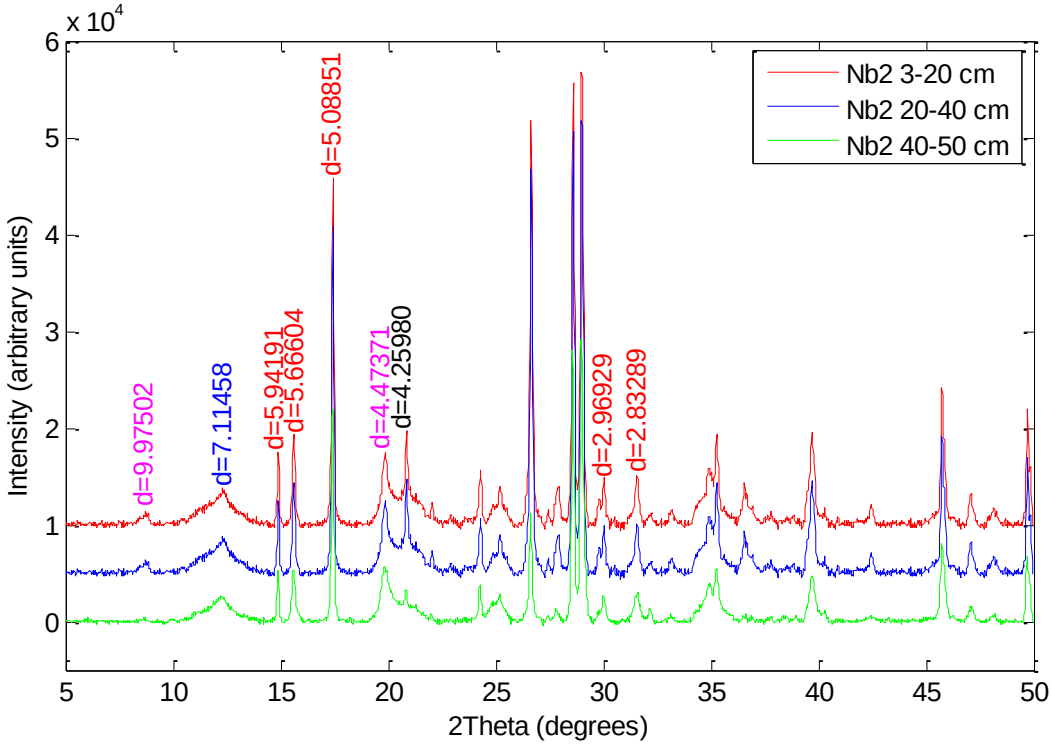

Figure 1.16: XRD pattern for the 3 horizons of Nb2.

Figure 1.17 is an overlay of a section of the XRD patterns of Nb2 (40–50 cm) and Nb4 (B-horizon). A broadening of the kaolinite peak observed at 7.11 Å compared to pristine soil may indicate a less crystalline kaolinite phase possibly transforming into halloysite.

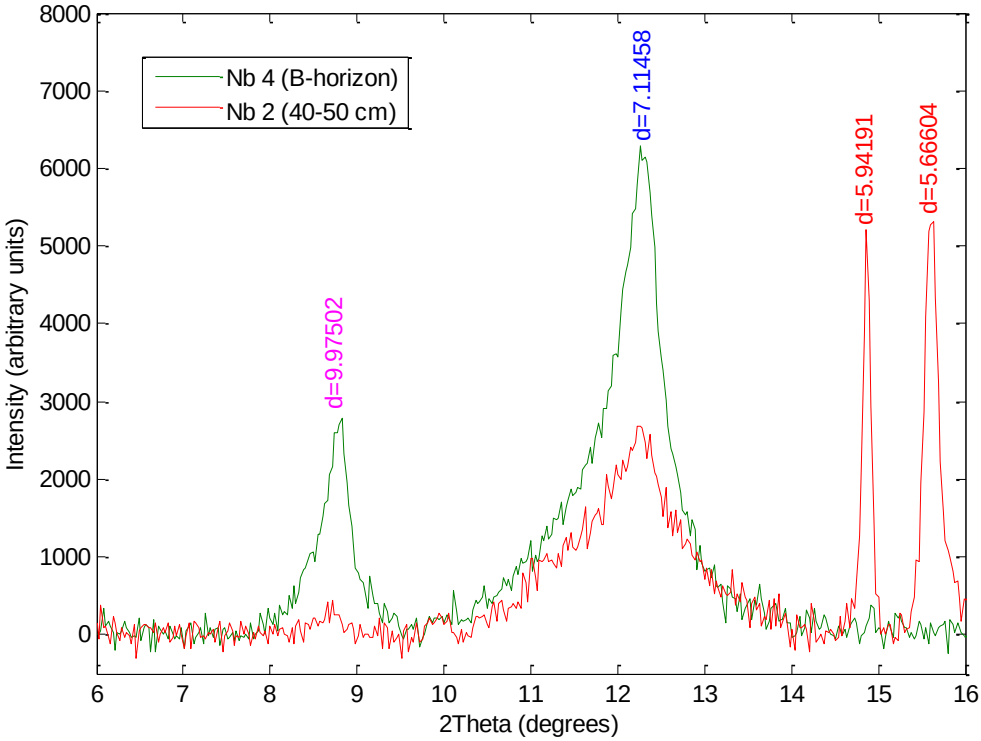

Figure 1.17: Section of XRD pattern that compares Nb4 (B-horizon) with Nb2 (40–50 cm).

A section of the crust was analyzed with XRD analysis and the two dominant minerals which fitted the peaks best were identified. The first of these minerals is apjohnite with chemical formula $MnAl_2(SO_4)_4 \cdot 22H_2O$. The second mineral is epsomite ($MgSO_4 \cdot 7H_2O$), a hydrated magnesium salt. Interestingly, no iron mineral is detected in the crust layer.

The XRD data for Nb3 is depicted in Figure 1.18. The XRD pattern for Nb3 has a very similar pattern to that of Nb2. The minerals identified here were again kaolinite, quarts, jarosite and illite, although the first peak of illite at 9.98 Å has very low intensity. As previously mentioned, this might be due to a low concentration of illite in the soil. It should be noted that the peaks generated during XRD analysis are, as previously mentioned, related to the concentration and crystallinity of minerals in the samples. This means that there are many shortcomings to XRD analysis for the analysis for poorly crystalline materials.

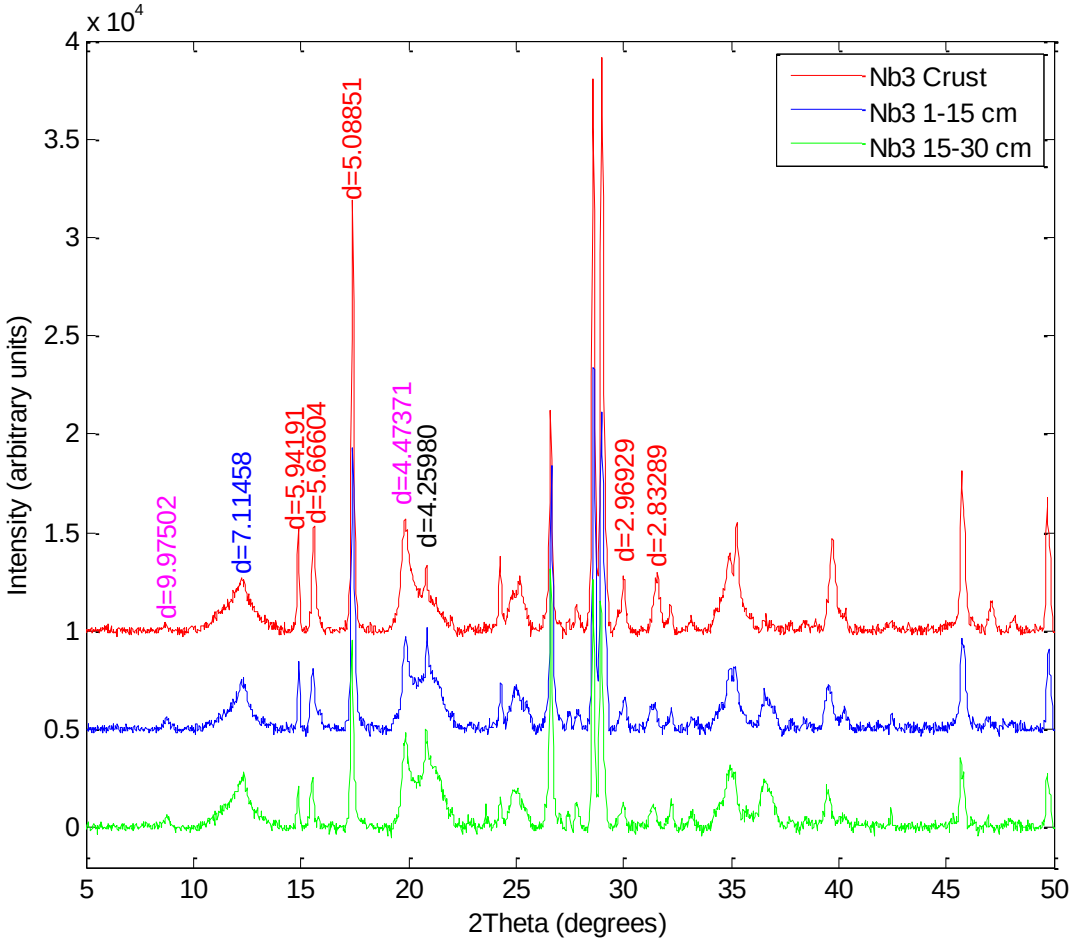

Figure 1.18: XRD data for the 3 horizons of Nb3.

The main differences in Fourier Transform infrared (FTIR) spectra between the contaminated soils and the pristine soils occur at the wavenumber values between 3700 cm^{-1} and 2800 cm^{-1}. The range of wavenumbers is given in Figure 1.19 for the contaminated soil (Nb2). The broad peak between 3500 cm^{-1} and 3000 cm^{-1} can be assigned to OH vibration of jarosite as identified by Sasaki et al. (1998) for peaks at 3390 cm^{-1} and 3365 cm^{-1}. The broadness of the peak may also be related to water bound to metals in more amorphous phases such as ferrihydrite (Russell, 1979).

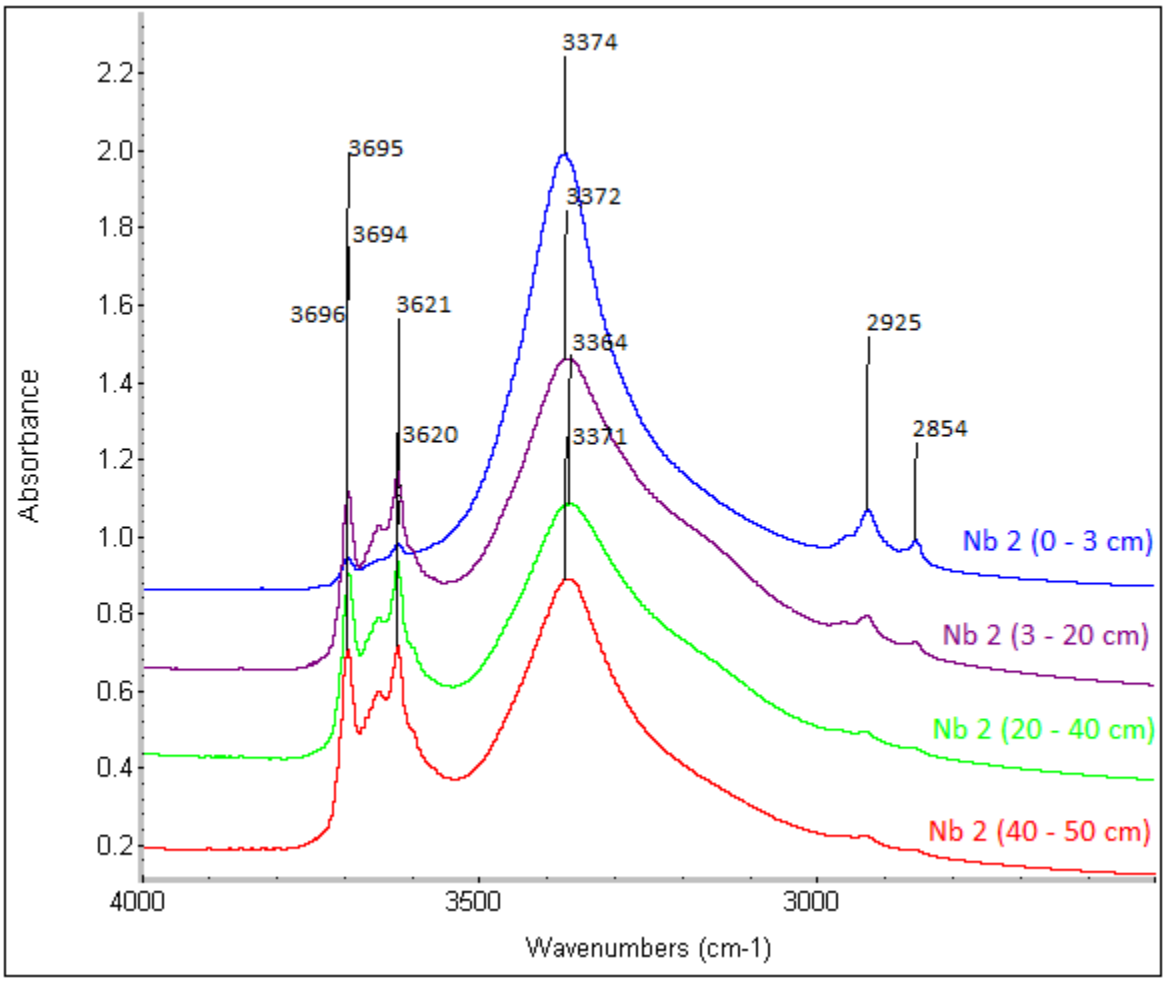

Figure 1.19: FTIR spectra for the contaminated soil Nb2, with special focus on the region of 4000–2500 cm^{-1} in order to emphasize the absorption bands.

3.8.4. Equilibrium modeling

The saturation indices were calculated for the contaminated soils using the Pitzer virial-coefficient approach for activity-coefficient determination (Figure 1.20). Epsomite was detected in the crust on the surface. The SI in the top-tailings layer for epsomite is below zero, despite being close to zero. Saturation of the solution, with respect to epsomite, may be reached upon drying and this will lead to epsomite ($MgSO_4 \cdot 7H_2O$) precipitation. The SI for both hematite and goethite is positive, which means these two minerals will precipitate on other mineral surfaces. Ferrihydrite's SI fluctuates around zero and is positive for the 2–30 cm and 40–50 cm layers, meaning it too will precipitate The results indicate that illite (SI = −9.28 to −11.77), montmorillonite (SI = −4.91 to −5.98) and kaolinite (SI = −4.35 to −5.91) are under-saturated with respect to the soil solution, which means these minerals are dissolving under the current conditions. Kaolinite and Illite were however detected in the horizons from 3–50 cm. The presence of these minerals possibly indicates that their dissolution kinetics could be relatively slow, hence preventing these minerals from disappearing from the soil. The conditions might also be changed during rainfall events when concentrations are diluted. No clear differences can be distinguished

between the different horizons, except for the presence of the epsomite in the 40–50 cm horizon, which also had the highest SI value. There is a small difference in SI value between the 3–20 cm and 20–40 cm depths of soil profile. The SI for gibbsite [$Al(OH)_3$] in the soil solution ranged from −4.83 to −3.95.

The Nb3 soil is considered to be less contaminated as it is located further away from the contamination point source. The saturation indices for the soil are presented in Figure 1.21. The SI values of montmorillonite (SI = −1.51 and −1.72) and illite (SI = −1.3 and −2.06) in Nb3 are still negative for the 1–15 cm and 15–30 cm horizons although not as negative as in Nb2 for the same horizons. For kaolinite, however, a positive SI was calculated, and these values for SI were 0.58 and 0.41 for the 1–15 cm and 15–30cm horizons respectively. As in Nb2, gibbsite is under-saturated with respect to the soil solution, while PHREEQC predicts that hematite and goethite would precipitate from soil solution. In Nb3, the ferrihydrate SI is positive for both horizons. The chemical modeling of both Nb2 and Nb3 illustrate that silicate clays are largely unstable in the current conditions. This is verified by the XRD data which shows low intensity or very broad peaks for the clay minerals.

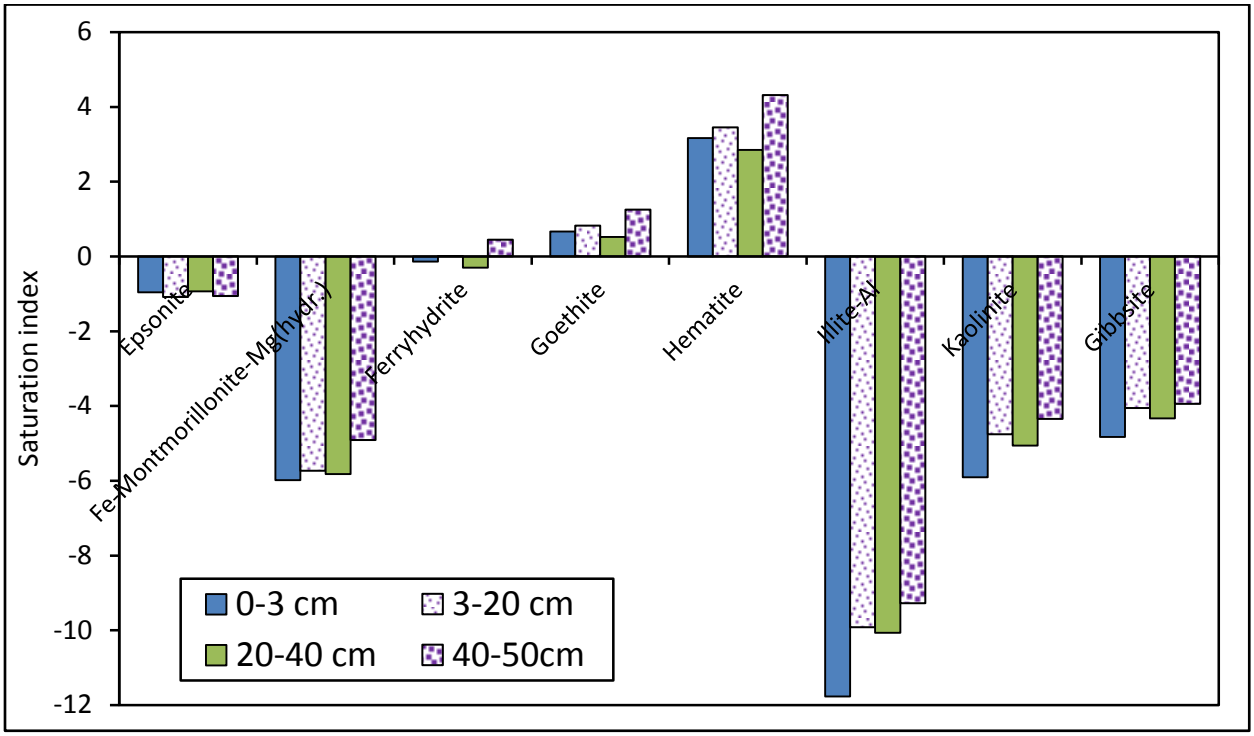

Figure 1.20: Saturation indices calculated in PHREEQC for selected minerals in Nb2 at different depths.

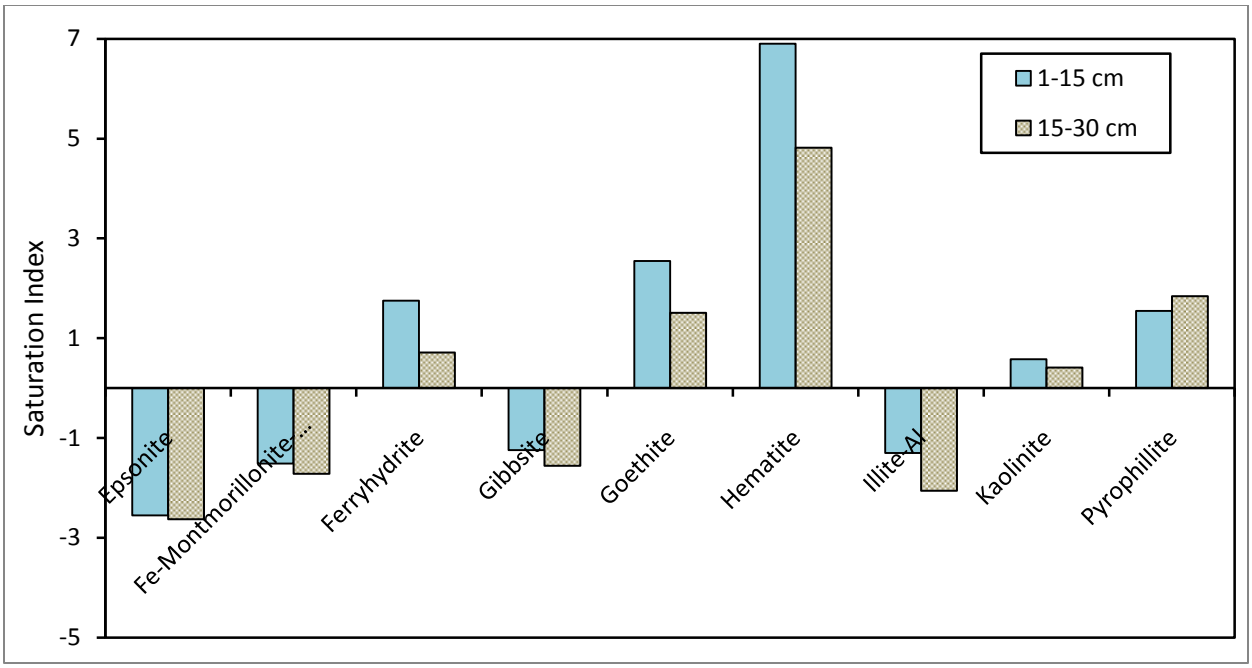

Figure 1.21: Saturation indices calculated in PHREEQC for selected minerals in Nb3 at different depths

Table 1.10 provides the total metal concentration data obtained for the whole soil samples which is compared to the data contained in a study by Hansen (2009), for which the upper percentile (75th percentile) of metal concentration values are given. Hansen (2009) investigated the anthropogenic influence on the soils of the Okiep Copper District. The total elemental analysis was conducted using a portable XRF, thus some metals measured by Hansen (2009) were below the detection limit of the instrument. Copper shows an extremely high concentration, for the Nb2 soil (370 ppm) and the A horizon of Nb4, with a concentration of 420 ppm. The value measured by Hansen (2009) for the upper percentile was 49 ppm. Table 1.10 indicates that Zn concentrations are well below those detected by Hansen (2009).

Sulfur was not determined in the study of Hansen (2009), but the sulfur contents of the pristine soil in this study were 4830, 3510 and 2840 ppm for the A, B1 and B2 horizons, respectively. Given that the parent material (granite-gneiss) does not contain sulfur, its presence in the soil indicates an external source and substantiates suspicions that the smelter furnace caused contamination of the surrounding environment. The fact that concentration decreases with depth supports an aerosol pollution source and this certainly challenges the overall pristine nature of the soil.

Table 1.10: Metals detected by Niton XRF gun compared with XRF data from Hansen (2009).

Metal	Nb2 (3-20 cm)	Nb3 (1-15 cm)	Nb4 A horizon	Hansen (2009) (75th percentile)
		ppm		
As	<LOD	<LOD	<LOD	5
Co	<LOD	<LOD	<LOD	14
Cr	<LOD	<LOD	<LOD	104
Cu	370	60	420	49
Nb	<LOD	<LOD	<LOD	24
Ni	140	<LOD	<LOD	26
Pb	40	60	90	34
Rb	110	110	130	202
Sb	<LOD	<LOD	<LOD	13
Sn	<LOD	<LOD	<LOD	1
Sr	80	90	100	193
Th	30	60	30	80
U	<LOD	<LOD	<LOD	2
V	<LOD	<LOD	<LOD	99
W	<LOD	<LOD	<LOD	7
Y	40	30	20	92
Zn	170	40	100	91
Zr	200	260	170	1520

LOD = limit of detection

4. Conclusions

The characterization of the AMD showed that the evaporative conditions of the area concentrated the solution to exceptionally high values of metals and sulfates. The highest concentration of metal was Fe (42.9 g/l) which was present in two oxidation states, namely ferrous (Fe^{2+}) and ferric (Fe^{3+}) iron. This phenomenon is possibly attributed to speciation with the sulfate ions in solution. The low pH (1.5) and high concentration of heavy metals renders this solution a hazard to the environment. Melanterite is one of the minerals that were sampled in the tailings and this ferrous sulfate crystal plays an import role in the immediate release of Fe and sulfate into the environment.

Pristine soils were classified as arenosols (WRB) and had a sandy texture (2–5.2 % clay). The pristine soils had a low pH (3.78–4.21, in KCl) given that it is from an arid region. The saturated paste extracts also indicated the presence of sulfate (0.152–0.239 mmol/l) which was not expected from soils derived from granite-gneiss and may suggest contamination by the smelter furnace in the nearby town of Nababeep. The clay minerals detected by XRD analysis were illite, kaolinite, montmorillonite and quarts.

The contaminated soils varied with an order of magnitude in their concentrations of metals due to their position and subsequently their exposure to AMD. The soil located closer to the leaching pond (Nb2) had for example 546.67 mmol/l Al in the 3–20 cm layer while Nb3 had a concentration 19.8 mmol/l Al in the 1–15 cm layer. Clay minerals in the contaminated soil seemed to have been altered by broadening of the XRD peaks which indicates dissolution of clay minerals into more amorphous phases. A new phase, namely jarosite, was also detected in the contaminated soil.

Chapter 2. Effect of acid mine drainage on mineral weathering

1. Introduction

In the previous chapter, the soils and AMD were characterized at a site contaminated by an abandoned Cu processing pond, where an acidic metal leachate spread into the nearby soils surrounding the source. The contaminated soils were compared to pristine soils. The most notable impact of the AMD on the surrounding soils was the introduction of a range of new chemical species to the soil solution, which caused a significant shift in the mineral equilibrium conditions. When the equilibrium conditions shift in such a radical way, many of the minerals that were stable under natural soil conditions begin dissolving, as was shown by the saturation indices that were calculated. Saturation indices, however, only indicate what is thermodynamically possible, but the kinetics of these reactions is disregarded. In this extended period of time the changes in soil can be monitored and investigated to reflect the influence of long term AMD exposure to the soils.

The main goal of the experiments described in this chapter is to simulate the weathering conditions encountered at the Nababeep mining site, in terms of the soil type, acid mine drainage (AMD) composition and climatic conditions. The effect of AMD in contact with pristine soils was investigated. The climate, as described previously, is arid with high evaporation, low precipitation and hot summers. The acidic solution is expected to dissolve the soil phases through mechanisms such as acid attack. Firstly the factors involved in weathering reactions will be reviewed.

1.1. Acid induced weathering

Proton-promoted weathering has been described by Furrer & Stumm (1986) and is based on the theory that protons that bind to surface oxide groups weaken the critical bonds and this leads to release of metal from the structure. Figure 2.1 is the representation of the different protonation steps that illustrates the release of a trivalent metal (M^{3+}) from a crystalline structure. The process is initiated by protonation of the mineral surface and reaches equilibrium with the solution quickly. The release of the metal from the structure (step 4) is the rate limiting step and the rate is then related to activity of the protonated species (species D in Figure 2.1).

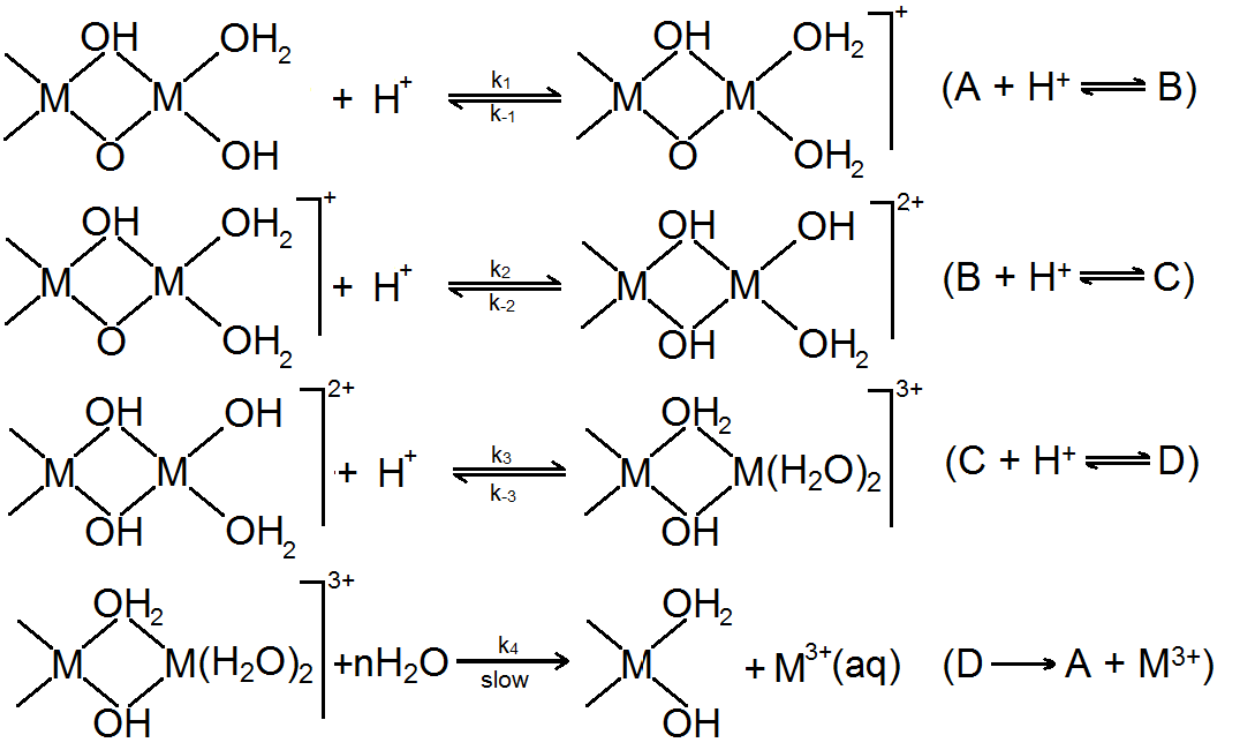

Figure 2.1: Schematic representation of the protonation steps that occur during the dissolution of a M_2O_3 surface site, promoted by protonation (adapted from Furrer & Stumm (1986)).

The number of protons bound to a surface is defined as C_H^s (moles/m^2) and the activity and, in effect the rate of dissolution of species D, is then derived to be related to $(C_H^s)^3$. Furthermore, the rate of proton-promoted dissolution is defined as R_L (moles.m^{-2}.h^{-1}):

$$R_L \propto (C_H^s)^3$$

This is, however, true for a mechanism, as depicted in Figure 2.1, where three protons are required for dissolution. The relation however is applicable to any proton-promoted dissolution where *n* protons are required for dissolution and the equation becomes:

$$R_L \propto (C_H^s)^n$$

The dissolution of a mineral is therefore related to the interaction of the surface of a mineral with the solution it is in contact with. Studies by Huertas et al. (1998) and Ganor et al. (2003) investigated the interaction between kaolinite and an acidic solution with specific reference to the surfaces. Ganor et al., (2003) established that the point of zero net proton charge (pH_{PZNPC}) occurs at a pH of approximately 5. Huertas et al. (1998) also found the pH_{PZNPC} to be 5.5 for kaolinite. When the pH is below this pH_{PZNPC}, a positive charge is generated by surface adsorption on Al sites of the octahedral sheets. In a study by Huertas et al. (1999), where the dissolution kinetics of kaolinite was investigated, it was found that kaolinite dissolves congruently at a pH below 4 and at 25 °C. Cama et al. (2002) expressed the rate of kaolinite dissolution in terms of the release of Si and Al in relation to pH and temperature. Two reaction paths were established of which one occurs below a pH of 0.5 and second reaction path that occurs at

pH ≥ 2.5. Between a pH of 0.5 and 2.5, both reaction paths influence the dissolution rate of kaolinite. Studies on proton promoted dissolution of montmorillonite have also been conducted, such as the study by Zysset & Schindler (1996) that investigated dissolution at pH between 1 and 5 and different concentrations of KCl. The Si and Al ratio in solution suggested congruent dissolution, but at lower KCl concentrations there was a deviation from congruent dissolution which is attributed to adsorption of Al on exchange sites. It was also concluded that the dissolution is predominantly observed on crystal edge surfaces.

Steudel and co-workers investigated acid activation on non-swelling clay minerals (Steudel, Batenburg, Fischer, Weidler, & Emmerich, 2009a) and swelling clay minerals (Steudel et al., 2009b) under different H_2SO_4 concentrations (1 M, 5 M and 10 M) at 80°C for several hours. It is reported that the chemical character, such as the chemical composition and initial particle size, plays an important role in the alteration of the mineral. For non-swelling clay minerals, edge attack resulted in dissolution of the octahedral sheets and the formation of a silica phase. It was determined that di-octahedral layers possessed greater resistance to acid than trioctahedral sheets and the order of dissolution of structural cations were Mg>Fe>Al. In the study of Steudel et al. (2009b) on swelling clays, the products after treatment with H_2SO_4 had lower layer charge, higher specific surface area and lower CEC. Another study by Jozefaciuk & Bowanko (2002) was conducted on bentonite, biotite, illite, kaolinite, vermiculite and zeolite and it was found that kaolinite and illite were the most resistant to acid attack by analysis with XRD. Aglietti et al. (1988) investigated acid treated kaolinite, and the evolution of an infrared (IR) band and XRD patterns were analyzed as a function of original Al content. This experiment was conducted at 170°C with a 1N solution of sulfuric acid. At 60 % Al extraction, a complete structural collapse was observed. Similarly, Hradil et al. (2002) used Al release in order to characterize kinetics of acidification of clay. The study compared a 0.5M and 5M sulfuric acid treatment with a 1M hydrochloric acid treatment at 25°C up to 240 hours (10 days) on kaolinites, illites and halloysite. The rate of dissolution for kaolinite was found to be three times higher in the 0.5 M H_2SO_4 solution than in the 1 M HCl with equivalent hydrogen concentration. Increasing the concentration of 2:1 clays such as illite decreases the rate of Al release, as these have a greater resistance to acid attack.

Swoboda-colberg & Drever (1993) compared the dissolution rates of minerals in a field-scale experiment to those in the laboratory. It was found that laboratory experiments overestimated dissolution rates by a factor of 200–400 times with exposure to HCl at pH of 2–3.5. The laboratory experiments, however, were carried out in a fluidized bed reactor, which provided greater exposure of the acid solution to mineral surfaces, and hence more efficient acid attack and dissolution of the minerals.

1.2. Influence of AMD on clay minerals

Komadel & Madejova (2006) report that acid attack naturally occurs when soils are exposed to AMD. This was in reference to studies by Galan et. al (1999) and Dubikova et al. (2002).

The study by Galan et al. (1999) was conducted on soils surrounding the Rio Tinto River in Spain which is infamous for high metal content and low pH generated by mining activities. In this study, samples from two different locations in the valley were tested. The first was a chlorite-rich slate and the second an area rich in smectite clays. The chlorite-slates were ground and sieved to obtain a mineral size fraction

of < 63 µm. For the soil samples, a clay extraction was conducted by to obtain a <2 µm size fraction. Subsamples were treated with natural acid sulfate water collected from the Rio Tinto River with pH of 2.2. The treatment times for clay minerals extended for 180 min for clay samples and 1 day for the slate sample at room temperature. For the chlorite-rich slate, the chlorites showed early transformation to vermiculite by alteration of octahedral sheets. There was no change in bulk mineralogy of the slate samples with the predominant mineral being mica. For the clay samples, there was however a significant change in mineralogy. Illite and kaolinite seemed to resist the treatment by AMD. The amount of smectite prior treatment was 70% in < 2 µm fraction, but no smectite was detected after treatment. Calcite was also present in the mineralogy of the soil and this rapidly dissolved to buffer the pH of the solution and increased the pH from 2.2 to 6.6. The dissolution of smectite and change in pH also resulted in precipitation of Fe and Al oxy-hydroxides as well as silica gels. These new amorphous silica phases that formed were enriched with Al and Mg, as a decrease in these metals was observed in the extracted solution.

In the second study by Dubikova et al. (2002), soil columns were treated with AMD to investigate the acid-soil interaction. The soils are cambisols originating from a mining area in Slovakia. The soils were treated with natural AMD (pH 2.1 and 2.3), sulfuric acid solutions with the same H_2SO_4 concentration as AMD, and distilled water. The experiments were conducted over a period of 30 weeks (210 days) at room temperature. It was found that the leachates of the 0.15 M H_2SO_4 treated column rose to 4.3 initially and stabilized at 3.4 which is a substantial change, since the initial solution pH was 0.8. A similar trend was observed for the AMD treated column. The leachate from the AMD column showed a 1 month retention of Mg while the Al was not leached initially, despite the leachate having a pH of 3.4 and their being a high Al concentration. A large percentage of Al and Fe were retained in the columns over the period. Almost 100% Fe and 25% Al was retained in column treated with AMD. The natural soil contained vermiculite, chlorite, illite, kaolinite and pyrophyllite. The 0.15 M H_2SO_4 treatment showed more severe dissolution of vermiculite than the treatment with AMD. The illite, kaolinite and pyrophyllite showed no or little alteration by laboratory treatment. Alteration of chlorite was also observed. Jarosite formed in the column treated with H_2SO_4 and AMD. It is also reported that a silica gel formed in the columns. Transmission electron microscopy (TEM) was conducted on samples from the treated columns and mohair particles were observed which had high Al and Si content.

1.3. Microbial enhanced weathering

The five soil forming factors are time, the presence and role of organisms, topography, climate and parent material. The interactions between these factors and the mechanisms by which they operate are a complex network of natural processes.

Organic acids are the products of metabolic activities of soil microbes in the soil and play an important role in the release of nutrients from parent materials (Uroz et al., 2009). Calvaruso et al. (2009) supported this idea with research showing a rapid increase in mineral weathering in the rhizosphere compared to that in the bulk soil. Vandevivere et al. (1994) investigated the dissolution of silicate minerals by bacteria and found that gluconate promoted the dissolution of albite, quarts and kaolinite. The study states that the mechanisms of microorganisms and how it increases the mineral dissolution rates are still unclear. In a review on mineral weathering by bacteria, Uroz et al. (2009) again stated (15

years later) that molecular weathering mechanisms of bacteria remain “poorly understood”. The previous mentioned studies investigated primary and silicate minerals, but Glasauer et al. (2003) and authors within investigated the dissolution of Fe(III)-hydroxides by the process of reduction which is induced by dissimilatory iron-reducing bacteria (DIRB). This facultative anaerobic organism can reduce iron from goethite, hematite and magnetite and hydrous ferric oxide bound on clay minerals.

Drever & Stillings (1997) report three mechanisms by which organic acids and their anions affect mineral weathering. These are: 1) the change in equilibrium in the soil solution brought about by decreasing the pH of the solution, or by forming complexes near the surfaces of minerals; 2) causing a change in saturation conditions in the soil solution, with regards to the mineral it is in contact with; and 3) by forming organo-metal complexes, such as the complexation of Al^{3+} in solution for example. Drever & Stillings (1997) state that feldspar dissolution rates are independent of pH when the pH of the solution is in the range of 4–5 to 8, but increase for pH values below 4–5 in the organic acid solutions. Welch & Ullman (1993) investigated the effect of organic acids on plagioclase dissolution and found that dissolution rates are the highest at a pH of around 3, and decreases as pH increases to more neutral values. This study found effective dissolution of plagioclase was induced by oxalate, citrate, succinate, pyruvate and 2-ketoglutarate, and that the rates for plagioclase dissolution by these organic acids were 10 times greater than for plagioclase dissolution by inorganic acids.

It can therefore be concluded that the rate of natural mineral weathering is significantly altered by presence of microbial life although mechanisms are not completely understood. One of the main mechanisms is a change in equilibrium brought by a change in pH and in the context of AMD that would also occur when AMD moves into pristine soil. Other mechanisms such as chelation of Al^{3+} depends on microbial activity and may not be a significant influence in the AMD affected system. In the discussion on AMD in the previous chapter, some attention has be given to acidophilic organisms living in AMD and therefore the presence of microbes cannot not be ruled out and little is known about the interaction with the soil environment.

1.4. Fourier Transform Infrared (FTIR) Spectroscopy of Soil Minerals

One potential problem with mineral weathering studies is the difficulty in identifying poorly crystalline phases. Fourier transform infrared (FTIR) spectroscopy is commonly used to identify minerals showing short-range order. A brief review of the technique is provided below.

The use of FTIR spectroscopy is commonly used in organic applications for the identification of functional groups of carbon or carbon-nitrogen compounds and an elaborate set of reference peaks exist. In mineral identification, XRD analysis is often used as mineral phases are very crystalline. In order to account for more amorphous phases, FTIR is useful. The main minerals identified in the soils sampled at Nababeep as reported in the previous chapter include illite, kaolinite, jarosite and montmorillonite and it is important to know which peaks are to be assigned to each of these minerals. Table 2.1 is the assignments for the different peaks of kaolinites given by Steudel et al. (2009a) and Vaculíková et al. (2011), and authors therein. The values agree for both different kaolinites and different authors.

Table 2.1: Infrared maxima for kaolinite as measured by FTIR spectroscopy in cm^{-1}.

Assignment	Kga-1b[a]	Sedlec[a]	Unanov[a]	13_Pol[b]	14_Kaolex[b]	15_Rogers[b]
OH stretching of inner-surface hydroxyl groups	3694	3696	3696			
OH stretching of inner-surface hydroxyl groups	3669	3669	3669			
OH stretching of inner-surface hydroxyl groups	3653	3653	3652			
OH stretching of inner hydroxyl groups	3618	3620	3620			
Si-O stretching (longitudinal mode)	1113	1113	1114	1110	1112	1110
Si-O stretching (perpendicular mode)	1098					
in-plane Si-O stretching	1033	1032	1032	1030	1033	1035
in-plane Si-O stretching	1009	1007	1007			
OH deformation of inner-surface hydroxyl groups	937	937	935	939	935	939
OH deformation of inner hydroxyl groups	913	913	912	917	916	917
Si-O	791	793	794	792	792	792
Si-O, perpendicular	752	755	754	754	754	754
Si-O, perpendicular	694	699	697			
Inner surface OH vibration				644	644	646
Si-O	645	641	644			
Al-O-Si deformation	540	537	537	539	541	539
Si-O-Si deformation	468	469	469	472	470	470
Si-O deformation	433	430	429	431	428	430

a. Vaculíková et al., 2011
b. Steudel et al., 2009a

Table 2.2 is the FTIR maxima for montmorillonite (Tyagi et al., 2006) and illite (Steudel et al., 2009a). Tyagi et al. (2006) also investigated acid attack on montmorillonite and argue that a broadness of the 3623 cm^{-1} band shows substitution of octahedral Al^{3+} by Fe^{2+} or Mg^{2+}. This is confirmed by bending vibrations forming peaks at 915 cm^{-1} (AlAlOH), 875 cm^{-1} (AlFeOH) and 836 cm^{-1} (AlMgOH).

Figure 2.2 shows the IR spectra for kaolinite and illite in an acid attack study (Used with permission from Steudel et al. (2009a)). The study of Steudel et al. (2009a) investigated acid attack on non-swelling clays and reports that the biggest alteration was observed for the bands between 400 and 1200 cm^{-1}. The intensity of the OH-deformation bands (912 and 877 cm^{-1}) and adsorption bands at 825 cm^{-1} and 750 cm^{-1} decreased after acid attack. Steudel et al. (2009a) showed that for illite the intensity of Si–O–Al bands at 538 cm^{-1} decreased after acid attack.

Table 2.2: Infrared maxima for Montmorillonite and Illite as measured by FTIR spectroscopy in cm^{-1}.

Assignments	Montmorillonite[a]	9_Illite[b]
OH stretching	3697	
OH stretching	3623	
OH stretching, hydration	3440	
OH bending, hydration	1639	
SiO stretching, out-of-plane	1113	1101
SiO stretching, in-plane	1035	1030
AlAlOH bending	915	912
AlFeOH bending	875	877
AlMgOH bending	836	823
Platy form of tridymite	793	
Si–O–Al vibration		750
Quartz	692	
Inner surface OH vibration		622
Si–O–Al (out-of-plane) bending (Al in tetrahedral sheet)		538
Si–O bending	529	431
Si–O (in-plane) bending associated with OH		472

a. Tyagi et al. (2006)
b. Steudel et al. (2009a)

Jarosite has the formula $MFe_3(SO_4)_2(OH)_6$ where M is a monovalent cation such as NH_4^+, Na^+, Ag^+ or Pb^+ which gives it distinctive names such as ammoniojarosite, natrojarosite, argentojarosite and plumbojarosite, respectively. When the monovalent cation is K^+ it is referred to as jarosite and this was the type identified in chapter 1 by XRD analysis. The FTIR spectra for jarosite are given in Table 2.3.

As mentioned before the breakdown of crystalline materials often leads to the formation of more amorphous materials. Allophane and imogolite are examples of the common poorly crystalline aluminosilicates often found in soils derived from volcanic material, but they are also found in wide range of other soils and parent materials (Harsh, 1999). The identification of these minerals using XRD analysis is difficult as they only give diffuse scattering (Farmer et al., 1979). Imogolite has a structural formula of $(OH)_3Al_2O_3SiOH$ and Al occurs in octahedral coordination. It has been established that the infrared band at 348 cm^{-1} is characteristic of imogolite (Farmer et al., 1979; Harsh, 1999). Other bands for imogolite exist at 925–935 cm^{-1} and 990–1010 cm^{-1} (Wada, 1978; and authors within). Harsh (1999) reports that the IR spectrum for allophane is similar to that of imogolite. This issue is also addressed by Wada (1978) and the author cites many studies that are for and against this argument. It is mentioned that the maxima for allophane with SiO_2/Al_2O_3 ratios of 2 to 1.5 would have broad maxima at 1010 and 945 cm^{-1} while the maxima for imogolite lie at 990, 995 and 925 cm^{-1}. In the same source it is stated that maxima often shift with maturity of soils and content of Al_2O_3.

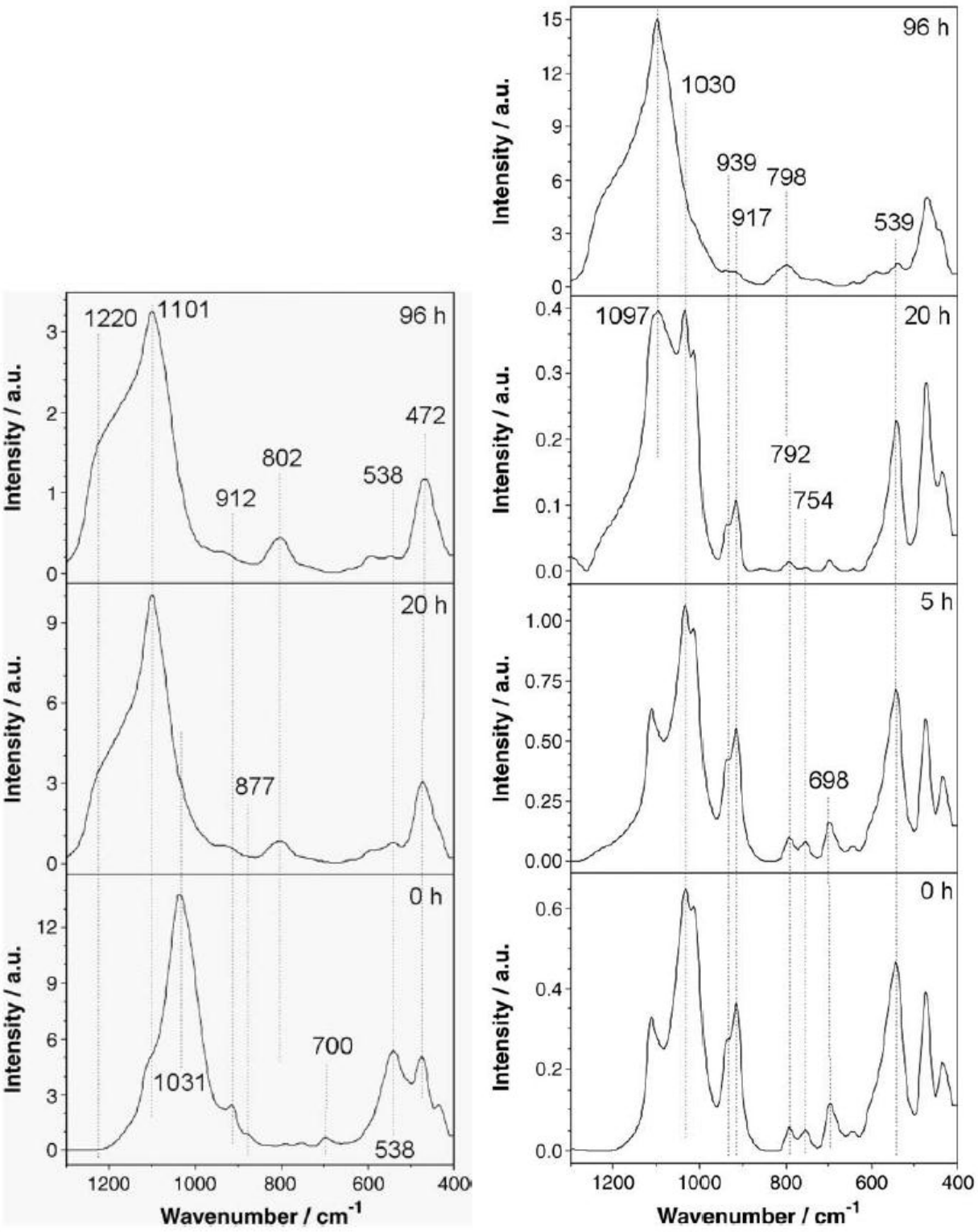

Figure 2.2: (Left) FTIR spectra for illite treated with 5 M H_2SO_4 at 80°C for 0, 20 and 96 hours. (Right) FTIR spectra for kaolinite treated with 5 M H_2SO_4 at 80°C for 0, 5, 20 and 96 hours (figures used with permission from Steudel et al. (2009a)).

Table 2.3: Jarosite spectra assignments for FTIR (Sasaki et al., 1998).

Assignment	Spectra maxima (cm^{-1})[a]
ν_{OH}	3390sp
ν_{OH}	3365
$\nu_3(SO_4^{2-})$	1190
$\nu_3(SO_4^{2-})$	1088s
δ(OH)	1028s
$\nu_1(SO_4^{2-})$	1010
$\nu_4(SO_4^{2-})$	660
$\nu_4(SO_4^{2-})$	630sp
ϒ(OH)	580
O-Fe	520
O-Fe	478
$\nu_2(SO_4^{2-})$	448

a. sp = sharp; s = strong

Poorly crystalline Fe-oxides are common soil constituents and precipitate from AMD. Brady et al. (1986) investigated Fe-oxide formation from AMD and found IR bands related to these poorly crystalline materials include OH-stretching at 3400 cm^{-1}, H–O–H deformation at 1620 cm^{-1} and octahedral vibrations [FeO_6] between 430 and 470 cm^{-1}. Webster et al. (1998) state that peaks at 797 and 890 cm^{-1} are characteristic of goethite. Parfitt & Henmi (1982) investigated allophane and spectra bands of clay fractions of andic soils in New Zeeland. In this study the bands at 3150, 3440 and 3520 cm^{-1} are assigned to goethite and gibbsite present with the allophane.

2. Materials and Methods

2.1. Weathering experiments

The soil on which the weathering experiments were conducted is the B2 horizon of the pristine soil (Nb4). The reason for selecting this particular horizon is that it is the horizon with the highest fine earth fraction (2.1–5.1 %). The surface area of finer particles is larger and weathering rates would occur at a higher rate. The soil was prepared by sieving with a 2 mm sieve, and the sieved (< 2 mm) fraction was used.

Sampling of the AMD was conducted at the end of the dry season, when the AMD solution was at its most concentrated. The AMD typically diffuses into the soils surrounding the abandoned copper treatment site during rainfall events, in which case the AMD is diluted. In order to achieve a more realistic AMD concentration, the unfiltered, but translucent AMD was diluted ten times with distilled water. This shifted the equilibrium of the highly saturated solution and therefore the new solution was left for 48 hours to allow the precipitation of any solid phases. The new solution was then filtered with Whatman® 40 filter paper to remove precipitates. Three replicates of the new solution were analyzed by inductively coupled plasma-atomic emission spectrometry (ICP-AES).

Three weathering systems were run parallel in this investigation. The first were replicate trials of treatment of a pristine soil with dilute AMD, while the third was a control. The control was a treatment of a pristine soil with a solution having the same EC as was measured for the pristine soil. This solution was a 0.438 mM $CaCl_2 \cdot 2H_2O$ solution in deionized water (18 MΩ·cm, Millipore, Billerrica, MA).

The weathering experiments were conducted over a period of nearly 8 months (12 December 2013 to 1 July 2014), a duration of 201 days. The experiments were conducted at a constant temperature of 30°C by immersing the sample containers in a water bath. The containers were high density plastic containers. The containers were all filled with 750 g of soil. At each new exposure to AMD, 115 ml of either control solution or AMD (AMD-1 and AMD-2) was added. The amount of liquid added was based on preliminary tests conducted on 50 g of soil in order to determine the amount of water needed to achieve field capacity. Briefly, the soil was saturated in conical filter paper positioned in funnel and excess water was then allowed to drain for 20 minutes. The wet soil was weighed and the amount of water calculated.

During the extent of the experiment, the soil was treated with the diluted AMD and allowed to evaporate until it was completely dry. The drying period varied between two weeks and a month. This reflects the high evaporation rate at the site of investigation. The samples were treated 9 times during this period with new AMD (Table 2.4).

Table 2.4: Timeline of long weathering experiment

Wetting Cycle	Date	Month	Year
1	12	Dec	2013
2	13	Jan	2014
3	29	Jan	2014
4	17	Feb	2014
5	10	Mar	2014
6	31	Mar	2014
7	23	Apr	2014
8	15	May	2014
9	30	May	2014
Sampling on 1 July			

2.2. Scanning Electron Microscopy (SEM)

Scanning electron microscopy (SEM) was used to determine morphological differences in the different treatment methods. The samples used were the long weathered soil control, one of the long weathered samples treated with AMD (LW-B) and the pristine soil that was used for long weathering experiments but not treated during the time. Since the largest effect of weathering is expected on the smaller particles with high surface area, the samples were sieved and only the <106 µm size fraction was used. The material was pressed in pellets by making dry paste of soil and a few drops of Mowiol (poly-(vinyl alcohol)). The paste was then pressed into a pellet by a hydraulic press, using less than 5 tons of pressure on disc. The pellets were dried for 24 hours at 60˚C.

The pellets were analyzed by SEM using a Leo® 1430VP Scanning Electron Microscope at the University of Stellenbosch. The pellets were mounted on a glass slide with double sided carbon tape and were covered with thin layer of gold or carbon for surface electrical conductivity. The beam conditions used during surface conditions were 7 kV and approximately 1.5 nA with spot size of 150. Images were then taken of surface structure. Clay powders were analyzed directly without any pre-treatment except for coating with gold.

2.3. Mineralogical and Chemical characterization

The mineralogy of clay fractions from the treated samples were determined by infrared (IR) spectroscopy and X-ray diffraction (XRD) analysis as described in Chapter 1. Clay separation techniques were conducted as described in previous chapter.

Saturated paste extracts of treated samples were prepared and analyzed as described in chapter 1.

3. Results and Discussion

3.1. Acid mine Drainage

In Table 2.5, the different parameters and concentrations of species are provided that were measured for the diluted AMD used at each treatment in the weathering experiments. The ratio of the concentrations between diluted and the concentrated AMD are related and will be discussed in next chapter.

Table 2.5: Concentration of species, Eh, EC and pH of the diluted AMD used for treatment in weathering experiments.

Element/ Parameter	Concentration/ Value	Standard Deviation[a]
pH	2.415	0.007
EC (mS/cm)	18.69	0.13
Eh (mV)	656.5	0.71
Al (mg/l)	2756.33	50.64
B (mg/l)	1.54	1.33
Ba (mg/l)	0.088	0.023
Ca (mg/l)	21.86	1.69
Cd (mg/l)	0.148	0.026
Co (mg/l)	12.23	0.26
Cr (mg/l)	1.91	0.031
Cu (mg/l)	403.20	13.26
Fe (mg/l)	4445.67	151.58
K (mg/l)	0.99	0.12
Mg (mg/l)	2170.00	74.18
Mn (mg/l)	351.70	7.21
Na (mg/l)	1.89	1.24
Ni (mg/l)	32.43	1.37
P (mg/l)	6.18	0.27
Pb (mg/l)	0.41	0.35
SO_4^{2-} mg/l	31175.19	1975.86
Si (mg/l)	1.59	0.06
Sr (mg/l)	0.011	0.008
Zn (mg/l)	175.63	3.61

a. Determined from triplicate samples (n = 3)

3.2. Soil Chemistry

The saturated paste extract data is given in Table 2.5 for control and two AMD treated soils (AMD-1 and AMD-2). It should be noted that these were closed systems in that no solution was removed, but water was purely evaporated. This means that species that are lower in concentration than the control were taken up in insoluble phases. This phenomenon is observed for Ca, K, Na and Si. The loss of K from solution could be taken up in the jarosite phase. The loss of Si could be related to the precipitation of amorphous Si phases. The diluted AMD added during the experiments had more Fe in solution than Al. For the saturated paste extracts, higher Al concentrations were extracted (11.17 mmol/l and 6.26 mmol/l) for the AMD soils (AMD-1 and AMD-2) than the concentration of Fe (4.27 mmol/l and 2.39 mmol/l). The lower mobility of Fe is related to either precipitation of Fe-phases and/or release of Al from the dissolution of clay minerals. In the latter case, an increase in Si would however be observed except if the Si was readily scavenged into new phases. The control had a low pH (3.86) and may be related to exchangeable acidity released by the addition of $CaCl_2$.

Table 2.6: Saturated paste pH, pe and elemental concentrations for the three treatments.

Element/ Parameter	Control	AMD-1	AMD-2
pH	3.86	1.95	2.36
pe	10.02	11.03	11.11
Al (mmol/l)	0.0377	11.1706	6.2635
Ca (mmol/l)	0.9671	0.1268	0.1226
Cd (mmol/l)	nd	0.000239	0.000128
Co (mmol/l)	0.000893	0.026114	0.014980
Cr (mmol/l)	0.000029	0.004662	0.002702
Cu (mmol/l)	0.2469	0.7640	0.4272
Fe (mmol/l)	0.0034	4.2690	2.3870
K (mmol/l)	0.37	nd	nd
Mg (mmol/l)	0.6237	9.9650	6.1222
Mn (mmol/l)	0.0434	0.7330	0.4367
Na (mmol/l)	0.6520	0.0277	0.0188
Ni (mmol/l)	0.0011	0.0572	0.0319
Pb (mmol/l)	0.000509	0.000318	0.000168
SO_4^{2-} (mmol/l)	0.0575	33.4945	20.0405
Si (mmol/l)	0.47320	0.00652	0.00529
Sr (mmol/l)	0.00792	0.00001	0.00001
Zn (mmol/l)	0.04887	0.31845	0.18232

3.3. Mineralogy

The soil used for the weathering experiments was the soil sampled from the B2-horizon of profile Nb4. In order to compare differences that might have occurred in the soil during the experimental treatment of the control, the XRD patterns for the B2 horizon and the control are displayed in Figure 2.3. Similar clay minerals were detected in both cases which are illite (peaks at d = 9.923, 2.562 and 2.06 Å), kaolinite (peaks at d = 7.298 and 3.563 Å) and quarts (peaks at d = 4.246 and 3.336). It should, however, be noted that montmorillonite is detected for the control weathering experiment (d = 14.932 and 4.448 Å), but not in the XRD pattern of the Nb4 B2 horizon.

Montmorillonite was however detected in the A horizon of this profile and is therefore possibly also found in the B horizons. Another possibility is that montmorillonite had formed during the weathering reactions. According to Eberl et al. (1984), the three mechanisms by which clay minerals form are inheritance, neoformation, and transformation. In this case, inheritance is immediately ruled out as a possibility as smectites were below the detection limits before experiments and the parent material is granite-gneiss. Kloprogge et al. (1999) reviewed several articles on smectite formation under different temperature conditions such as low temperature (<100 °C and ambient pressure), hydrothermal conditions (100–1000 °C and high pressures) and extreme hydrothermal conditions (>1000 °C or >10 kbars). The review therefore focus on neoformation of different smectites and Kloprogge et al. (1999) mentions that smectites are one of the most difficult clay minerals to study. One of the articles cited in

the review is a study conducted on the formation of montmorillonite at 3 °C, 20 °C and 60 °C by Harder (1972). For these experiments, Al, Si and Mg were mixed in solution at different concentrations and it is reported that the first changes in the XRD patterns were detected 10 days after initiation and aging the samples for longer than a year gave no better results. Three conditions were found to favor the formation of montmorillonite of which the first is low silica concentration so that the solutions are undersaturated with respect to amorphous silica.

Secondly, the concentration of elements in solution that make up the smectite should be similar to the composition of the solid phase. Thirdly, pH plays an important role, and under basic conditions (pH 10) less Mg (10 ppm) is necessary in solution for the formation of smectite minerals. At neutral conditions it is still possible to form smectite minerals if the composition of the precipitate contains more than 6% MgO. Mg was the third highest ion extracted the in the saturated paste after Ca (38.8 mg/l) and Cu (15.7 mg/l) with a concentration of 15.1 mg/l. With the low pH of the paste, a much higher Mg content should be required for smectite formation.

In a study by Istok & Harward (1982), smectite formation through transformation was investigated. In this case the soil moisture was related to the conversion of serpentine and/or chlorite to smectite. Serpentine is similar to kaolinite with trioctahedral Mg layer (brucite) replacing the dioctahedral Al (gibbsite) layer in kaolinite. Smectite was only observed in soils in the landscape position that are poorly drained and it was concluded that these conditions favored the conversion from serpentine and/or chlorite to smectite. With the weathering experiments, the soil water conditions were disturbed as it was saturated frequently over the duration of the experiments. However, the formation of smectite in the absence of high Mg minerals at the low pH of the pristine soil is difficult to explain.

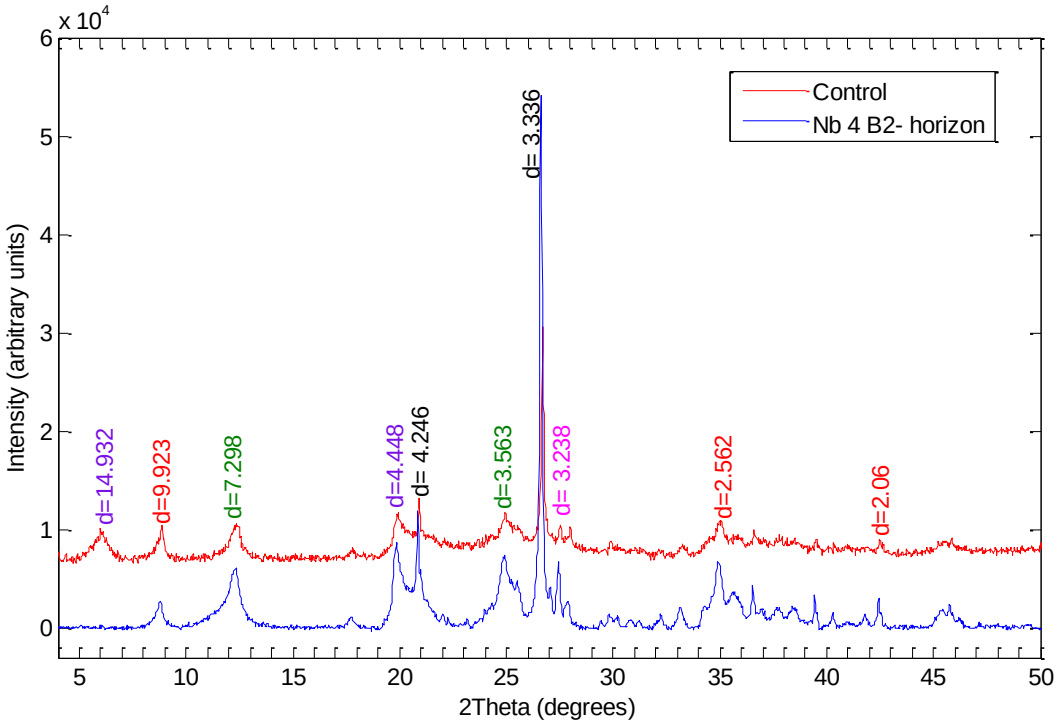

Figure 2.3: XRD pattern for weathering experiment control and B2 horizon of Nb4.

In Figure 2.4 the XRD pattern of the control is compared to those treated with AMD. The distinct peaks for the clays are shown in control (lowest pattern) for montmorillonite, illite and kaolinite at d-distances of 14.932 Å, 9.923 Å and 7.298 Å respectively. These peaks however, are not prominent in the XRD patterns for AMD-1 and AMD-2. This loss of intensity points to either a loss of crystallinity and/or to total dissolution of these minerals. Montmorillonite seems to be the most affected as the peak at 14.932 Å almost completely decrease below detection limit. The change of other peaks is difficult to observe because of the overlapping of peaks of other minerals. For illite the reduction of peak intensity can also be observed at 2.061 Å. The mineral not observable in the control is jarosite ($KFe_3(SO_4)_2(OH)_6$), with primary peak at 3.116 Å and other peaks observable at 5.944, 5.714, 5.095, 3.204, 1.982 and 1.828 Å. As previously stated, the intensity of the XRD peaks is a function of both crystallinity and concentration. The relative intensity could, however, be useful to compare. Working from zero as a baseline, the relative intensity to the control for the quarts peak at 3.336 Å for AMD-1 and AMD-2 was 50.3 % and 56.2 % respectively. This might be attributed to the dissolution of clay-sized quarts particles from the soil which would mean that more silica would be present in the extracted soil solution. The peak assigned to quarts at 3.336 Å for control extends beyond peak quarts of treatment B and C in Figure 2.4 and hides these respective peaks. The crystal structure of quarts could have possibly also been modified to more amorphous phases which would lead to lower intensity peaks.

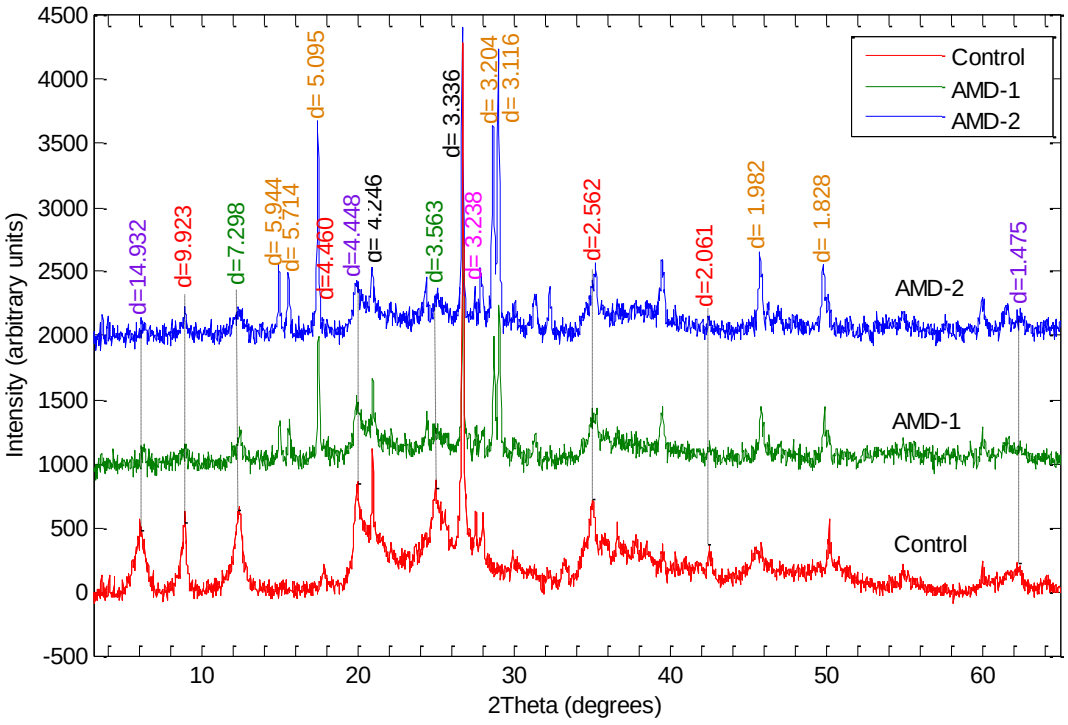

Figure 2.4: XRD pattern for clays of control and AMD weathered soil (AMD-1 and AMD-2).

Galan et al. (1999) treated smectite rich soils for 180 min with acid water that had a pH of 2.2. The XRD results of these treatments also showed the disappearance of the smectite peaks and chemical changes were observed in the solution within 30 minutes of treatment. The observed chemical changes included an increase in Al, Mg and Fe from octahedral positions and Si and Al from tetrahedral positions. By measuring the release of Fe from the smectite (nontrolite) structure it has been found that the

dissolution of octahedral and tetrahedral layers occurs simultaneously (Luca & Maclachlan, 1992). In the long term acid weathering experiment conducted by Dubikova et al. (2002) on a cambisol, the dissolution of vermiculite occurred, but kaolinite and illite seemed to be stable in both a pure 0.15 M H_2SO_4 and AMD treated samples. Dubikova et al. (2002) further reports that the amorphous Fe-oxyhydroxides that are precipitated in the pore spaces and on surfaces of clay minerals acts as a barrier preventing dissolution of these minerals. This is because the exchangeable positions on minerals are blocked by Fe-oxyhydroxides and therefore may have prevented clay minerals from completely dissolving.

The FTIR spectra for the clay fractions of the different weathering treatments are depicted in Figure 2.5. Two peaks at approximately 3596 and 3621 cm^{-1} are assigned to OH-stretching of inner hydroxyl groups of either kaolinite or montmorillonite (Tyagi et al., 2006; Vaculíková et al., 2011). A peak with high intensity is also observed at wavelength of 1031–1032 cm^{-1} which is assigned to Si–O stretching in kaolinite, montmorillonite or illite (Steudel et al., 2009a; Tyagi et al., 2006; Vaculíková et al., 2011). The peak in this position is also more prominent in the control weathering spectrum than in weathering experiment B and C where this peak collapses to about the same intensity of a second peak at 1008–1009 cm^{-1}. The peak in this position (1008–1009 cm^{-1}) could also be assigned to in plane Si–O stretching (Vaculíková et al., 2011) for kaolinite. A prominent peak exists at 912–914 cm^{-1} for all three cases which is assigned to OH-deformation of inner hydroxyl groups of kaolinite or AlAlOH bending of montmorillonite or illite (Steudel et al., 2009a; Tyagi et al., 2006; Vaculíková et al., 2011). A lower intensity peak exists at 798–799 cm^{-1} which is clearly visible for control and AMD-1 spectra but is somewhat smaller, but still visible in AMD-2. The peak in this wavenumber range could be assigned to goethite (Webster et al., 1998). Webster et al. (1998) also report that another characteristic peak for goethite occurs at 890 cm^{-1} which cannot be identified in Figure 2.5, possibly being hidden by the intensity of peak at 912–913 cm^{-1}. A peak which is easily identifiable at 694 cm^{-1} for control weathering experiment, but which appears less distinct for the other two cases due to change in spectra, can be assigned to Si–O perpendicular vibrations (Vaculíková et al., 2011). A peak at 535–536 cm^{-1}, which is observed in all three cases, is due to Al–O–Si deformation of kaolinite and illite (Steudel et al., 2009a; Vaculíková et al., 2011). Another peak characteristic of kaolinite is at a wavenumber range of 469-470 cm^{-1} assigned to Si–O–Si deformation (Vaculíková et al., 2011). A clear peak is observed at 431 cm^{-1} for the control weathering experiment and AMD-1, however for the second AMD weathering experiment (AMD-2), the peak has collapsed and is only observable as a shoulder. This peak could possibly be assigned to Si–O deformation of kaolinite (Vaculíková et al., 2011).

Some other major differences between the control experiment and the AMD treated trials (AMD-1 and AMD-2) are, firstly, the emergence of a distinct but broad peak at 3388–3393 cm^{-1} in the acid treated samples. These peaks are assigned to the hydroxyl vibration of jarosite (Sasaki et al., 1998). Secondly, a strong peak is observed at 1088–1089 cm^{-1} and at 631 cm^{-1}, assigned to SO_4^{2-} vibration of jarosite (Sasaki et al., 1998). In Table 2.3, the spectra for jarosite as given by Sasaki et al. (1998) are given. No peaks are observed between 700 and 1000 cm^{-1} for jarosite, but several peaks are assigned to the vibrational mode of SO_4^{2-} between 1000 and 1200 cm^{-1} and overlaps with the Si–O stretching of Si–O in clay minerals.

The broad peak at 3388–3393 cm^{-1} can also be assigned to structured water bonds. This band associated with water and deeper in structure has been observed for ferrihydrite (Russell, 1979). Madejova et al. (2002) also assigned a band at 3435 cm^{-1} for structural water on montmorillonite. It is however difficult to distinguish between the bands for different water-cation interactions. The cation-water interaction does influence the position and intensity of the peak. The broad peak area around 3696–3000 cm^{-1} can therefore also be related to water bonded to amorphous phases.

A very broad and low intensity peak exists for the control weathering experiment at a wavenumber value of 1652 cm^{-1}. Although this peak is broad it seems to shift slightly to wavelengths of 1636–1637 cm^{-1}. Peaks occurring at 1620 cm^{-1} may be assigned to H–O–H deformation of Fe-oxides as Brady et al. (1986) report. Tyagi et al. (2006) report of OH-bending that occurs at 1639 cm^{-1} for montmorillonite, which might be also related to the broad peak observed at 1652 cm^{-1}.

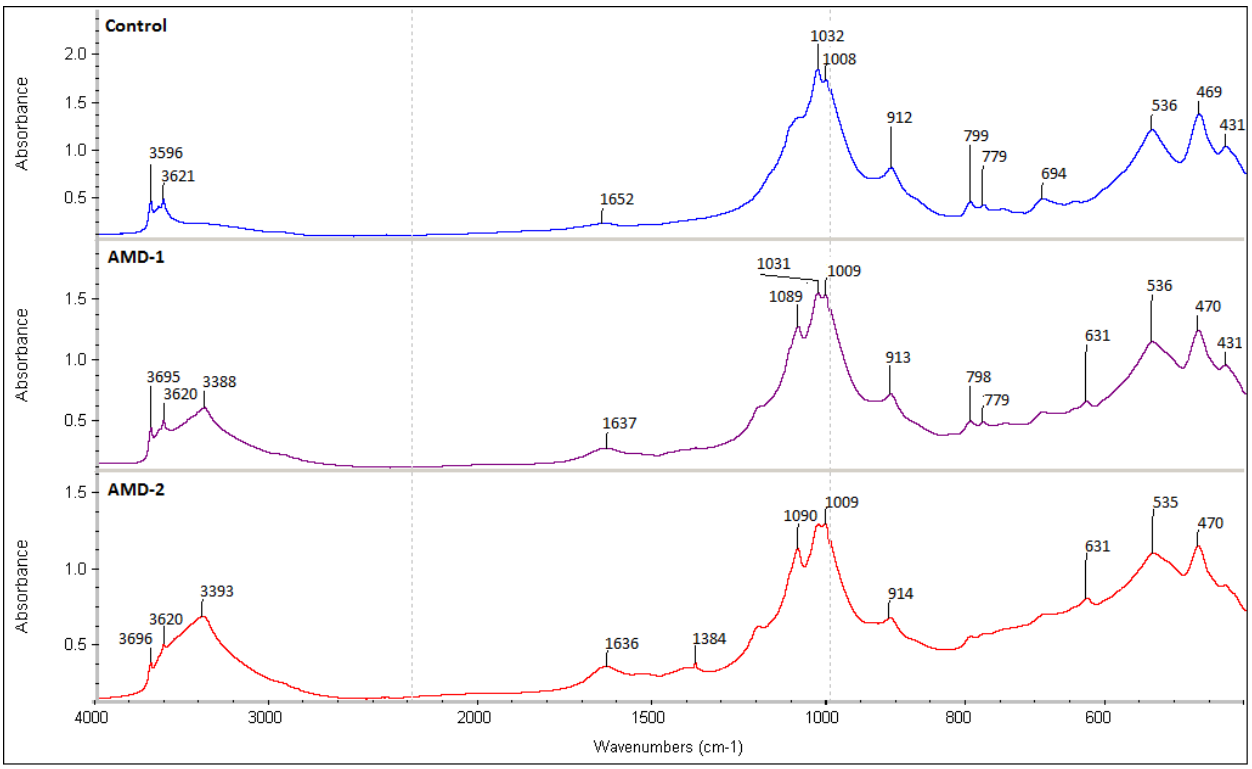

Figure 2.5: FTIR Spectra of three different weathering experiments with wavelengths 4000–400 cm^{-1}.

Interpreting the spectra of a mixture of minerals can be quite challenging given that peaks of different minerals may overlap and weaker peaks may be hidden by stronger peaks. No distinct peaks were identified for imogolite or allophane. The spectral range was from 4000 to 400 cm^{-1} and hence the characteristic peak of imogolite at 348 cm^{-1} could not be investigated. Other characteristic peaks for these amorphous silicates exist at 925–935 cm^{-1} and 990–1010 cm^{-1} (Wada, 1978), however at these wavenumber ranges, strong peaks of other functional groups were observed and may have made identification impossible. It should be noted that for the separation of the clay fraction from the other soil particle sizes, this particle size fraction was suspended in solution. It was further saturated with either K^{+} or Mg^{2+}, which means that only relatively insoluble minerals would be observed in the XRD

patterns and IR spectra. This, however, does not rule out the possible formation of more soluble phases that also play an important role in acid buffering and element cycles.

3.4. Mineral Stabilities

The saturated paste solutions of the three different treatments were modeled in PHREEQC using the Pitzer model. The saturation indices (SI's) are depicted in Figure 2.6 for a selection of minerals with respect to soil solution of control. The SI's with respect to soil solution are positive for all minerals depicted in Figure 2.6 with the exception of Mg-Montmorillonite and thus it is not likely to form or to be stable in the soil solution. A second group of montmorillonite species that are stable, however, is Fe-montmorillonite. Montmorillonite was detected by XRD analysis and could thus be assigned to the latter group of montmorillonites. The soil solution therefore agrees with the minerals detected by XRD analysis and little change in soil mineralogy has occurred over the course of the weathering experiment for the control.

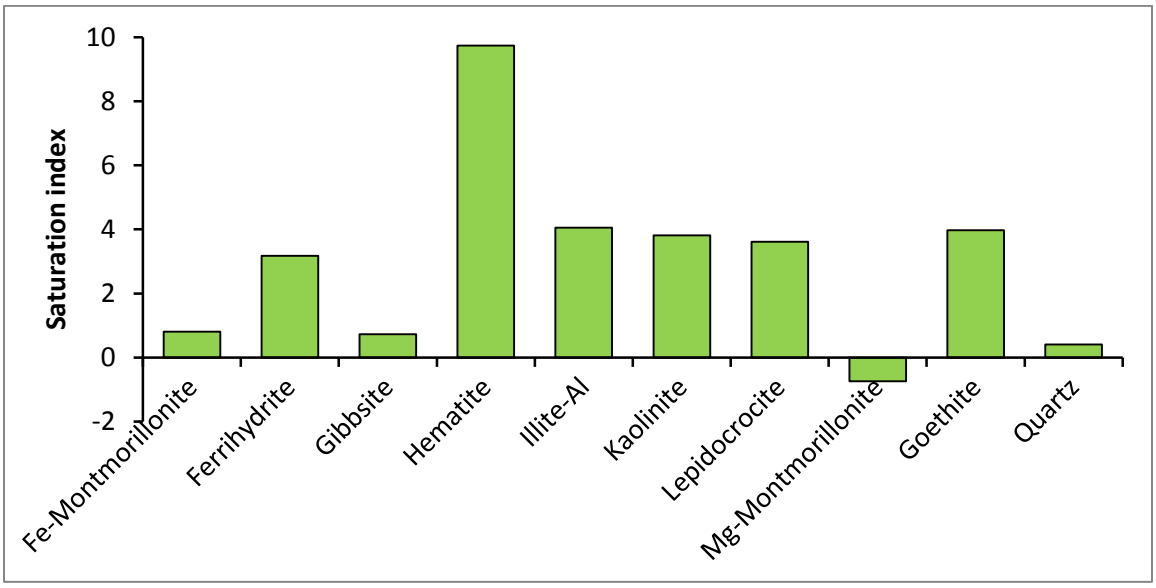

Figure 2.6: Saturation indices with regard to the weathering control soil solution.

The SI's were calculated for the AMD treated soil solutions (AMD-1 and AMD-2) as well as for the diluted AMD (Figure 2.7) with PHREEQC. Solution chemistry of the AMD suggests that ferrihydrite, goethite and lepidocrocite would precipitate from solution. Precipitates did form during the dilution process due to an increase in pH, but were filtered out. The diluted AMD used in the experiments was observed to be translucent, and homogeneous. Precipitation of these minerals is thus kinetically very slow or were formed as small colloids. The positive SI for of the Fe-oxyhydroxides (ferrihydrite, lepidocrocite and goethite) also supports the idea, postulated by Dubikova et al. (2002), that precipitates of these Fe-oxyhydroxides on surfaces of minerals would act as a stable barrier to the acidic solution. This was however not observed for the clay minerals in this study, as these minerals were dissolved.

For the AMD treatment, the saturated paste extracts indicate that in all cases, the soil solution was under-saturated with respect to kaolinite, montmorillonite and quarts. This supports the observed disappearance or reduction in peak intensity for these minerals in the XRD diffractograms. Illite is not

shown in Figure 2.7 as K was not detected in the saturated paste extracts of the AMD treated samples, which is one of the elements that make up this mineral. Potassium was detected in the AMD itself and the PHREEQC calculated SI for illite was –14.16. This low saturation means illite is unstable and therefore would dissolve.

The saturation index of ferrihydrite is positive for AMD-2 and AMD and slightly negative (−0.38) for AMD-1. For other Fe-minerals, such as goethite and lepidocrocite, the SI values are positive with respect to the soil solution for AMD-1, AMD-2 and diluted AMD. This means Fe-phases would precipitate in these solutions. This would explain the low amount of Fe extracted from the saturated pastes, as seen in Table 2.6. Amorphous silica also has a saturation index of less than zero which means the formation of amorphous silica phases such as imogolite and allophane are probably inhibited.

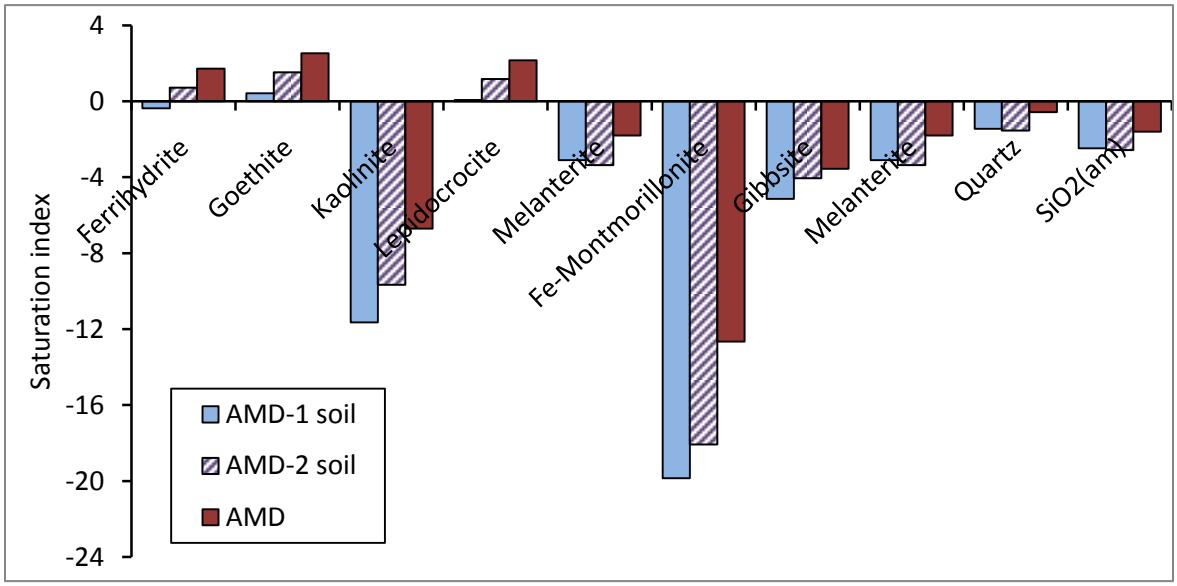

Figure 2.7: Saturation indices of soil solutions of AMD treated weathering experiments (AMD-1 and AMD-2) and raw AMD.

3.5. Soil Morphology

The morphologies of the soil for the different treatments were investigated by micrographs obtained from a scanning electron microscope (SEM). In Figure 2.8, three micrographs are displayed for the control weathering experiment (Figure 2.8a–c), the AMD treated weathering experiment (Figures 2.8d–f) and the untreated B2 horizon of the pristine soil (Figures 2.8g–i). Structural similarities occur between the control weathering experiment and the untreated pristine soil, since they both show larger crystalline particles (Figures 2.8a, b, g and i). Clay particles with a size of 2 µm or less (Gee & Bauder, 1986) are observed in Figures 2.8a, b, c and h. The clay sized particles observed are smooth and oblong to oval in shape. Figures 2.8d, e and i are micrographs of the AMD treated sample and portray a very different morphology compared to the two other cases. In Figures 2.8d and f, the sample has an amorphous mass that covers or binds the particles so that it is difficult to distinguish among the larger particle edges. In both of these micrographs (Figures 2.8d and f), linear crystal structures which have formed on the surface of this amorphous mass can be observed. In Figure 2.8f, it is also possible to

identify smaller clay size particles. This micrograph was collected at a different scale to the other micrographs. Figure 2.8e shows a strikingly unique morphology when compared to the other micrographs. The morphology observed in this case can be described as a “shattered” appearance and is probably as a result of artifacts from sample preparation. The particles are clay to silt size (2–50 µm) with sharp corners.

Micrographs were also collected for the clay fraction (Figure 2.9) for the control, AMD-weathered and pristine soil. Subtle differences can be observed between the control and pristine soil. For the AMD-weathered sample, the edges appeared to be more corroded than the smooth edges observed in the control. These observations are in all likelihood attributable to the attack on the edges of the clay minerals, and a shift to more amorphous phases.

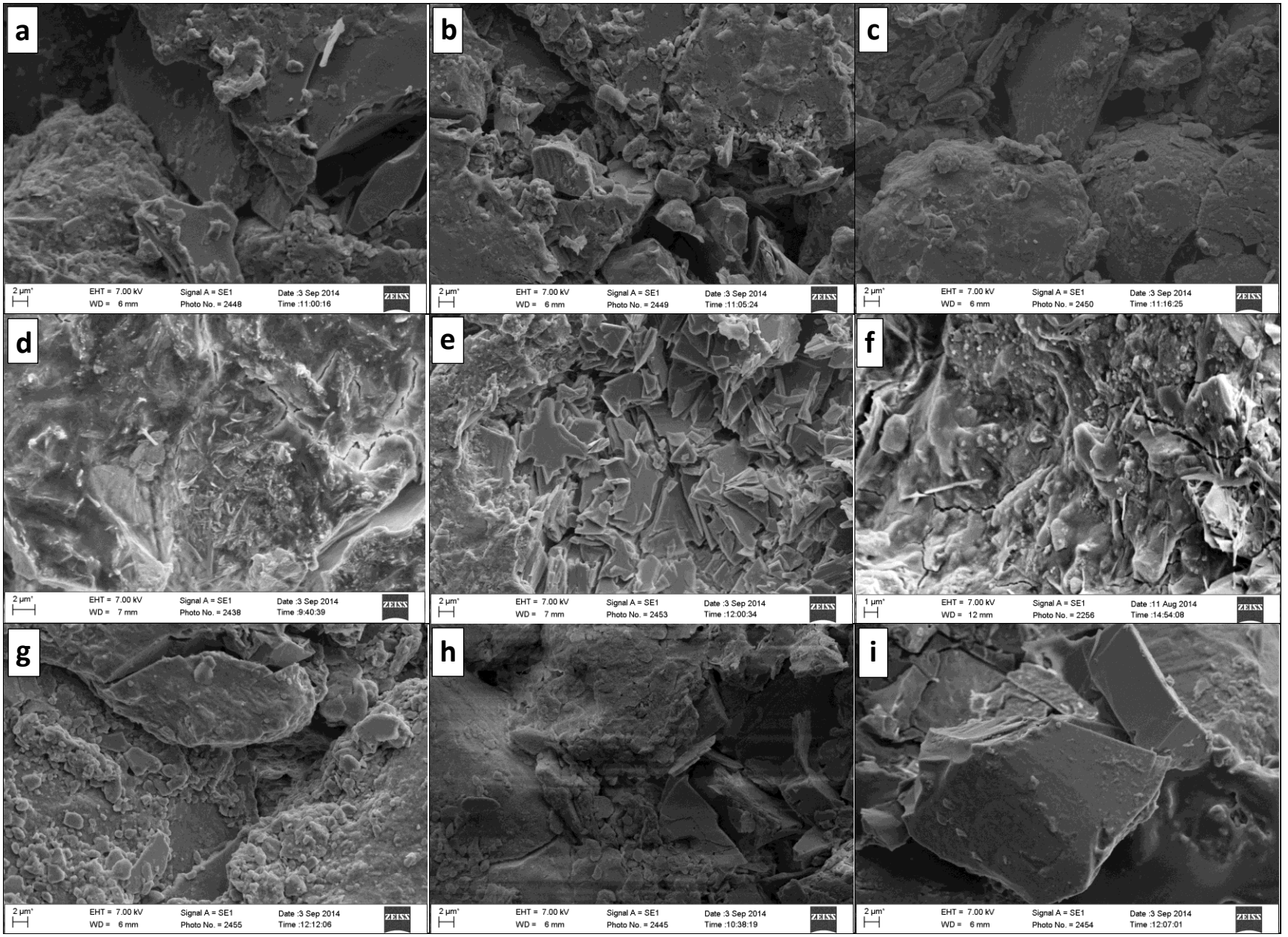

Figure 2.8: Micrographs for control weathered sample (a–c), AMD weathered sample (d–f) and pristine soil B horizon (g–i).

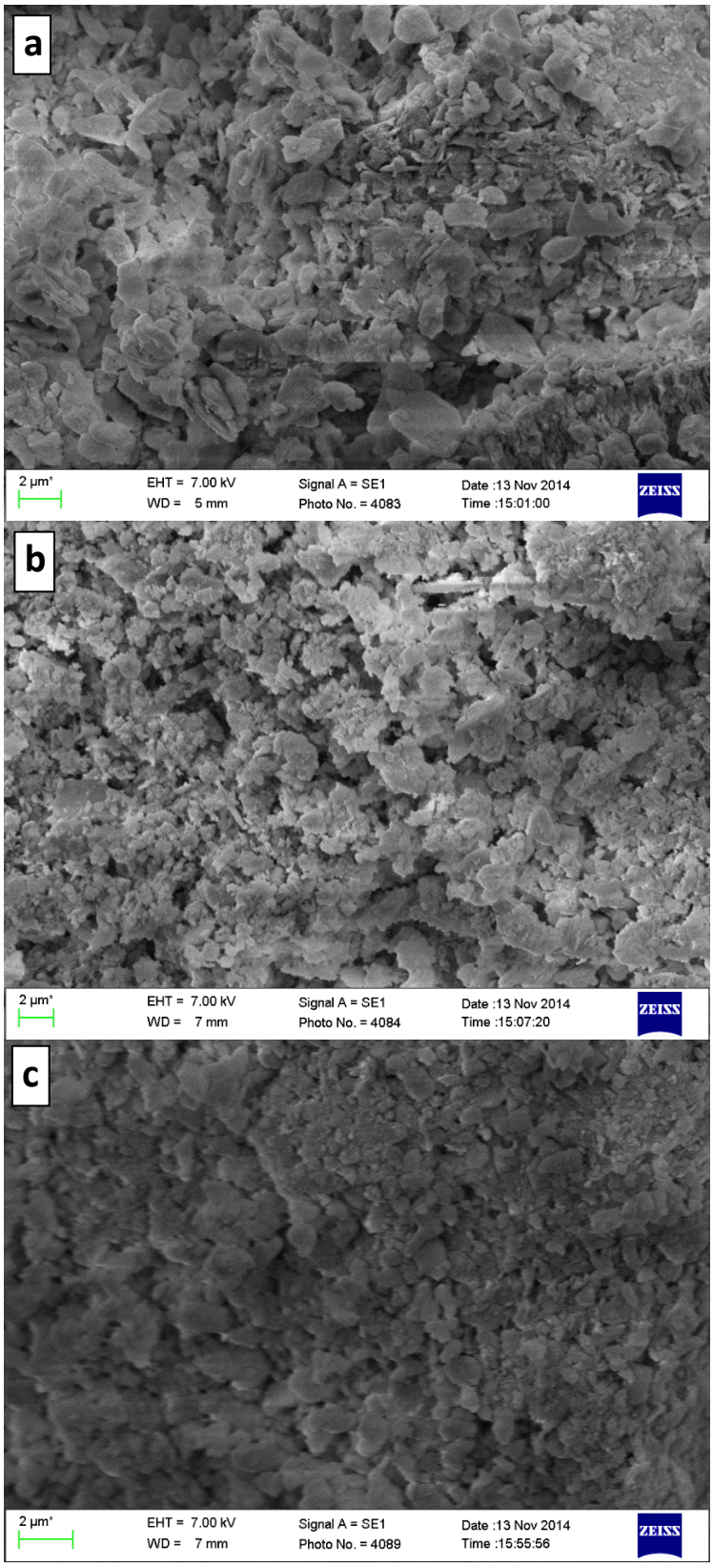

Figure 2.9: Micrographs of clay fraction for the control weathered sample (a), AMD weathered sample (b) and pristine soil (c).

4. Conclusion

An attempt was made to assess the impact of AMD on mineral weathering under evaporative conditions.

The XRD patterns indicated severe changes to the clay fraction of the control and AMD treated soil experiments. Montmorillonite is almost completely dissolved by the AMD, while the kaolinite and illite also show alterations in the minerals with broadening and collapsing of peaks. The changes were not only observed in the XRD patterns, but observations from the IR spectra supported the idea of these mineral changes too, by observations such as the reduction of peak intensity of the Si–O stretching assigned to kaolinite. Jarosite ($KFe^{3+}_3(SO_4)_2(OH)_6$) is a predominant mineral that precipitated from solution in the AMD treated experiments. This mineral is insoluble and is likely to be an important sink for sulfate. The precipitation of jarosite leads to the removal of K^+ from solution which may contribute to weathering of minerals with K^+ in their structure, such as illite for example.

The stabilities of soil minerals were evaluated with the modeling of soil solution in PHREEQC. The low pH of the AMD (2.42) is one of the main reasons why the soil solutions are under-saturated with respect to clay minerals such as montmorillonite, illite and kaolinite. Fe-oxyhydroxides, such as ferrihydrite and goethite, are stable in the soil solutions, and it is possible that minerals such as kaolinite and illite were coated with these Fe-phases, and were therefore protected from total dissolution.

The morphology of the AMD treated samples was observably different to that of the control treatment. A more amorphous matrix was observed from the micrographs. The morphologies of the pristine and control weathering experiments were fairly similar in nature. For clay powders, the edges of the acid treated soils had a corroded appearance not observed in the control, and could therefore be indicative of the mechanism of acid attack on these minerals.

Chapter 3. Metal mobility in the Nababeep soils

1. Introduction

In this chapter, the focus is on the mobility and the availability of chemical species in the soils of the Nababeep site, especially associated with the AMD. Soil has a capacity to attenuate metals and buffer the acidity of AMD. Rate et al. (2000) lists the mechanisms by which metals are retained in soils as ion exchange, outer- and inner-sphere complexes (adsorption), and precipitation or co-precipitation. The soil is a pathway for the polluted water but in this process the polluted solution is modified by interaction with soil. In order to establish the impact of the acid mine drainage (AMD) on the environment, it is important to gain an understanding firstly, of what species are available or soluble under different conditions and secondly, how mobile these species are in the soil. This is of high importance since this, in effect, determines the extent of pollution and how far the heavy metals and acidic solution would spread into the surrounding area, including nearby water bodies such as underlying aquifers. Studies have shown that underground water can be acidified and contaminated by heavy metals and sulfur leaching from AMD sources (Miao et al., 2013; Lei et al., 2010). At the site of investigation, the contamination source is located upslope from an ephemeral stream, which may be at risk of receiving polluted water from the AMD source. The spread of water from the processing pond is most likely to occur during the rainy season when soils surrounding the pond reach their water holding capacity. Evidence of salt pollution was present in a direct line below the pond towards the streambed, suggesting there is movement of polluted waters from the pond.

Understanding the movement and availability of metals in the soil could provide better management strategies in order to protect water resources and to stabilize the mobile fraction of trace elements in the soil. The aim of this chapter is i) to determine the metal retention and buffer capacity of the Nababeep soils, by applying AMD to the pristine soils and ii) to determine the mobility and leachability of metals in the contaminated Nababeep soils. Understanding the metal release and retention capacity of the soil will allow an estimation to be made of the contamination risks to nearby water sources. Leaching experiments were conducted to determine the capacity of the soil to retain AMD. This is to simulate conditions when soils are exposed to AMD as it moves into the environment close to the processing pond. The metal partitioning was also determined by sequential extraction to evaluate the mobility of metals in the soils exposed to AMD. First, a review of the current literature pertaining to metal sorption in soils and sequential extraction techniques is presented.

2. Review on metal mobility in soils

2.1. Sorption reactions in soils

The mechanisms that are assumed to be responsible for heavy metal retention in soil systems are given by Selim & Amacher (1996). This is firstly the adsorbed fraction by cation exchange which is readily exchangeable. Ion exchange is a rapid process and a fully reversible reaction (Selim & Amacher 1996). The second mechanism is where ions with a high affinity are sorbed onto specific sites on the soil matrix.

Sposito (1989) define the first type as ion exchange. The second type is another group of reactions that has stronger retention strength such as inner-sphere complexes, surface precipitation and the possible penetration of metals into the crystal lattices of minerals found in soils. The second kind of metal retention is often referred to as specific sorption (Tiller et al., 1984).

Sposito (1989) explains three types of adsorption reactions which are inner-sphere complexes, outer-sphere complexes and diffuse ion clouds. The outer-sphere complexes occur on the solid surface and include the solvation shell. Diffuse ion clouds are ions that neutralize the surface charge but are not attached to the solid surface. The outer-sphere complex and the diffuse ion cloud involve mostly electrostatic bonding and are therefore considered to be the exchangeable ions in soils. Inner-sphere complexes are found in the siloxane cavity of clays and involve either ionic or covalent bonding. Since covalent bonds require a specific electron configuration, these reactions are considered to be specific sorption and will only occur on specific surface groups. Specific sorption studies can also occur rapidly (within one hour) yet true equilibrium can take longer to establish (Benjamin & Leckie, 1981). The initial equilibrium can therefore only be considered a pseudo-equilibrium.

Metals in soil are adsorbed onto specific sites at low concentrations. At higher concentrations these specific sites become saturated with metals and the less permanent exchange sites are then filled (Mclean & Bledsoe, 1996; and references therein). O'Conner et al. (1984), for instance, investigated Cd adsorption on calcareous soils and characterized the retention with a two-part Freundlich relationship. The first part was for Cd-specific adsorption sites, and the second was a combination of highly Cd-specific sites and nonspecific sites attributed to exchange reactions. These relationships are strongly dependent on concentrations of the metals. A metal's affinity for a specific soil surface is related to the tendency to form a strong bond. Table 3.1 was compiled by Mclean & Bledsoe (1996), and shows the affinities of certain metals for different soils and soil constituents. Puls & Bohn (1988), for instance found that Cd has a higher affinity for kaolinite than Zn whilst a study by Forbes et al. (1976) found that both Zn and Co have a higher affinity for goethite than Cd does. In general, Pb and Cu has higher affinities for different soil constituents than Zn and Ni does. In a study by Tiller et al. (1984) on Cd, Zn and Ni adsorption on soils, it was found that the high-affinity sites depended on pH, equilibrium time and surface saturation that is specific to each respective clay in soil.

Table 3.1: Relative affinity of different soils and soil constituents for metals as given by Mclean & Bledsoe (1996).

Soil or Soil constituent	Relative order of sorption	Reference
Goethite	Cu>Pb>Zn>Co>Cd	Forbes et al. (1976)
Fe Oxide	Pb>Cu>Zn>Cd	Benjamin & Leckie (1981)
Montmorillonite	Cd=Zn>Ni	Puls & Bohn (1988)
Kaolinite	Cd>Zn>Ni	Puls & Bohn (1988)
Soils	Pb>Cu>Zn>Cd>Ni	Bidappa et al. (1981)
Soils	Zn>Ni>Cd	Tiller et al. (1984)
Mineral soils	Pb>Cu>Zn>Cd	Elliott et al. (1986)
Organic soils	Pb>Cu>Cd>Zn	Elliott et al. (1986)
Soil	Pb>Cu>Zn>Ni	Harter (1986)

Another mechanism that influences the mobility of metals in the soil is co-precipitation. This process occurs when phases precipitate from solution and is usually associated with a change in pH or a change in concentration with additions of new salts. Co-precipitation has been investigated to be a method of removing trace metals from AMD by authors such as Lee et al. (2002) and Sánchez España et al. (2006). Co-precipitation is however not limited to human induced reactions and has be observed "naturally" or unintentionally in AMD systems. Smith & Williams (2000) report on the removal of Cd, Co, Ni, V and Cr from AMD downstream from an AMD source. This removal is attributed primarily to co-precipitation with crystalline sulfates of which melanterite is the most prevalent. Bortnikova et al. (2001) investigated the response of the solution in a reservoir to an inflow of an AMD stream. In this study, co-precipitation is suggested as one of the main mechanisms by which metals are removed from solution. This occurs through sorption of ions onto the neo-formed Fe-compounds. The phases that formed in solution were gypsum, jarosite and Fe-oxides. Johnson (1986) also showed that amorphous Fe-oxyhydroxides regulated the concentrations of Cd and Zn in a river contaminated with AMD by specific binding to the surfaces of these amorphous Fe precipitates.

Although artificial metal removal is beyond the scope of this study, a few concepts are worth noting. In the study by Lee et al. (2002), the importance of different phases for the removal metals is highlighted. The phases of importance include firstly, Fe-oxides, where ferrihydrite forms at pH values below 4 and schwertmannite, which forms at pH values above 4. Secondly, Al-rich phases which form at pH values of approximately 5 are also important. Thirdly, the other important phase in soils include the Mn-compounds, which precipitate at a pH of approximately 8. It is stated that the removal of metals depends on the formation of these three phases. Sánchez España et al. (2005) support the importance of pH on metal removal rates from AMD and also include the importance of the activity of SO_4^{2-} which determines the speciation of metals. At high activities of SO_4^{2-} (> 10^{-1} mol/L), metals such as Al, Zn, Cd, Pb and U form anionic bisulfate complexes, which enable these metals to be sorbed at pH values below 5 (Sánchez España et al. 2006).

2.2. Leaching of metals and pollution potential

The subject of metal mobility is important with the regards to the pollution potential of a metal loaded solution such as AMD. As discussed above, soils and soil constituents have a significant influence on the removal and retention of metals, although there are limitations to their capacity for attenuation. Lei et al. (2010) investigated groundwater in close proximity to a tailings storage facility of a nickel sulfide mine. It was found that the groundwater from drilling holes was acidic and that the concentrations of Co, Cu, Zn, Cd, Al and Mn were 1 to 2 orders of magnitude higher than the background groundwater concentrations. Rösner (1998) reported significant As, Cd, Pb, Zn, Fe and Mn pollution in groundwater in the vicinity of a mine in Arizona, yet another nearby mining site yielded no evidence of groundwater contamination (Rösner 1998). The different responses to contamination were attributed to soil chemical reactions, different groundwater systems and dilution effects.

Some remediation strategies attempt to immobilize metals by the addition of amendments to the soil. Amendments such as $CaCO_3$, iron grit, fly ash, manure, bentonite and bone meal (Hodson et al. 2001; Concas et al, 2007; Houben et al., 2012) have been evaluated as possible metal immobilization agents in soil. One of the factors that reduces the leaching of heavy metals is the increase in alkalinity.

Remediation will not be investigated in this dissertation, but the importance of leaching behavior should be considered to understand the extent of pollution of metals and to evaluate future solutions to the problem.

2.3. Determination of metal partitioning

Metals can partition into a number of different soil phases. The phase that a metal partitions into determines the mobility and bioavailability of the metal (Filgueiras et al., 2002). Sequential extraction is a procedure which selectively dissolves certain phases in the soil sediment or sludge, allowing predictions to be made about metal mobility and bioavailability (Filgueiras et al., 2002). Sequential extraction is a multi-step process where metals are separated by extracting one or several metal fractions at each step using a different solvent.

The procedure that was followed in this study is based on the method described by Tessier et al. (1979) for fluvial bottom sediments. The basic procedures and chemicals used are outlined in Table 3.2.

Since then the procedure was adapted and used in many applications. The Community Bureau of Reference (BCR), which is now called Standards, Measurement and Testing Programme, developed a three step sequential extraction method with three fractions (acid soluble, reducible and oxidizable) (Ure et al., 1993). The applications and adaptions of sequential extractions vary to such an extent that a comprehensive review was done by Filgueiras et al. (2002) on sequential extraction procedures over the previous decade of publication and more than 400 papers were reviewed. One of the aims of this review is to assess comparability between the different techniques. Figure 3.1 is a summary of the different defined extractable phases with the corresponding chemicals used in each stage. The selection of different stages and chemicals is dependent on the different applications as listed by Filgueiras et al. (2002) which are (1) pollution source characterization, (2) determining metal bioavailability and availability, and (3) for determining the binding sites important for assessment of the metal accumulations, transport mechanisms and pollution.

Sequential extraction has been applied to many different materials such as sewage sludge, river sediments, fly ash and soil (Filgueiras et al., 2002). Maiz et al. (1997) conducted a two-step sequential extraction procedure on soils contaminated by mining, steel factory and traffic emissions. The order of metal availability was proposed to be Cd>Pb>Zn~Cu>Mn>Ni>Fe~Cr. In a study by Barona et al. (1999), Cu, Ni and Zn were sequentially extracted in a 3-step procedure on soils contaminated by smelters and a steel factory. Copper was found to be the most abundant in the non-residual fraction and hence most available while Ni was mostly extracted from residual fraction. In a long-term experiment by McGrath & Cegarra (1992), soils were treated with sewage sludge or inorganic fertilizers over a long period (1942–1961). The soils were then analyzed by a four step sequential extraction. During the first ten years of sewage sludge additions, it was found that for the metals Pb, Cu, Zn and Cd there was an increase in the proportions of metals in at least one of the first three fractions extracted. These were the fractions representing exchangeable, organically bound and carbonate forms and thus the more mobile fractions in soil. For a period of more than 30 years of sewage sludge addition as fertilizer, there was little change in the distribution of the metals extracted in the distinctive fractions. Chrome was mostly found in the residual fraction for most of the cases.

Table 3.2: Summary of the sequential extraction procedure described by Tessier et al. (1979).

Fraction number	Operationally-defined phase	Procedure summary
Fraction 1	Exchangeable	8 ml - 1M $MgCl_2$, pH 7 **or** 1 M NaOAc, pH 8.2 Continuous agitation 1 hour at room temperature ± 22 °C
Fraction 2	Bound to carbonates	8 ml - 1M NaOAc pH 5 (HOAc adjusted) Continuous agitation 5 hours at room temperature ± 22 °C
Fraction 3	Bound to Fe-Mn oxides	20 ml - 0.3 M $Na_2S_2O_4$ + 0.175 M Na citrate + 0.025 M H-citrate - **or** 0.04 M $NH_2OH{\cdot}HCl$ in 25% (v/v) HOAc Occasional agitation 6 hours at 96 ± 3 °C
Fraction 4	Bound to Organic Matter	3 ml 0.2 M HNO_3 5 ml 30% H_2O_2 pH 2 (HNO_3 adjusted) intermittent agitation 1st - 2 hours at 85 ± 3 °C 2nd - for 3 hours at 85 ± 3 °C Allow to cool 5 ml 3.2 M NH_4OAc in 20% (v/v) HNO_3 Dilute sample to 20 ml and agitate for 30 min
Fraction 5	Residual	Residue digested with HF-$HClO_4$

Differences in the distribution of heavy metals of the sludge compared to the soil treated with inorganic fertilizers were also observed by McGrath & Cegarra (1992). Lead was found to be most abundant in a fraction extracted by ethylenediaminetetraacetic acid (EDTA) which represents the acid soluble fraction in the fertilized-treated soils. In the sludge treated soils, lead was more predominant in residual fraction. Copper was more predominant in the NaOH fraction assigned to organic matter, however NaOH could also attack aluminosilicates and clays (Gleyzes et al., 2002). Lastly, Cd was mostly found in the exchangeable fraction ($CaCl_2$) in experiments by McGrath & Cegarra (1992).

Abdel-Saheb et al. (1994) characterized soils contaminated by mining and smelting activities by sequential extraction. In this study by Abdel-Saheb et al. (1994), the different fractions extracted were sulfide, carbonate, organic, sorbed and exchangeable fractions and the sulfide fraction had the highest concentration of heavy metals. Another sequential extraction study on sandy and loamy texture soils found that metals from anthropogenic sources are more mobile than the metals inherited from the parent material (Chlopecka et al., 1996). It was found in this study by Chlopecka et al. (1996) that soil type, cation exchange capacity (CEC), texture or organic matter did not influence the proportion of metal forms. The pH, however, did play a role in that soils with a pH of less than 5.6 had higher relative proportions of Cd, Pb and Zn in the exchangeable fraction than in soils with a pH of more than 5.6.

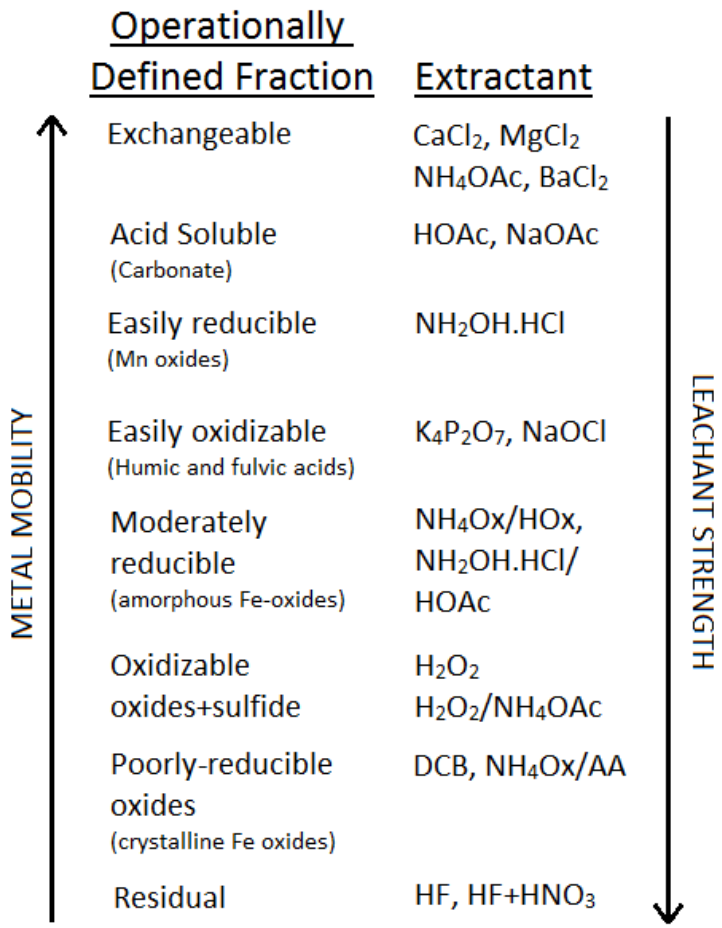

Figure 3.1: Figure depicting the relationship between the metal mobility for each fraction and examples of chemicals used for each fraction (adapted from Filgueiras et al. (2002)).

Although there are known limitations to sequential extraction techniques (Martin et al., 1987), it is one of the only ways to gather information on the lability of metals. This is important as it determines the potential for AMD to move through the soil into nearby water bodies when soil conditions change.

3. Materials and Methods

3.1. Metal retention experiments

The acid mine drainage used in this experiment was collected from the leach pond (as described in Chapter 2). At the time of collection (end of the dry season), the AMD was highly concentrated. To simulate the dilution that would take place in the rainy season (when movement of AMD into the soil is most likely) it was diluted 10 times. The diluted AMD was filtered to remove the precipitates that formed during the dilution process. The composition of the diluted AMD was analyzed by ICP-AES.

A 250 ml separating funnel was used as the leaching column. A glass wool and filter paper pulp plug was used to prevent the soil leaving the vessel. The filter paper pulp was prepared by blending torn pieces of Whatman 40 paper in distilled water. A small amount of this pulp was added on top of the glass wool layer. The glass wool and filter paper pulp layer was not thicker than 1 cm.

The amount of liquid added was slightly higher than field capacity (previously determined) and for 80 g of soil this was around 13 ml of liquid. It was, however, decided to add 15 ml of AMD to the air dried soil at the first leach cycle to ensure enough liquid could be extracted from the first run for analysis. Thereafter 13 ml of liquid was added. To make sure the solution moved right through the column the tap was left open until the added solution reached the plug filter. The solution was allowed to equilibrate with the soil for 24 hours before being extracted under vacuum. This leaching cycle was repeated 10 times. The leachates were filtered through 0.45 µm syringe filters, diluted and analyzed by ICP-AES.

3.2. Sequential Extraction

The sequential extraction procedure was based the procedure described by Tessier et al. (1979). This five step procedure was developed for river sedimentary samples and is summarized in Table 3.2.

The sequential extraction was performed on three different soil samples: the first was from the long weathering experiment, the second was the control from the long weathering experiment (both described in Chapter 2) and the third was the B horizon (15–30 cm) from the contaminated Nb3 profile (Chapter 1).

Table 3.3 is a modification of the Tessier method (Tessier, 1979) used for the sequential extraction in this study. For each soil, 1 g of soil was used and samples were prepared in triplicate. The first deviation from the method by Tessier et al. (1979) is the introduction of a water soluble fraction in the first treatment.

The soils exposed to AMD have a substantial amount of soluble salts that have precipitated in the soil matrix, but are however not associated with the solid fractions of the original soil. The last residue was not treated with HF-$HClO_4$.

The soil samples were analyzed before and after sequential extraction by X-ray fluorescence (XRF) spectrometry in order to determine bulk elemental composition, using a handheld Niton® XL3t GOLDD^{TM}++ Analyzer by Thermo Scientific.

The experiments were conducted in 50 ml polypropylene centrifuge tubes. Between the operationally-defined phases, separation was accomplished by centrifuging at 8000 rpm for 20 minutes. The supernatant was then carefully removed with a micro-pipet without extracting the residual fraction. The supernatant was added to a volumetric flask and solution was made up as indicated in Table 3.3 and then subsequently analyzed by ICP-AES. After each fraction (except first fraction), the residual fraction was washed by adding 10 ml Deionized (DI) water (18 MΩ·cm, Millipore, Billerrica, MA), shaking the sample for 10 minutes, and then centrifuging it. The second supernatant was discarded. The reagents used for all procedures were analytical grade and were tested for contamination by a blank control run for each fraction.

Table 3.3: Summary of experimental procedure followed for sequential extraction.

Fraction number	Operationally-defined phase	Procedure summary
Fraction 1	Soluble fraction	Add 30 ml of DI water Continuous agitation 1 hour at room temperature ± 22 °C Repeat Decant in 100 ml volumetric flask and make up with DI water
Fraction 2	Exchangeable	Add 10 ml - 1M $MgCl_2$ Continuous agitation 1 hour at room temperature ± 22 °C
Fraction 3	Bound to carbonates	Add 8 ml - 1M NaOAc pH 5 (HOAc adjusted) Continuous agitation 5 hours at room temperature ± 22 °C Decant to 25 ml volumetric flask and make up with DI water
Fraction 4	Bound to Fe-Mn oxides	Add 20 ml - 0.3 M $Na_2S_2O_4$ + 0.175 M Na citrate + 0.025 M H-citrate Occasional agitation 1st - 5 hours at 96 ± 3 °C 2nd (repeat)- 3 hours at 96 ± 3 °C Decant to 50 ml volumetric flask and make up with DI water
Fraction 5	Bound to Organic Matter	Add 3 ml 0.2 M HNO_3 Add 5 ml 30% H_2O_2 pH 2 (HNO_3 adjusted) Intermittent agitation 2 hours at 85 ± 3 °C Add 5 ml 30% H_2O_2 pH 2 (HNO_3 adjusted) Intermittent agitation 3 hours at 85 ± 3 °C Allow to cool 5 ml 3.2 M NH_4OAc in 20% (v/v) HNO_3 Dilute sample to 20 ml and agitate for 30 min Decant to 50 ml volumetric flask and make up with DI water

4. Results and Discussion

4.1. AMD dilution

The AMD that was used in the treatment of weathering experiments in the previous chapter is the same AMD now used in the metal retention experiments. The AMD was not filtered prior to dilution, this would give the true effect of rain-induced dilution on the composition of the AMD. The ratio between the concentrated and diluted AMD is given to evaluate conservative and non-conservative behavior of species (Table 3.4). A ratio of less than ten indicates that dilution results in dissolution of particulate species whereas a ratio of more than ten suggests non-conservative behavior or removal of the species from solution. After the dilution of the concentrated AMD, a translucent yellow/red precipitate formed that would be assigned to be amorphous Fe-oxyhydroxides. The ratio for Fe is, however, slightly less than 10 (9.66) which indicates a release of Fe into the solution.

The ratio between concentrated and diluted AMD for Na is 10.73. Sodium should act conservatively with dilution, therefore it can be used as threshold for comparison with other metals. Calcium and heavy metals such as Cd, Co, Cr and Ni have a ratio of close to 10 with values of 10.54, 10.34, 10.35, 10.40 and 10.49 respectively and could be considered to have behaved conservatively. Pb, however, shows some non-conservative behavior with a ratio of 14.02. The removal of this metal could be attributed to co-adsorption with Fe-oxyhydroxides. The pH value increased from 1.5 to a value of 2.42.

Table 3.4: Metal/Species concentration of concentrated and diluted AMD

Element/ Species	AMD mg/l	AMD10 mg/l	Ratio --
Al	26896.67	2756.33	9.76
B	24.12	1.54	15.67
Ca	230.33	21.86	10.54
Cd	1.53	0.15	10.34
Co	126.57	12.23	10.35
Cr	19.89	1.91	10.40
Cu	3819.00	403.20	9.47
Fe	42923.33	4445.67	9.66
K	7.86	0.99	7.97
Mg	20493.33	2170.00	9.44
Mn	3447.67	351.70	9.80
Na	20.25	1.89	10.73
Ni	340.23	32.43	10.49
P	52.17	6.18	8.44
Pb	5.72	0.41	14.02
SO_4^{2-}	318352.60	31175.19	10.21
Si	16.57	1.59	10.45
Zn	1688.33	175.63	9.61

4.2. Metal retention experiments

Figure 3.2 depicts the average pH for every 24 hour leachate cycle. The horizontal (red) line is the pH of the AMD that was introduced to the column. The first phenomenon observed in Figure 3.2 is the low pH for the first two leach cycles (1.35 and 1.39 for the first and second cycle, respectively). This is lower than the AMD pH (2.42). This decrease in pH can possibly be attributed to the precipitation of amorphous Fe oxyhydroxides which acidifies the solution. Another explanation could be the release of reserve acidity. A large difference was observed between the pH in water and KCl in Chapter 1 (Table 1.4) and the AMD would therefore release exchangeable acidity. After the first two leach cycles the pH stabilizes close to the pH of the AMD.

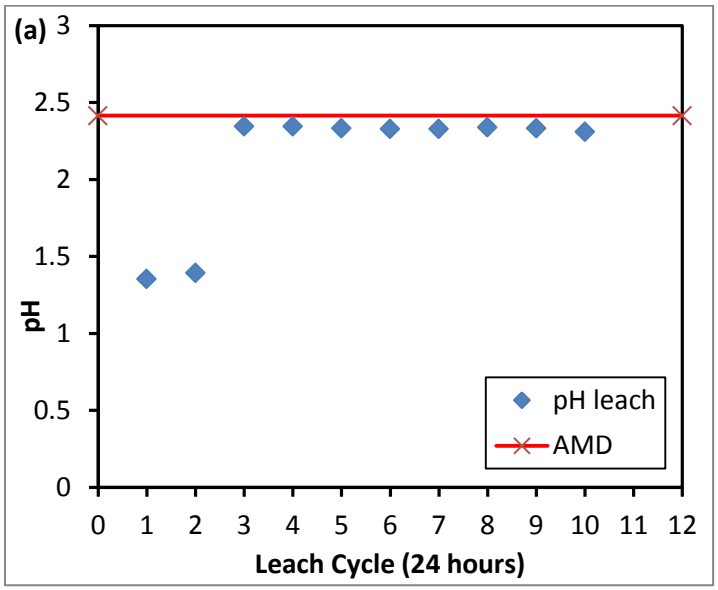

Figure 3.2: Measured pH values of leachates extracted (blue diamonds) from soil columns every 24 hours. Red line indicates pH of the introduced AMD.

Figure 3.3 depicts the concentration of Si, Fe, Al and Mn in the leachate after each leach cycle. In Figure 3.3b, a clear decrease in Fe concentration in the leachate can be observed for the first three cycles after which the concentration gradually approaches the concentration of the AMD and then plateaus off to more or less the same concentration of AMD. This supports the theory stated above that the precipitation of Fe-oxyhydroxides occurs which leads to the acidification of the solution. The precipitation of these Fe-oxyhydroxides is limited as the concentration of AMD is unaffected after 5 leach cycles. The Si concentration measured in the AMD is 1.65 mg/l, but for the first leachate 77.2 mg/l was extracted and would mean Si is being released from the soil. The source of Si in leachate could be attributed to the dissolution of acid soluble Si phases. Smectite was identified in the Nb4 profile, and smectite is unstable in acid soils (Kloprogge et al., 1999). Smectite also has a high surface area, thus it is likely that this would be one of the first mineral phases to dissolve. The release of Si decreases with progressive leaching until the curve plateaus. Interestingly, this is still above the concentration of the AMD. Reasons for this may be a gradual dissolution of clay minerals such as illite and kaolinite ($Al_2Si_2O_5(OH)_4$).

No specific trend can be observed for Al in Figure 3.3. The first of cycle of leachate had a concentration of 2585 mg/l which is lower than the concentration of the AMD (2756 mg/l). In the leachate from the second cycle, the Al concentration spiked above the AMD concentration (3122 mg/l). From the third leach cycle onwards the concentration of Al in the leachate is above the concentration of the AMD which means a net release of Al from the soil. The loss of Al supports the theory that clay minerals such as kaolinite and montmorillonite are dissolving. This also implies that no Al-minerals precipitate in the solution and Al is one of the most mobile cations in the soil.

The concentration of Mn in the leachate rapidly drops over the first three leach cycles from an average of 963 mg/l to approximately the value of the AMD (351 mg/l in Figure 3.4d). The rapid removal indicates that the Mn is easily released from the soil into solution. The source of this Mn remains unexplained. It may be attributed to primary minerals, but in chapter 1 the reported minerals found in the granite-gneiss is biotite ($K(Mg, Fe)_3(AlSi_3O_{10})(F, OH)_2$), hornblende ($(Ca, Na)_2(Mg, Fe, Al)_5(Al, Si)_8O_{22}(OH)$) and feldspar ($CaAl_2Si_2O_8$). A sample of the weathered granite was also analyzed by XRD and the phases identified included microcline ($KAlSi_3O_8$) and albite ($NaAlSi_3O_8$) and none of these minerals contain Mn in its chemical composition.

In Chapter 1 saturated paste extractions were also conducted on the same soil and could be compared to the first leach cycle. The Mn for the saturated paste extracted with DI water was only 2.66 mg/l. This means the 963 mg/l value for first leachate would include the Mn added by AMD but also a fraction that was solubilized by mechanisms such as acid attack induced by AMD.

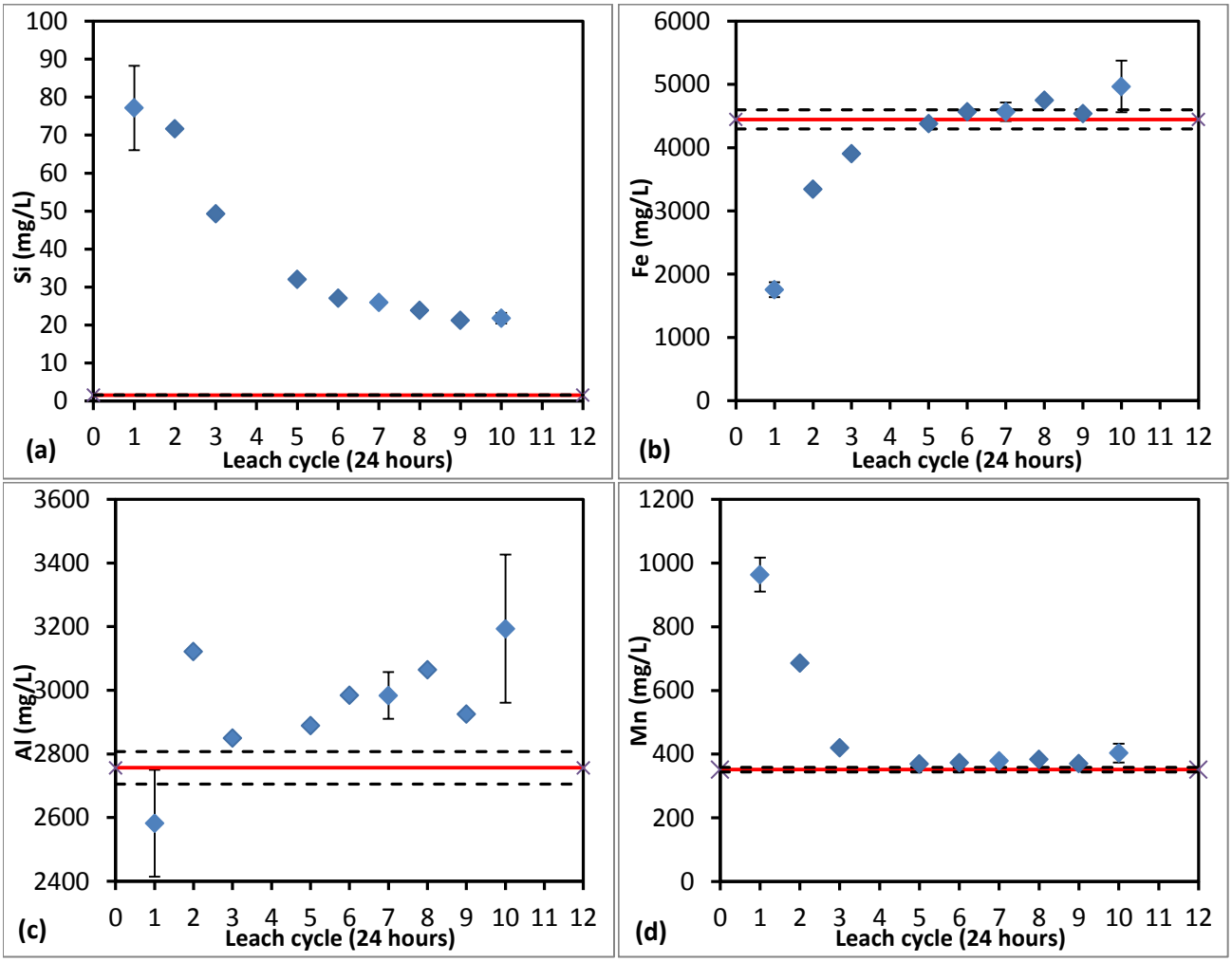

Figure 3.3: Concentration of Si (a), Fe (b), Al (c) and Mn (d) in leachate for each leach cycle with upper and lower standard deviation given for cycle 1, 7 and 10. Red line indicates concentration of species in AMD and black dashed lines indicate upper and lower standard deviation.

Figure 3.4 depicts the concentrations of basic cations in the leachate at every leach cycle. A similar pattern is observed for Na, K and Ca (Figures 3.4a, c and d) which is a high concentration of the cation in the initial leachate followed by a rapid decrease in concentration over the cycles 2 to 4, after which the concentration plateaus close to the concentration of the AMD. This means again that these cations are rapidly removed from the soil within three or four leaching cycles. This behavior was also observed for Ca in leaching experiments by Dubikova et al. (2002) and corresponds with the exchangeable and soluble species in the soil. During the first leach cycle, 6.88 mg/kg soil Na, 9.06 mg/kg soil K and 110 mg/kg soil Ca was removed from soil and would be exchanged with high Mg in AMD. Mg however shows different pattern to the other basic cations (Figure 3.4b). The concentration observed for Mg in the leachate is always higher than the average AMD concentration (2170 mg/l). The highest Mg concentration is observed in the last leach cycle (cycle 10) which is 2521 mg/l Mg. This release of higher Mg concentration only later in leaching cycles may be related to dissolution of clay minerals and primary

minerals, such as biotite. The lag in release of Mg from the soil was also observed by Dubikova et al. (2002) was assigned to the dissolution of clay minerals. It does however not reflect the same pattern as Mn that showed a high release into solution initially. The cations contained in the AMD suppress the release of alkali and alkali-earth metals from the soil (Dubikova et al., 2002).

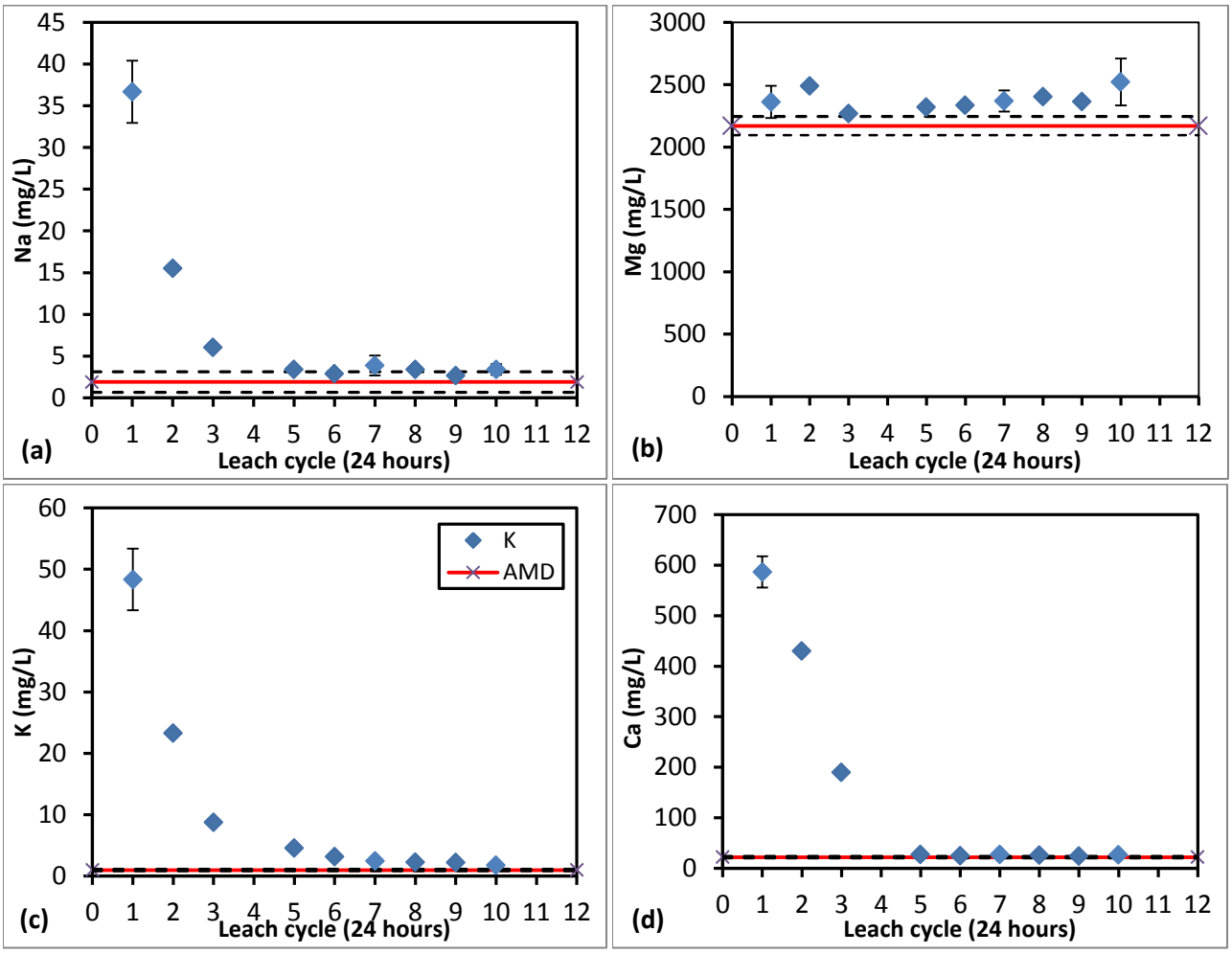

Figure 3.4: Concentration of Na (a), Mg (b), K (c) and Ca (d) in leachate for each leach cycle with upper and lower standard deviation given for cycle 1, 7 and 10. Red line indicates concentration of species in AMD and black dashed lines indicate upper and lower standard deviation.

Figure 3.5 depicts the concentration in leachates for heavy metals (Co, Ni, Cu and Zn). Cobalt shows a trend similar to that of the Mn where the metal is rapidly removed during the first 3 leach cycles and thus removed from the soil. After the first three leach cycles, the curve plateaus off and the concentration remains close to that of the AMD introduced at the top of leaching column. During the first leach cycle 22.11 mg/l of Co is measured in the leachate equivalent to 4.15 mg/kg soil and thus an amount of Co is released from soil into solution. This could possibly be Co associated with Mn-oxides. The leachate curves for Ni, Cu and Zn follow a similar trend to each other with leachate concentrations fluctuating around the concentration of AMD. In all three cases, the Ni, Cu and Zn concentrations for the first cycle were lower than the AMD which can be associated with the co-precipitation of Fe-

oxyhydroxides, a removal mechanism discussed by authors such as Johnson (1986) and Smith & Williams (2000).

The results demonstrate that the soils show a low capacity to retain the metals in the soil. For the heavy metals only the first cycle seemed to have had an influence in retaining the metals. On the contrary a number of metals, such as Al, Mn and Co seemed to have been released from the soil into the soil solution. The AMD also strips the soil from basic cations. The mechanisms for this may be cation exchange and dissolution of clay minerals but the effect is permanent and would have irreversible effects on the soil. This would make remediation of the soil challenging. Iron was precipitated from the AMD solution and this mechanism may responsible for the initial removal of some heavy metals such as Cu, Zn and Ni, heavy metals through co-precipitation. This capacity seems limited, however, with the leachate soon attaining equilibrium with the leachate.

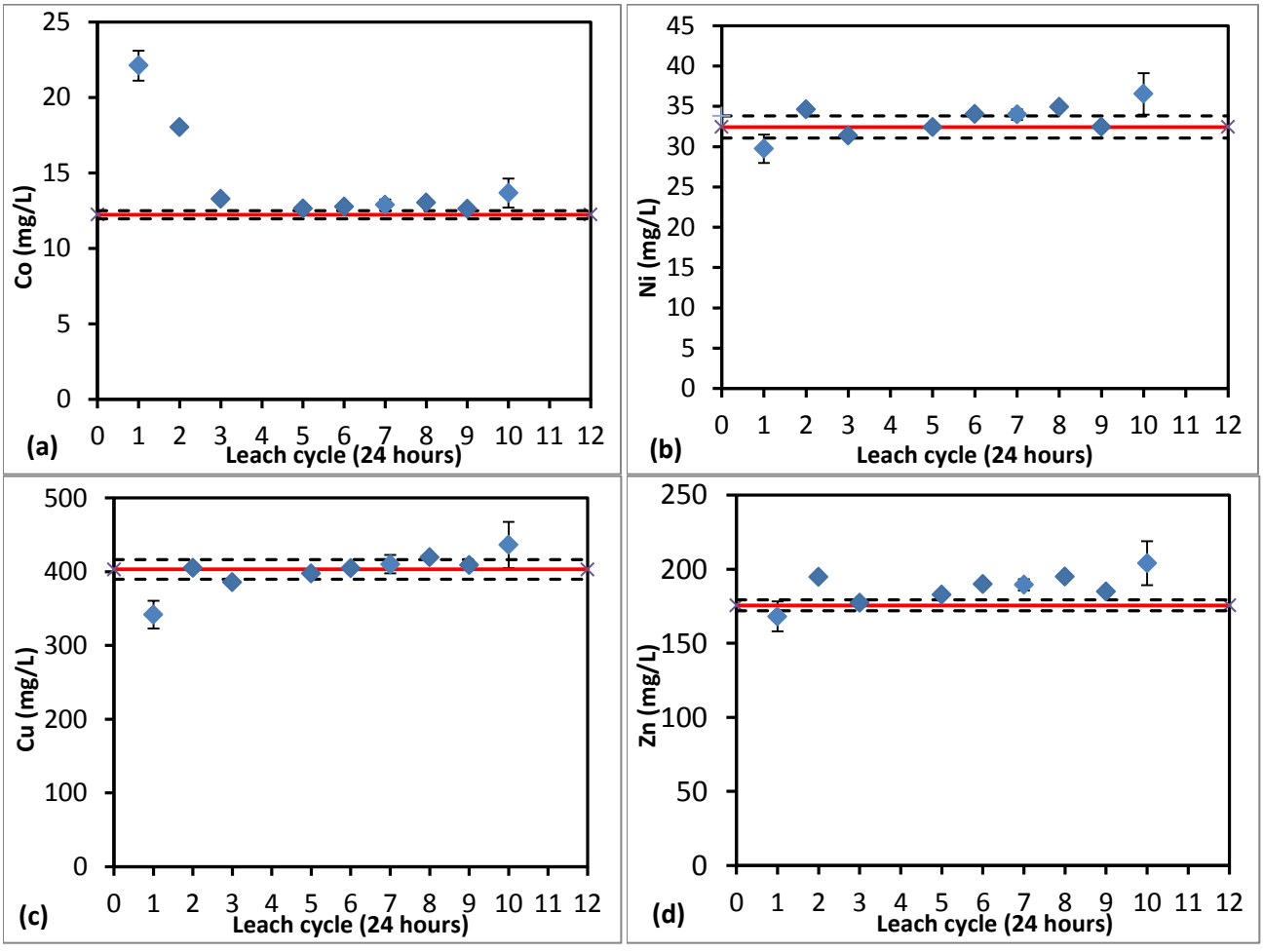

Figure 3.5: Concentration of Co (a), Ni (b), Cu (c) and Zn (d) in leachate for each leach cycle with upper and lower standard deviation given for cycle 1, 7 and 10. Red line indicates concentration of species in AMD and black dashed lines indicate upper and lower standard deviation.

4.3. Sequential Extraction

The initial phase extracted from the soil was the water extractable phase. Table 3.5 gives this extraction data for the long weathering treatment along with the cumulative concentrations of metals added to the soil during the weathering experiment. The cumulative metal concentrations are the total metal loads added to the soil in nine wetting events. The water soluble metals are expressed as a percentage of the cumulative metal concentrations (Table 3.5). For Fe, only 14 % of the added metal concentration was released in the soluble fraction. It can therefore be assumed that the Fe phases that precipitated out from the AMD were insoluble in water. As previously discussed the jarosite phase was detected in the clay phase and this could be one of the main sinks for Fe. Although a low amount of K was added in AMD over the experiments (1.36 mg/kg), none of this K was detected in the soluble phase which supports the theory that this element is part of jarosite's chemical composition.

Table 3.5: Comparison of the input of weathering experiments to the soluble fraction of sequential extraction.

Element	Input over experiments*	Fraction 1 (Soluble fraction)	% soluble
	mg/kg soil		
Al	3803.74	2035.67	53%
Ba	0.12	0.61	500%
Ca	30.16	94.27	313%
Co	16.88	9.65	57%
Cr	2.64	0.82	31%
Cu	556.42	319.5	57%
Fe	6135.02	870.6	14%
K	1.36	nd	0%
Mg	2994.6	1665.67	55%
Mn	485.35	258.73	53%
Na	2.61	nd	0%
Ni	44.75	25.69	57%
Pb	0.56	nd	0%
S	14360.74	6875.33	47%
Si	2.19	11.62	531%
Sr	0.015	0.057	367%
Zn	242.37	127.93	52%

* $\frac{x \times 0.115\ \text{l AMD} \times 9\ \text{treatments}}{0.75\ \text{kg soil}}$

where x – concentration of species in AMD

Of the heavy metals Co, Cu, Ni and Zn that were added, between 50 and 60 % were water extractable which means that more than half of metals added were present in labile phases in the soil. The same is true for Al, Mn and Mg, which had between 50 and 60% water extractability for the amount of metals added. Chrome and Pb seemed to have the highest affinity for the soil, with only 31% and 0% being extracted by water, respectively. Some elements, namely Ba, Ca, Sr and Si, were released from soil so

that a higher concentration was detected in the soluble fraction than the amount that was introduced through AMD. This can be largely attributed to the dissolution of silicate minerals by the addition of AMD.

Table 3.6 gives the metal concentrations released in each extractant for the long weathering control, the AMD treated soil and the Nb3 (15–30 cm) subsoil. The concentrations of Al and Fe in the water soluble fraction of the control was 87 and 50 mg/kg soil, respectively, while for the water soluble fraction of the AMD treated sample, the concentration of Al and Fe was 2036 and 870 mg/kg soil, respectively. For the AMD treated sample, the highest amount of Al was extracted in this water soluble fraction. As previously discussed, clear dissolution of montmorillonite, illite and kaolinite was observed and this could be the source of Al species which is extracted in this fraction. The dissolution of these minerals would also lead to Si being available in the more soluble fractions.

Table 3.6: Selected elemental concentrations of different sequential extraction fractions of control, AMD treated long weathering experiments and contaminated soil (Nb3 15-30 cm).

Fraction		mg/kg soil									
		Al	Fe	Mn	Si	Ca	Co	Cr	Cu	Pb	Zn
Soluble	AMD	2035.67	870.60	258.73	11.62	94.27	9.65	0.82	319.50	nd	127.93
Exchangeable	AMD	88.97	36.62	1.16	3.14	8.60	nd	nd	9.21	nd	0.79
Acid Soluble	AMD	14.80	387.67	1.12	26.10	10.83	nd	nd	12.63	0.27	0.89
Reducible	AMD	596.17	6925.00	11.12	1987.17	48.63	nd	6.00	51.78	14.17	19.72
Oxidizable	AMD	260.48	143.00	3.30	297.05	220.88	0.16	0.51	29.36	3.84	3.72
Soluble	Control	86.89	49.74	0.98	137.90	13.45	0.05	nd	3.78	nd	1.20
Exchangeable	Control	12.39	13.73	2.98	2.16	61.72	nd	nd	28.57	2.58	3.64
Acid Soluble	Control	25.32	105.59	2.07	21.08	10.83	nd	nd	24.56	3.12	0.95
Reducible	Control	678.67	4515.50	19.90	1781.17	90.20	nd	6.05	77.15	10.77	24.10
Oxidizable	Control	274.97	154.23	3.04	282.27	263.25	0.13	0.55	58.31	3.50	4.25
Soluble	Nb3 15-30 cm	69.85	57.90	17.92	12.36	905.27	0.44	nd	12.53	nd	6.24
Exchangeable	Nb3 15-30 cm	124.05	21.08	0.48	3.62	71.00	nd	nd	2.06	nd	0.65
Acid Soluble	Nb3 15-30 cm	26.57	20.97	0.50	27.90	11.36	nd	nd	4.21	nd	0.36
Reducible	Nb3 15-30 cm	998.67	21175.0	14.73	3070.17	78.65	nd	15.85	41.53	8.00	10.65
Oxidizable	Nb3 15-30 cm	412.23	165.02	2.67	589.67	24.08	0.16	0.71	4.04	1.76	4.13

nd = not detected

The concentration of Si in this sample is lower in first three fractions (water soluble, exchangeable and acid soluble) compared to the reducible fraction and this suggests that Si has been scavenged into less soluble phases. Another observation is that Al remains in the most mobile fraction of the soil and is not bound to neoformed phases. An example of this is alunite ($K_2Al_6(SO_4)_4(OH)_{12}$), which is not water soluble. Alunite has been observed in precipitates of AMD by several studies (i.e. Sánchez España et al., 2006; Filipek et al., 1987; Jones et al., 2011; Lee et al., 2002; Sánchez España et al., 2005). Alunite precipitation may be limited by lack of K in solution. The heavy metal content was significantly higher for Co, Cr, Cu

and Zn in the AMD treated soil than in control. These metals are associated with soluble salts from the metal laden AMD solution.

For the exchangeable fraction, the concentration of all elements in Table 3.6, except Al, Fe and Si, were higher in the control than for AMD treated soil. Due to the low organic matter content the clay phase is responsible for the exchangeable fraction and the clay content of the soil was measured to be only 5.12 %. The introduction of the metal laden AMD to soil increases the competition of exchangeable sites. The concentration of Al extracted in the exchangeable fraction for the AMD treated soils was 88 mg/kg soil which the second lowest value in the fractions for the AMD treated soil in this metal partitioning experiment.

The acid soluble fraction is usually associated with carbonates which are not dominant in the parent material. The values observed for this fraction is somewhere in between the values of other fractions. The concentration of Fe for AMD treated soil is 387.7 mg/kg soil. Claff et al. (2010) investigated Fe partitioning in acid soils and although a stronger acid was used than in this study (1M HCl) as an acid extractant, it is reported that in this fraction, poorly ordered sulfides and oxides are also dissolved. The release of Fe can thus be assigned to dissolution of phases such as ferrihydrite. The use of acetic acid in this fraction may also release metals by cation exchange.

The extracted concentration of Fe for the control was 4515 mg/kg soil and 6925 mg/kg soil for the AMD treated sample in the reducible fraction. The Fe is significantly higher for the AMD treated soil ($p = 0.0029$) and this additional release can be attributed to neoformed minerals such as jarosite. In Chapter 1, the formation of Fe-compounds was discussed in terms of pe-pH diagrams. In Figure 1.10, formation conditions of jarosite are shown which is at low pH and high pe (oxidizing conditions). When minerals such as jarosite are therefore exposed to reducing conditions, the solid Fe-phases dissolve. Dold (2003) did a two part reducible fraction extraction and found jarosite dissolving in the reducible fraction amongst other phases of ferric (Fe^{3+}) minerals. No jarosite was detected in the control phase. The release of Fe is however also related to other Fe phases such as goethite and hematite. For the control, the highest amount of Al extracted was in the reducible fraction (679 mg/kg soil). Aluminium is however not a redox sensitive element and the release of Al must be related to phases that do contain redox sensitive cations. The amount of Al extracted in reducible fraction for the control is higher than soil treated with AMD (596 mg/kg soil). This can be attributed to a change in mineralogy of the AMD treated sample. The average concentration of Si in the reducible fraction is significantly higher in the AMD treated soil ($p = 0.031$). The highest Pb concentration was detected in the reducible fraction of the control and AMD treated soil. The Pb was significantly higher in the AMD treated soil ($p = 0.027$) which can be attributed to its release upon the dissolution of Fe-phases. The release of metals from the reducible fraction was also observed for Cr, Cu and Zn.

The oxidizable fraction is the fraction associated with organic matter and supergene sulfides. There is no significant difference in the concentrations between the AMD treated and control weathering experiments which means the organic matter remained unaffected over the experiments. Calcium was the highest in the oxidizable fraction for both AMD treated soil (220.9 mg/kg soil) and control (263.3 mg/kg soil).

The extracted Cu concentration was higher in the control for all fractions except the water soluble fraction of AMD treated soil (Table 3.6). The pristine nature of the Nb4 sampled site soil has been questioned previously in this dissertation and this release of Cu supports the idea of possible contamination from previous mining activities. It may also be attributed to the naturally elevated Cu concentrations resulting from the presence of Cu-ore mineral deposits in the area.

All the metals in the soluble fraction of the AMD treated soil are significantly higher (p-values < 0.001) than in the contaminated soil (Nb3 15-30 cm) which suggests that the soluble species have already been removed from these soils. Significantly more Al and Si are observed in exchangeable, acid soluble, reducible and oxidizable fractions of the contaminated soil than in the AMD treated soil. The elevated amounts are ascribed to the extended years of exposure to AMD resulting in an accumulation of these species. Iron concentration is also more than three times higher in the reducible fraction for the contaminated soil (21175 mg/kg soil) than AMD treated soil. Copper concentrations were significantly higher in all the fractions for the AMD treated soil and this would suggest that for an open soil system, metal attenuation is less effective. The Pb and Zn concentrations in the reducible fraction of the AMD treated soil is higher than contaminated soil and supports the notion that metal attenuation is limited in natural environments. The comparability of the contaminated and AMD treated soil is also questionable. The AMD treated soil was pristine soil treated for 201 days while contaminated soil sample is exposed to AMD conditions for several years. The 15–30 cm layer of the contaminated soil is above a rock layer and therefore more saturated with water. Therefore, the layer is prone to water saturation and reducing conditions probably prevail, which would, in turn, influence metal mobility and mineralogy significantly.

The water soluble, exchangeable and acid soluble fractions are often considered to be bioavailable (Maiz et al., 1997). As discussed, the soluble fraction for the AMD treated soils is the highest. This is because this is a closed system where metals accumulated over the period of the experiment and cannot be directly compared to the contaminated soil. It is, however, interesting to note that total Cu for the bioavailable fraction (water soluble + exchangeable + acid soluble) in the control is 56.91 mg/kg soil. This value is only 18.8 mg/kg soil for the contaminated soil. The total extracted Cu is 192.37 mg/kg soil and 64.37 mg/kg soil for the control and contaminated soil respectively. This puts the amount of Cu in the contaminated soil into perspective in that it is lower than in the control where no Cu was added. This is also true for Pb with a bioavailable fraction of 5.7 mg/kg in the pristine soil and no detected Pb in the bioavailable fraction of contaminated soil. One explanation for this is that the heavy metals in the contaminated soil have already been released.

In the comparison between AMD and the control, slight differences were observed that showed that the AMD altered the soil to some degree. There is however no convincing evidence that heavy metals in general are retained in the soil and retained in the more immobile fractions such as reducible and oxidizable fractions. The comparison between the contaminated soil and AMD treated soil showed that, even though this soil has been exposed to contamination for several years, only Cr is retained more in the non-mobile fractions (15.9 mg/kg soil in reducible fraction) than the AMD treated soil. For the other heavy metals, the AMD treated soil retained more Cu, Pb and Zn in the reducible and oxidizable fractions.

In summary, the control weathering experiment showed high release of Si (137.9 mg/kg) and Al (86.9 mg/kg) in the water soluble fraction. This favours precipitation of clay minerals such as kaolinite. For the exchangeable and acid soluble fraction, no extractions were noteworthy, except for high Cu concentrations. The highest concentration for all metals was obtained for the reducible fraction, except for Ca which was in the oxidizable fraction. One significant metal that was released is Mn, which was the highest among all three different treatments (19.9 mg/kg). The greatest quantity of heavy metals was released in the reducible fraction, which means that these are not bioavailable.

The AMD treated soil had high amounts of metals which was extracted in the water soluble fraction. This was the highest for Al (2036 mg/kg), Mn (259 mg/kg), Co (9.65 mg/kg), Cu (319.5 mg/kg) and Zn (128 mg/kg). This was a closed system experiment to mimic the highly evaporative conditions of Namaqualand and thus a large amount of the metals precipitated as salts. Secondly, this can be attributed to dissolved minerals such as Mn-oxides. Again no noteworthy concentrations were obtained in the exchangeable and acid soluble fractions, but for the reducible fractions, the concentrations of Al (596 mg/kg), Fe (6925 mg/kg) and Si (1987 mg/kg) were very high. This is due to the dissolution of reducible Fe phases such as jarosite, hematite and goethite, which are neoformed and originate from the pristine soil before the experiments.

The contaminated soil had a high amount of Ca (905.3 mg/kg) in the water soluble fraction that was possibly released from the tailings. A high concentration of Al was extracted in the exchangeable fraction (124 mg/kg). Exceptionally high Al (999 mg/kg), Fe (21175 mg/kg) and Si (3070 mg/kg) were released in the reducible fraction. This may be attributed to several years of exposure to AMD that led to the precipitation of both crystalline and amorphous Fe-phases. In the reducible fraction, a high concentration of Cr (15.9 mg/kg) was also extracted.

5. Conclusions

In this chapter an attempt was made to understand the mobility of metals both in the context of metals added to pristine soils and metals released from contaminated soils. Two approaches were followed in order to investigate metal mobility. Firstly, metal attenuation studies were conducted on pristine soil with AMD and secondly, sequential extraction was conducted on the contaminated soil, AMD weathering experiment soil, and the control weathering experiment.

The metal attenuation experiments showed that Fe was initially removed from the AMD solution, possibly through precipitation in the form of amorphous Fe-oxyhydroxides. The dissolution of aluminosilicate phases such as clays is also suspected due to the release of Si and Al from the soil. Basic cations such as Na, K and Ca were stripped from the soil. The removal can be attributed to cation exchange with other metals and dissolution of clay size particles and is therefore irreversible soil deterioration. Heavy metals such Cu, Ni and Zn showed some removal during the first cycle of removal. This capacity is however limited and after first cycle the sites were saturated and these metals were mobile so that the same concentration was collected in the leachate as in the AMD. A net release of Co and Mn form soil was observed. The conclusion can be made that the capacity of the soils to attenuate metals are low. The reason for this is that the parent material from which the soils are derived, are acidic granite-gneiss characterized by an absence of secondary carbonates. Secondly, the soils in this

arid region are poorly developed and have a low clay content, a component that is responsible for most of the surface reactions that immobilize metals. Thirdly, air pollution from the nearby smelter may have possibly also added to the acidity of the soil.

Sequential extraction showed that the soluble fraction of the AMD treated soil is high for most elements, although elements were still taken up in less mobile fractions. For example, of the amount of Fe introduced over the weathering experiments, only 14 % was released in the soluble fraction. In the AMD treated soil, a large proportion of metals were also extracted from the reducible fraction. This shows the importance of Fe-phases as a mechanism to retain metals. Jarosite, for example, is assumed to be one of the dominant sinks for both Fe and subsequently K.

Overall, the soil showed a limited capacity to remove metals from solution. It should be noted that the soil falls in a sandy texture class and would therefore naturally have low cation exchange capacity. Secondly, the AMD is also highly metal-laden, which requires significant adsorption sites to reduce the concentration of metals. A large fraction of the metals are therefore mobile and would spread further into soil pedons or underground water resources.

Chapter 4. General conclusions and further work

The aim of this study was to gain an understanding as to what the impact of the AMD is on soils in terms of mineral weathering and mineralogy. Related to this, is the mobility and bioavailability of metals in the soil system, as well as the soil solution chemistry. These concepts are important in understanding the metal cycling and toxicity present at a site contaminated by AMD. The focus of this study is on contaminated soils located near a copper mine close to Nababeep, Northern Cape, South Africa. This is located in the Namaqualand region which is an arid region but is also known to be a diversity hotspot with a high level of endemism.

The major conclusions that can be drawn from this study are outlined, and then elaborated upon in the paragraphs that follow.

The corrosive nature of the water (AMD) can be visibly observed on the granite-gneiss rock that has been weathered within the leach pond. Melanterite crystals were observed that formed beneath the tailings. This ferrous sulfate crystal is associated with solutions with exceptionally high concentrations of Fe and sulfate. This, together with the orange colouration of the water, suggests both ferrous and ferric iron species are present in the AMD. The composition of the AMD reflected high concentrations of metals such as Fe, Al and Cu, Mn and Mg. The reason for these high concentrations is attributed to the evaporative environment that has been accumulating the metals for an extensive period of time.

The clay minerals that were identified in the pristine soils close to the processing pond are kaolinite, illite, quarts and montmorillonite. High levels of sulfate and Cu, and a low pH, was observed in the pristine soil. This might be indicative of air pollution which emanated from the smelter plant during its operation. The soils in the pond show alterations in its mineralogy in comparison with the pristine soil. These changes include the disappearance of montmorillonite and the broadening of the kaolinite XRD peaks, suggesting a transformation to a more amorphous mineral. Neoformed jarosite was also detected in the clay phase of the pond soils.

Long term weathering experiments were conducted by exposing the pristine soil to AMD and a $CaCl_2$ control for 8 months. An interesting phenomenon was observed in that montmorillonite was detected in the control experiment, but no montmorillonite was detected in the original soil used for the experiments. The formation of montmorillonite in the control could not easily be explained as the soil solution was acidic. Saturated paste extracts of the AMD treated soils showed that the soil solution was undersaturated with respect to minerals such as illite and kaolinite. Alteration of these minerals was observed in collapsed and broader XRD peaks. Illite and kaolinite did not completely disappear, which may be related to this process being kinetically slow. Another contributing factor may be a precipitate layer of Fe-oxides or oxyhydroxides on the surfaces of these minerals. This acts like a barrier to prevent total dissolution of the mineral (Dubikova et al., 2002).

Scanning electron microscope (SEM) images of the AMD treated soils and control, when compared with each other, showed differences. The AMD treated soil had a more amorphous nature. Secondly, a more corroded appearance was observed for the clay fraction of the AMD treated soil compared to the control. The amorphous nature of the soil was confirmed by a broad IR band representing structured water molecules, indicative of metal coordination, which was not observed in the control soil. Jarosite also formed in the soils treated with AMD, which is a possible explanation why K was not detected in the saturated paste extracts of theses soils.

Metal retention experiments were conducted in order to gain a better understanding into the capacity of the pristine soils to buffer pH and immobilize metals. Fe-phases precipitated in the soil initially but no prolonged Fe removal from solution into less soluble phases was observed, however. An amount of Cu was retained in the soil initially, but its concentration in solution soon matched that of the AMD Cu concentration, suggesting Cu attenuation was limited. A metal such as Co, for example, was released by the soil rather than retained. This may have to do with dissolution of Mn-oxide phases as Mn also showed a net release from the soil. The basic cations Na, K and Ca were also removed from the soil solution into the extract. This may be attributed firstly to cation exchange, but also to dissolution and replacement of clay structures. These results demonstrated that the soils have a very low capacity to retain metals. The metals of greatest concern are heavy metals that are toxic at low concentrations. Only slight attenuation was observed for Cu. In many respects, leaching the soils with AMD actually increased the metal and salt load of the solution. The low capacity of the soils to attenuate metals is attributed to the acidity of the parent material, the absence of secondary carbonates, the low clay content of the soils and the fact that the pristine soils have already been contaminated by air pollution. In addition to this, the AMD is highly concentrated and therefore the limited metal retention capacity of the soil will become saturated rapidly.

Metal mobility and bioavailability of the contaminated soils was assessed by means of a sequential extraction. For the soils exposed to AMD for 8 months, high amounts of metals were extracted in the water soluble fraction. This is related to the metal salts that precipitated in the closed system which are highly mobile and bioavailable. In the contaminated pond soil, which represents an open system, the reducible phase showed the highest metal concentrations. This suggests the incorporation of metals in Fe- and Mn-oxide phases. Jarosite may also be responsible for metal attenuation in the reducible phase. This means the metals that are attenuated by the soils partition into phases that are not bioavailable, but the relatively low concentrations of metals extracted from all phases, confirm the low metal attenuation capacity of the soils. A very high Cu concentration was extracted from the pristine soil in the exchangeable, acid soluble, reducible and oxidizable fractions, which may relate to naturally high background levels of Cu in the soils or significant Cu contamination from the mining operations in the area.

The AMD has a significant influence on the soils that were investigated. What was observed is an substantial change in the mineralogy and chemistry of the soil. The soil also does not show a high capacity to retain the metals, in order to prevent these metals from spreading further into the environment. This means nearby water systems are at great risk to be polluted by heavy metals and acidic solutions.

Further work

One of the main gaps that still exist for these contaminated sites is the quality of water of the surrounding water systems. Due to the aridity and highly evaporative conditions, rivers are non-perennial, but unconfined aquifers continue to move water through underground systems and the contamination of this water is of great concern. The sampling of borehole water should also be conducted in order to monitor changes that would occur in the water bodies.

Effective remediation strategies should be implemented at these contaminated sites. Johnson & Hallberg (2005) reviewed different remediation strategies for AMD. Two main streams of neutralization exist, one is biological and the other chemical. These two strategies are subdivided to each have active and passive treatment systems. The area of Namaqualand is, however, arid and this might pose some unique challenges for strategies that aim to bring remarkable differences and preserve the soil and natural resources.

The mineral jarosite was detected in a soil from the contaminated site, and was also neoformed in the long weathering experiment conducted in the laboratory. This mineral is important as it contains K in its structure that is not only a major nutrient but also an integral part in the structures of minerals such as illite. No detectable K was found in the saturated paste extracts of AMD treated soils. Another species in the structure of this phase is sulfate, and this mineral may be an important sink for the removal of sulfates from soil solution. Understanding the chemistry of this mineral's formation is important as it plays a key role in the regulating and/or cycling of these elements and chemical species. Research has been conducted on this mineral (Dutrizac & Jambor, 2000), but there is still a gap in knowledge with respect to applications to this investigation site.

References

Abdel-Saheb, I., Schwab, A. P., Banks, M. K., & Hetrick, B. A. (1994). Chemical characterization of heavy-metal contaminated soil in southeast Kansas. *Water, Air, and Soil Pollution*, *78*(1-2), 73–82.

Aglietti, E. F., Porto Lopez, J. M., & Pereira, E. (1988). Structural Alterations in Kaolinite by Acid Treatment. *Applied Clay Science*, *3*, 155–163.

Akcil, A., & Koldas, S. (2006). Acid Mine Drainage (AMD): causes, treatment and case studies. *Journal of Cleaner Production*, *14*(12-13), 1139–1145. doi:10.1016/j.jclepro.2004.09.006

Alpers, C. N., Blowes, D. W., Nordstrom, D. K., & Jambor, J. L. (1994). Secondary Minerals and Acid mine-water Chemistry. In J. L. Jambor & D. W. Blowes (Eds.), *Environmental Geochemistry of Sulfide Mine Wastes1* (pp. 247–270). Waterloo, Ontario: Mineralogical Scociety of Canada.

Barona, A., Aranguiz, I., & Elias, A. (1999). Assessment of Metal Extraction, Distribution and Contamination in Surface Sois by a 3-Step Sequential Extraction Procedure. *Chemosphere*, *39*(11), 1911–1922.

Benjamin, M. M., & Leckie, J. O. (1981). Multiple-Site Adsorption of Cd , Cu , Zn , and Pb on Amorphous Iron Oxyhydroxide. *Journal of Colloid and Interface Science*, *79*(1), 209–221.

Bidappa, C. C., Chino, M., & Kumazavra, K. (1981). Adsorption, desorption, potential and selective distribution op heavy metals in selected soils of Japan. *Journal of Environmental Science and Health, Part B: Pesticides, Food Contaminants, and Agricultural Wastes*, *16*(4), 511–528.

Bigham, J. M., & Murad, E. (1996). Mineralogy of ochre deposits formed by the oxidation of iron sulfide minerals. *Advances in Geoecology*, *30*, 193–225.

Bigham, J. M., Schwertmann, U., Traina, S. J., Winland, R. L., & Wolf, M. (1996). Schwertmannite and the chemical modeling of iron in acid sulfide waters. *Geochimica et Cosmochimica Acta*, *60*(12), 2111–2121.

Blowes, D. W., Reardon, E. J., Jambor, J. L., & Cherry, J. A. (1991). The formation and potential importance of cemented layers in inactive sulfide mine tailings. *Geochimica et Cosmochimica Acta*, *55*, 965–978.

Bortnikova, S. B., Smolyakov, B. S., Sidenko, N. V., Kolonin, G. R., Bessonova, E. P., & Androsova, N. V. (2001). Geochemical consequences of acid mine drainage into a natural reservoir: inorganic precipitation and effects on plankton activity. *Journal of Geochemical Exploration*, *74*(1-3), 127–139. doi:10.1016/S0375-6742(01)00179-0

Brady, K. S., Bigham, J. M., Jaynes, W. F., & Logan, T. J. (1986). Influence of sulfate on Fe-oxide formation: Comparisons with a stream receiving Acid Mine Drainage. *Clay and Clay Minerals*, *34*(3), 266–274.

Brewer, G. J. (2010). Copper toxicity in the general population. *Clinical Neurophysiology : Official Journal of the International Federation of Clinical Neurophysiology*, *121*(4), 459–60. doi:10.1016/j.clinph.2009.12.015

Brindley, G. W. (1955). *Identification of clay minerals by x-ray diffraction analysis*.

Buckley, A. N., & Woods, R. (1987). THE SURFACE OXIDATION OF PYRITE. *Applied Surface Science*, *27*, 437–452.

Cairncross, B. (2004). History of the Okiep Copper District, Namaqualand, Northern Cape Province, South Africa. *Mineralogical Record*, *35*, 289–317.

Calvaruso, C., Mareschal, L., Turpault, M.-P., & Leclerc, E. (2009). Rapid Clay Weathering in the Rhizosphere of Norway Spruce and Oak in an Acid Forest Ecosystem. *Soil Science Society of America Journal*, *73*(1), 331. doi:10.2136/sssaj2007.0400

Cama, J., Metz, V., & Ganor, J. (2002). The effect of pH and temperature on kaolinite dissolution rate under acidic conditionsEnvironmental. *Geochimica et Cosmochimica Acta*, *66*(22), 3913–3926.

Chlopecka, A., Bacon, J. R., Wilson, M. J., & Kay, J. (1996). Forms of Cadmium, Lead, and Zinc in Contaminated Soils from Southwest Poland. *Journal of Environmental Quality*, *25*(1), 69–79.

Claff, S. R., Sullivan, L. A., Burton, E. D., & Bush, R. T. (2010). Geoderma A sequential extraction procedure for acid sulfate soils : Partitioning of iron. *Geoderma*, *155*(3-4), 224–230. doi:10.1016/j.geoderma.2009.12.002

Clarke, C. E., le Roux, S. G., & Roychoudhury, A. N. (2014). The role of evaporation on the formation of secondary Cu-hydroxy minerals in the arid Namaqualand soil system of South Africa. *Applied Geochemistry*, *47*, 52–60. doi:10.1016/j.apgeochem.2014.05.013

Clifford, T. N., & Barton, E. S. (2012). The O'okiep Copper District, Namaqualand, South Africa: a review of the geology with emphasis on the petrogenesis of the cupriferous Koperberg Suite. *Mineralium Deposita*, *47*(8), 837–857. doi:10.1007/s00126-012-0403-x

Concas, A., Montinaro, S., Pisu, M., & Cao, G. (2007). Mechanochemical remediation of heavy metals contaminated soils: Modelling and experiments. *Chemical Engineering Science*, *62*(18-20), 5186–5192. doi:10.1016/j.ces.2007.02.024

Department of Water Affairs and Forestry. (1996). *South African Water Quality Guidelines. Volume 7: Aquatic Ecosystems*. *Volume 7: Aquatic* (Vol. 7).

Department of Water and Sanitation. (n.d.). *Hydrological Services - Surface Water (Data, Dams, Floods and Flows)*.

Desmet, P. G. (2007). Namaqualand—A brief overview of the physical and floristic environment. *Journal of Arid Environments*, *70*(4), 570–587. doi:10.1016/j.jaridenv.2006.11.019

Dold, B. (2003). Speciation of the most soluble phases in a sequential extraction procedure adapted for geochemical studies of copper sulfide mine waste. *Journal of Geochemical Exploration*, *80*, 55–68. doi:10.1016/S0375-6742(03)00182-1

Drever, J. I., & Stillings, L. L. (1997). The role of organic acids in mineral weathering. *Aquatic Colloid and Surface Chemistry*, *120*(1-3), 167–181.

Dubikova, M., Cambier, P., Vladimı, S., & Caplovicova, M. (2002). Experimental soil acidification. *Applied Geochemistry*, *17*, 245–257.

Dutrizac, J. E., & Jambor, J. L. (2000). Jarosites and their application in hydrometallurgy. *Reviews in Mineralogy and Geochemistry*, *40*(2), 405–452.

Eberl, D. D., Farmer, V. C., & Barrer, R. M. (1984). Clay Mineral Formation and Transformation in Rocks and Soils [and Discussion]. *Philosophical Transactions of the Royal Society of London. Series A, Mathematical and Physical Sciences*, *311*(1517), 241–257.

Edwards, K. J., Bond, P. L., Gihring, T. M., & Banfield, J. F. (2000). An Archaeal Iron-Oxidizing Extreme Acidophile Important in Acid Mine Drainage. *Science*, *287*(5459), 1796–1799. doi:10.1126/science.287.5459.1796

Elliott, H. A., Liberati, M. R., & Huang, C. P. (1986). Competitive Adsorption of Heavy Metals by Soils. *Journal of Environmental Quality*, *15*(3), 214–219.

España, J. S., & Ercilla, M. D. (2008). Geochemical Modelling of Concentrated Mine Waters: A Comparison of the Pitzer Ion-Interaction Theory with the Ion-Association Model for the Study of Melanterite Solubility in San Telmo Mine (Huelva, Spain). In O. Stefansson (Ed.), *Geochemistry Research Advances*.

España, J. S., Pamo, E. L., Pastor, E. S., Andrés, J. R., & Rubí, J. a. M. (2006). The Removal of Dissolved Metals by Hydroxysulphate Precipitates during Oxidation and Neutralization of Acid Mine Waters, Iberian Pyrite Belt. *Aquatic Geochemistry*, *12*(3), 269–298. doi:10.1007/s10498-005-6246-7

Farmer, V. C., Fraser, A. R., & Tait, J. M. (1979). Characterization of the chemical structures of natural and synthetic aluminosilicate gels and sols by infrared spectroscopy. *Geochimica et Cosmochimica Acta*, *43*, 1417–1420.

Filgueiras, A. V, Lavilla, I., & Bendicho, C. (2002). Chemical sequential extraction for metal partitioning in environmental solid samples. *Journal of Environmental Monitoring*, *4*(6), 823–857. doi:10.1039/b207574c

Filipek, L. H., Nordstrom, D. K., & Ficklin, W. H. (1987). Interaction of acid mine drainage with waters and sediments of West Squaw Creek in the West Shasta Mining District, California. *Environmental Science & Technology*, *21*(4), 388–96. doi:10.1021/es00158a009

Food and Agricultural Organization of the United Nations, F. (2014). *World reference base for soil resources 2014 World reference base for soil resources 2014*.

Forbes, E. A., Posner, A. M., & Quirk, J. P. (1976). THE SPECIFIC ADSORPTION OF DIVALENT Cd, Co, Cu, Pb, AND Zn ON GOETHITE. *Journal of Soil Science*, *27*(2), 154–166.

Fosmire, G. J. (1990). Zinc. *The American Journal of Clinical Nutrition*, (51), 225–227.

Fowler, T. A., Holmes, P. R., & Crundwell, F. K. (1999). Mechanism of Pyrite Dissolution in the Presence of Thiobacillus ferrooxidans. *Applied and Environmental Microbiology*, *65*(7), 2987–2993.

Francis, M. L., Fey, M. V., Prinsloo, H. P., Ellis, F., Mills, a. J., & Medinski, T. V. (2007). Soils of Namaqualand: Compensations for aridity. *Journal of Arid Environments*, *70*(4), 588–603. doi:10.1016/j.jaridenv.2006.12.028

Frau, F. (2000). The formation-dissolution-precipitation cycle of melanterite at the abandoned pyrite mine of Genna Luas in Sardinia , Italy : environmental implications. *Mineralogical Magazine*, *64(6)*(December), 995–1006.

Furrer, G., & Stumm, W. (1986). The coordination chemistry of weathering : I . Dissolution kinetics of sigma-Al203 and Be0. *Geochimica et Cosmochimica Acta*, *50*, 1847–1860.

Galan, E., Carretero, M. I., & Fernandez-Caliani, J. C. (1999). Effects of acid mine drainage on clay minerals suspended in the Tinto River (Rio Tinto , Spain). An experimental approach. *Clay Minerals*, *34*, 99–108.

Ganor, J., Cama, J., & Metz, V. (2003). Surface protonation data of kaolinite—reevaluation based on dissolution experiments. *Journal of Colloid and Interface Science*, *264*(1), 67–75. doi:10.1016/S0021-9797(03)00298-4

Ghosh, S. K., & Tomar, K. P. (1974). Effect of cation saturation and air-drying of samples on the diffractogram obtained from parallel-oriented specimen Gosh tomar.pdf. In *Proceedings of the Symposium on Clay Minerals in Indian Soils, held at the Indian Agricultural Research Institute, New Delhi, on 10-12 October 1972. No. 50. Indian National Science Academy* (pp. 270–281).

Glasauer, S., Weidler, P. G., Langley, S., & Beveridge, T. (2003). Controls on Fe reduction and mineral formation by a subsurface bacterium. *Geochimica et Cosmochimica Acta*, *67*(7), 1277–1288. doi:10.1016/S0016-7037(00)01199-7

Gleyzes, C., Tellier, S., & Astruc, M. (2002). Fractionation studies of trace elements in contaminated soils and sediments: a review of sequential extraction procedures. *TrAC Trends in Analytical Chemistry*, *21*(6-7), 451–467. doi:10.1016/S0165-9936(02)00603-9

Goldich, S. S. (1938). A Study in Rock-Weathering. *The Journal of Geology*, *46*(1), 17–58.

Gray, N. F. (1997). Environmental impact and remediation of acid mine drainage : a management problem. *Environmental Geology*, *30*(1-2), 62–71.

Hammarstrom, J. M., & Smith, K. S. (2002). Geochemical and mineralogic characterization of solids and their effects on waters in metal-mining environments. In R. R. Seal II & N. K. Foley (Eds.), *Progress on geoenvironmental models for selected mineral deposit types* (pp. 8–54). US Geological Survey.

Hansen, R. N. (2009). Non-parametric statistical analysis and spatial distribution of the regional geochemical data of the Okiep Copper District, Namaqualand, South Africa: Implications for anthropogenic influence and risk assessment. Unpublished Report.

Harder, H. (1972). The Role of Magnesium in the Formation of Smectite Minerals. *Chemical Geology*, *10*(1), 31–39.

Harsh, J. (1999). Poorly Crystalline Aluminosilicate Clays. In M. E. Summer (Ed.), *Handbook of Soil Science* (p. F–169–182). CRC Press.

Harter, R. D. (1986). Effect of Soil pH on Adsorption of Lead, Copper, Zinc, and Nickel. *Soil Science Society of America Journal*, *47*(1), 47–51.

Hodson, M. E., Valsami-jones, E., Cotter-howells, J. D., Dubbin, W. E., & Kemp, A. J. (2001). Eff□ect of bone meal (calcium phosphate) amendments on metal release from contaminated soils - a leaching column study. *Environmental Pollution*, *112*, 233–243.

Hohne, S., & Hansen, R. N. (2008). *Preliminary conceptual geo-environmental model of the abandoned copper mines of the Okiep Copper District, Namaqualand, Northern Cape. Council for Geoscience*.

Houben, D., Pircar, J., & Sonnet, P. (2012). Heavy metal immobilization by cost-effective amendments in a contaminated soil: Effects on metal leaching and phytoavailability. *Journal of Geochemical Exploration*, *123*, 87–94. doi:10.1016/j.gexplo.2011.10.004

Hradil, D., Hostomský, J., & Soukupová, J. (2002). ALUMINIUM RELEASE RATES FROM ACIDIFIED CLAY STRUCTURES : COMPARATIVE KINETIC STUDY. *Geologica Carpathica*, *5*(2), 117–121.

Huertas, F. J., Chou, L., & Wollast, R. (1998). Mechanism of kaolinite dissolution at room temperature and pressure : Part 1 . Surface speciation. *Geochimica et Cosmochimica Acta*, *62*(3), 417–431.

Huertas, F. J., Chou, L., & Wollast, R. (1999). Mechanism of kaolinite dissolution at room temperature and pressure Part II : Kinetic study. *Geochimica et Cosmochimica Acta*, *63*(19), 3261–3275.

Istok, J. D., & Harward, M. E. (1982). Influence of Soil Moisture on Smectite Formation in soils Derived from Serpentinite. *Soil Science Society of America Journal*, *46*(5), 1106–1108.

Jerz, J. K., & Rimstidt, J. D. (2004). Pyrite oxidation in moist air. *Geochimica et Cosmochimica Acta*, *68*(4), 701–714. doi:10.1016/S0016-7037(03)00499-X

Johnson, C. A. (1986). The regulation of trace element concentrations in river and estuarine waters contaminated with acid mine drainage: The adsorption of Cu and Zn on amorphous Fe oxyhydroxides. *Geochimica et Cosmochimica Acta*, *50*(4), 2433–2438.

Johnson, D. B. (1998). Biodiversity and ecology of acidophilic microorganisms. *FEMS Microbiology Ecology*, *27*(4), 307–317. doi:10.1111/j.1574-6941.1998.tb00547.x

Johnson, D. B., & Hallberg, K. B. (2005). Acid mine drainage remediation options: a review. *The Science of the Total Environment*, *338*(1-2), 3–14. doi:10.1016/j.scitotenv.2004.09.002

Jones, A. M., Collins, R. N., & Waite, T. D. (2011). Mineral species control of aluminum solubility in sulfate-rich acidic waters. *Geochimica et Cosmochimica Acta*, *75*(4), 965–977. doi:10.1016/j.gca.2010.12.001

Jozefaciuk, G., & Bowanko, G. (2002). EFFECT OF ACID AND ALKALI TREATMENTS ON SURFACE AREAS AND ADSORPTION ENERGIES OF SELECTED MINERALS. *Clays and Clay Minerals*, *50*(6), 771–783.

Kelso, C., & Vogel, C. (2007). The climate of Namaqualand in the nineteenth century. *Climatic Change*, *83*(3), 357–380. doi:10.1007/s10584-007-9264-1

Kempton, H., & Atkins, D. (2000). Delayed Environmental Impacts from Mining in Semi-Arid Climates. *In Proceedings from the Fifth International Conference on Acid Rock Drainage,May 20-24, Denver, Colorado*, *2*, 1299–1308.

Kisters, A. F. M., Charlesworth, E. G., Gibson, R. L., & Anhaeusser, C. R. (1996). Steep structure formation in the Okiep Copper District , South Africa: bulk inhomogeneous shortening of a high-grade metamorphic granite-gneiss sequence. *Journal of Structural Geology*, *18*(6), 735–751.

Kloprogge, J. T., Komarneni, S., & Amonette, J. E. (1999). Synthesis of Smectite Clay Minerals: A Critical Review. *Clays and Clay Minerals*, *47*(5), 529–554.

Komadel, P., & Madejova, J. (2006). Acid activation of clay minerals. In F. Bergaya, B. K. G. Theng, & G. Lagaly (Eds.), *Handbook of Clay Science - Developments in Clay Science, Vol. 1* (Vol. 1, pp. 263–287). Elsevier Ltd. doi:10.1016/S1572-4352(05)01008-1

Lee, G., Bigham, J. M., & Faure, G. (2002). Removal of trace metals by coprecipitation with Fe, Al and Mn from natural waters contaminated with acid mine drainage in the Ducktown Mining District, Tennessee. *Applied Geochemistry*, *17*(5), 569–581. doi:10.1016/S0883-2927(01)00125-1

Lei, L., Song, C., Xie, X., Li, Y., & Wang, F. (2010). Acid mine drainage and heavy metal contamination in groundwater of metal sulfide mine at arid territory (BS mine, Western Australia). *Transactions of Nonferrous Metals Society of China*, *20*(8), 1488–1493. doi:10.1016/S1003-6326(09)60326-5

Luca, V., & Maclachlan, D. J. (1992). SITE OCCUPANCY IN NONTRONITE STUDIED BY ACID DISSOLUTION A N D MOSSBAUER SPECTROSCOPY. *Clays and Clay Minerals*, *40*(1), 1–7.

Madejova, J., Janek, M., Komadel, P., Herbert, H., & Moog, H. C. (2002). FTIR analyses of water in MX-80 bentonite compacted from high salinary salt solution systems. *Applied Clay Science*, *20*, 255–271.

Maiz, I., Esnaola, M., & Millfin, E. (1997). Evaluation of heavy metal availability in contaminated soils by a short sequential extraction procedure. *Science of The Total Environment*, *206*(2-3), 107–115.

Mandarino, J. A., & Fleischer, M. (1999). *Fleischer's glossary of mineral species 1999*.

Martin, J. M., Nirel, P., & Thomas, A. J. (1987). SEQUENTIAL EXTRACTION TECHNIQUES : PROMISES AND PROBLEMS *. *Marine Chemistry*, *22*(May 1986), 313–341.

McGrath, S. P., & Cegarra, J. (1992). Chemical extractability of heavy metals during and after long-term applications of sewage sludge to soil. *Journal of Soil Science*, *43*(2), 313–321.

Mcgregor, R. G., Blowes, D. W., Jambor, J. L., & Robertson, W. D. (1998). The solid-phase controls on the mobility of heavy metals at the Copper Cliff tailings area , Sudbury , Ontario , Canada. *Journal of Contaminant Hydrology*, *33*(3-4), 247–271.

Mckibben, M., & Barnh, H. L. (1986). Oxidation of pyrite in low temperature acidic solutions : Rate laws and surface textures. *Geochimica et Cosmochimica Acta*, *50*, 1509–1520.

Mclean, J. E., & Bledsoe, B. E. (1996). Behavior of Metals in Soils. In J. R. Boulding (Ed.), *EPA Environmental assessment Sourcebook* (p. 19).

Miao, Z., Carroll, K. C., & Brusseau, M. L. (2013). Characterization and quantification of groundwater sulfate sources at a mining site in an arid climate: The Monument Valley site in Arizona, USA. *Journal of Hydrology*, *504*, 207–215. doi:10.1016/j.jhydrol.2013.09.030

Mill, A. J. B. (1980). Colloidal and macromolecular forms of iron in natural waters 2: Their occurrence in rivers of South West England. *Environmental Technology Letters*, *1*(2), 109–124. doi:10.1080/09593338009383956

Miller, D. (1995). 2000 years of indigenous mining and metallurgy in Southern Africa - A review. *South African Journal of Geology*, *98*(2), 232–238.

Mosser-Ruck, R., Devineau, K., Charpentier, D., & Cathelineau, M. (2005). EFFECTS OF ETHYLENE GLYCOL SATURATION PROTOCOLS ON XRD PATTERNS : A CRITICAL REVIEW AND DISCUSSION. *Clays and Clay Minerals*, *53*(6), 631–638. doi:10.1346/CCMN.2005.0530609

Mucina, L., Jürgens, N., le Roux, A., Rutherford, M. C., Schmiedel, U., Esler, K. J., … Midgley, G. F. (2006). Succulent Karoo Biome. In L. Mucina & M. C. Rutherford (Eds.), *The vegetation of South Africa, Lesotho and Swaziland* (pp. 220–299). Pretoria.

Nesbitt, H. W., & Muir, I. J. (1994). X-ray photoelectron spectroscopic study of a pristine pyrite surface reacted with water vapour and air. *Geochimica et Cosmochimica Acta*, *58*(21), 4667–4679.

Nordstrom, D. K. (1982). *Aqueous pyrite oxidation and the consequent formation of secondary iron minerals. Acid Sulfate weathering* (pp. 37–56).

Nordstrom, D. K., & Wilde, F. D. (2005). *National Field Manual, Chapter A6, Section 6.5: Reduction Oxidation Potential (Electrode Method)* (Vol. 2, pp. 1–22).

Norrish, K., & Tiller, K. (1976). Subplasticity in Australian soils. V. Factors involved and techniques of dispersion. *Australian Journal of Soil Research*, *14*(3), 273. doi:10.1071/SR9760273

O'Connor, G. A., O'Connor, C., & Cline, G. R. (1984). Sorption of Cadmium by Calcareous Soils: Influence of Solution Composition. *Soil Science Society of America Journal*, *48*(6), 1244–1247.

Parfitt, R. L., & Henmi, T. (1982). Comparison of an oxalate-extraction methon and an infrared spectroscopic method for determining allophane in soll clays. *Soil Science and Plant Nutrition*, *28*(2), 183–190. doi:10.1080/00380768.1982.10432435

Peppas, A., Komnitsas, K., & Halikia, I. (2000). Use of organic covers for acid mine drainage control. *Minerals Engineering*, *13*(5), 563–574.

Pieterson, K., Titus, R., & Cobbing, J. (2009). *Effective Groundwater Management in Namaqualand: Sustaining Supplies*.

Puls, R. W., & Bohn, H. L. (1988). Sorption of Cadmium, Nickel, and Zinc by Kaolinite and Montmorillonite Suspensions. *Soil Science Society of America Journal*, *52*(5), 1289–1292.

Rate, A. W., Robertson, A. E., & Borg, A. T. (2000). Distribution of heavy metals in near-shore sediments of the Swan river estuary, Western Australia. *Water, Air, and Soil Pollution*, *124*, 155–168.

Reid, D. L., & Barton, E. S. (1983). Geochemical Characterization of Granitoids in the Namaqualand Geotraverse. *Spec. Publ. Geol. Soc. S. Afr.*, *10*, 67–82.

Rösner, U. (1998). Effects of historical mining activities on surface water and groundwater - an example from northwest Arizona. *Environmental Geology*, *33*(4), 224–230.

Russell, J. D. (1979). Infrared spectroscopy of ferrihydrite: evidence for the presence of structural hydroxyl groups. *Clay Minerals*, *14*, 109–114.

Sánchez España, J., López Pamo, E., Santofimia, E., Aduvire, O., Reyes, J., & Barettino, D. (2005). Acid mine drainage in the Iberian Pyrite Belt (Odiel river watershed, Huelva, SW Spain): Geochemistry, mineralogy and environmental implications. *Applied Geochemistry*, *20*(7), 1320–1356. doi:10.1016/j.apgeochem.2005.01.011

Sasaki, K., Tanaike, O., & Konno, H. (1998). Distinction of jarosite-group compounds by raman spectroscopy. *The Canadian Mineralogist*, *36*, 1225–1235.

Schaetzl, R. J., & Anderson, S. (2005). *Soils: Genesis and geomorphology* (pp. 75–81).

Schrenk, M. O., Edwards, K. J., Goodman, R. M., Hamers, R. J., & Banfield, J. F. (1998). Distribution of Thiobacillus ferrooxidans and Leptospirillum ferrooxidans: Implications for Generation of Acid Mine Drainage. *Science*, *279*(5356), 1519–1522. doi:10.1126/science.279.5356.1519

Selim, H. M., & Amacher, M. C. (1996). *Reactivity and transport of heavy metals in soils*. CRC Press.

Singer, P. C., & Stumm, W. (1970). Acidic Mine Drainage : The Rate-Determining Step. *Science*, *167*(3921), 1121–1123.

Smalberger, J. M. (1975). *A History of Copper Mining in Namaqualand 1846-1931*. Struik.

Smith, T. M., & Williams, B. (2000). Hydrochemical characterization of acute acid mine drainage at Iron Duke mine , Mazowe , Zimbabwe. *Environmental Geology*, *39*(January), 272–278.

Soil Classification Working Group, S. (1991). *Soil Classification - A Taxonomic System for South Africa*. Pretoria: The Department of Agricultural Development RSA.

Sposito, G. (1989). *The Chemistry of Soils*. New York: Oxford University Press.

Steudel, a., Batenburg, L. F., Fischer, H. R., Weidler, P. G., & Emmerich, K. (2009a). Alteration of non-swelling clay minerals and magadiite by acid activation. *Applied Clay Science*, *44*(1-2), 95–104. doi:10.1016/j.clay.2009.02.001

Steudel, a., Batenburg, L. F., Fischer, H. R., Weidler, P. G., & Emmerich, K. (2009b). Alteration of swelling clay minerals by acid activation. *Applied Clay Science*, *44*(1-2), 105–115. doi:10.1016/j.clay.2009.02.002

Stumm, W., & Morgan, J. J. (1996). *Aquatic chemistry, chemical equilibra and rates in natural waters*. *Environmental science & technology*. New York, United States: John Wiley and Sons.

Swoboda-colberg, N. G., & Drever, J. I. (1993). Mineral dissolution rates in plot-scale field and laboratory experiments. *Chemical Geology*, *105*, 51–69.

Tessier, A., Campbell, P. G. C., & Bisson, M. (1979). Sequential Extraction Procedure for the Speciation of Particulate Trace Metals, *51*(7), 844–851.

Tiller, K. G., Gerth, J., & Brummer, G. (1984). THE SORPTION OF Cd, Zn AND Ni BY SOIL CLAY FRACTIONS: PROCEDURES FOR PARTITION OF BOUND FORMS AND THEIR INTERPRETATION. *Geoderma*, *34*, 1–16.

Tutu, H., McCarthy, T. S., & Cukrowska, E. (2008). The chemical characteristics of acid mine drainage with particular reference to sources, distribution and remediation: The Witwatersrand Basin, South Africa as a case study. *Applied Geochemistry*, *23*(12), 3666–3684. doi:10.1016/j.apgeochem.2008.09.002

Tyagi, B., Chudasama, C. D., & Jasra, R. V. (2006). Determination of structural modification in acid activated montmorillonite clay by FT-IR spectroscopy. *Spectrochimica Acta. Part A, Molecular and Biomolecular Spectroscopy*, *64*(2), 273–8. doi:10.1016/j.saa.2005.07.018

Ure, A. M., Quevauviller, P., Muntau, H., & Griepink, B. (1993). Speciation of Heavy Metals in Soils and Sediments. An Account of the Improvement and Harmonization of Extraction Techniques Undertaken Under the Auspices of the BCR of the Commission of the European Communities. *International Journal of Environmental Analytical Chemistry*, *51*(1-4), 135–151.

Uroz, S., Calvaruso, C., Turpault, M.-P., & Frey-Klett, P. (2009). Mineral weathering by bacteria: ecology, actors and mechanisms. *Trends in Microbiology*, *17*(8), 378–87. doi:10.1016/j.tim.2009.05.004

Vaculíková, L., Plevová, E., Vallová, S., & Koutník, I. (2011). Characterization and Differentiation of Kaolinites from Selected Czech Deposits Using Infrared Spectroscopy and Differential Thermal Analysis. *Acta Geodynamica et Geomasteralia*, *8*(1), 59–67.

Valente, T. M., & Gomes, C. L. (2009). Occurrence, properties and pollution potential of environmental minerals in acid mine drainage. *The Science of the Total Environment*, *407*(3), 1135–52. doi:10.1016/j.scitotenv.2008.09.050

Vandevivere, P., Welch, S. A., Ullman, W. J., & Kirchman, D. L. (1994). Enhanced Dissolution of Silicate Minerals by Bacteria at Near-Neutral pH. *Microbial Ecology*, *27*, 241–251.

Wada, K. (1978). Allophane and imogolite. In T. Sudo & S. Susumu (Eds.), *Clays and clay minerals of Japan* (pp. 147–187). Tokyo: Elsevier Ltd.

Webster, J. G., Swedlund, P. J., & Webster, K. S. (1998). Trace Metal Adsorption onto an Acid Mine Drainage Iron (III) Oxy Hydroxy Sulfate. *Environmental Science & Technology*, *32*(10), 1361–1368.

Welch, S. A., & Ullman, W. J. (1993). The effect of organic acids on plagioclase dissolution rates and stoichiometry. *Geochimica et Cosmochimica Acta*, *51*, 2125–2136.

Whitney, D. A. (2011). Chemical Soil Test Procedures for the North Central Region, *221*(221), 59–60.

Yu, J.-Y. (1996). Precipitation of Fe and Al compounds from the acid mine waters in the dogyae area, Korea: A qualitative measure of equilibrium modeling applicability and neutralization capacity?. *Aquatic Geochemistry1*, *2*(1), 81–105.

Yu, J.-Y., Heo, B., Choi, I.-K., Cho, J.-P., & Chang, H.-W. (1999). Apparent solubilities of schwertmannite and ferrihydrite in natural stream waters polluted by mine drainage. *Geochimica et Cosmochimica Acta*, *63*(19), 3407–3416.

Zysset, M., & Schindler, P. W. (1996). The proton promoted dissolution kinetics of K-montmorillonite. *Geochimica et Cosmochimica Acta*, *60*(6), 921–931. doi:10.1016/0016-7037(95)00451-3

Appendices

Appendix A - Permissions

ELSEVIER LICENSE
TERMS AND CONDITIONS

Oct 08, 2014

This is a License Agreement between Ian Smuts ("You") and Elsevier ("Elsevier") provided by Copyright Clearance Center ("CCC"). The license consists of your order details, the terms and conditions provided by Elsevier, and the payment terms and conditions.

All payments must be made in full to CCC. For payment instructions, please see information listed at the bottom of this form.

Supplier	Elsevier Limited The Boulevard,Langford Lane Kidlington,Oxford,OX5 1GB,UK
Registered Company Number	1982084
Customer name	Ian Smuts
Customer address	40 Bosman Street Stellenbosch, Western Cape 7600
License number	3484240909574
License date	Oct 08, 2014
Licensed content publisher	Elsevier
Licensed content publication	Geochimica et Cosmochimica Acta
Licensed content title	Schwertmannite and the chemical modeling of iron in acid sulfate waters
Licensed content author	J.M. Bigham,U. Schwertmann,S.J. Traina,R.L. Winland,M. Wolf
Licensed content date	June 1996
Licensed content volume number	60
Licensed content issue number	12
Number of pages	11
Start Page	2111
End Page	2121
Type of Use	reuse in a thesis/dissertation
Portion	figures/tables/illustrations
Number of figures/tables/illustrations	1
Format	both print and electronic

Are you the author of this Elsevier article?	No
Will you be translating?	No
Title of your thesis/dissertation	The effect of Acid Mine Drainage on clay mineral weathering
Expected completion date	Nov 2014
Estimated size (number of pages)	150
Elsevier VAT number	GB 494 6272 12
Permissions price	0.00 USD
VAT/Local Sales Tax	0.00 USD / 0.00 GBP
Total	0.00 USD

Permission for the use of Figure

ELSEVIER LICENSE
TERMS AND CONDITIONS
Dec 08, 2014

This is a License Agreement between Ian Smuts ("You") and Elsevier ("Elsevier") provided by Copyright Clearance Center ("CCC"). The license consists of your order details, the terms and conditions provided by Elsevier, and the payment terms and conditions.

All payments must be made in full to CCC. For payment instructions, please see information listed at the bottom of this form.

Supplier	Elsevier Limited The Boulevard,Langford Lane Kidlington,Oxford,OX5 1GB,UK
Registered Company Number	1982084
Customer name	Ian Smuts
Customer address	40 Bosman Street Stellenbosch, Western Cape 7600
License number	3524190455011
License date	Dec 08, 2014
Licensed content publisher	Elsevier
Licensed content publication	Applied Clay Science
Licensed content title	Alteration of non-swelling clay minerals and magadiite by acid activation
Licensed content author	A. Steudel,L.F. Batenburg,H.R. Fischer,P.G. Weidler,K. Emmerich

Licensed content date	April 2009
Licensed content volume number	44
Licensed content issue number	1-2
Number of pages	10
Start Page	95
End Page	104
Type of Use	reuse in a thesis/dissertation
Portion	figures/tables/illustrations
Number of figures/tables/illustrations	2
Format	both print and electronic
Are you the author of this Elsevier article?	No
Will you be translating?	No
Title of your thesis/dissertation	The effect of Acid Mine Drainage on clay mineral weathering on the soils of Nababeep
Expected completion date	Dec 2014
Estimated size (number of pages)	100
Elsevier VAT number	GB 494 6272 12
Permissions price	0.00 USD
VAT/Local Sales Tax	0.00 USD / 0.00 GBP
Total	0.00 USD

Appendix B - Information Tables

Table B1 is a summary of the chemical species found as secondary minerals in AMD (Hammarstrom & Smith, 2002). The relative solubility is also indicated on this table but the mineral solubility is dependent on the degree of crystallinity and the particle sizes.

Table B1: Secondary minerals forming from AMD (Hammarstrom & Smith, 2002). Species indicated with * are highly soluble, ◊ - relatively insoluble. Chemical formulae obtained from Mandarino & Fleischer (1999).

Sulfate Minerals		Carbonate Minerals	
alunogen*	$Al_2(SO_4)_3{\cdot}17H_2O$	aurichalcite	$(Zn,Cu)_5(CO_3)_2(OH)_6$
alunite	$K_2Al_6(SO_4)_4(OH)_{12}$	azurite	$Cu_3(CO_3)_2(OH)_2$
anglesite◊	$PbSO_4$	cerussite	PbCO
antlerite◊	$Cu_3SO_4(OH)_4$	hydrozincite	$Zn_5(CO_3)_2(OH)_6$
argenojarosite◊	$Ag_2Fe^{3+}{}_6(SO_4)_4(OH)_{12}$	malachite◊	$Cu_2CO_3(OH)_2$
barite◊	$BaSO_4$	smithsonite	$ZnCO_3$
basaluminite	Al4(SO4)(OH)10·5H2O	**Iron oxyhydroxide (ochre) minerals**	
bassanite*	2CaSO4·H2O	akageneite	β-Fe^{3+}(O,OH,Cl)
beaverite◊	$Pb(Cu^{2+},Fe^{3+},Al)_6(SO_4)_4(OH)_{12}$	bernalite	$Fe^{3+}(OH)_3{\cdot}nH_2O$ (n=0 to 0.25)
beudantite	$PbFe^{3+}{}_3(AsO_4)(SO_4)(OH)_6$	ferrihydrite	$5Fe^{3+}{}_2O_3{\cdot}9H_2O$
bianchite*	$(Zn,Fe^{2+})SO_4{\cdot}6H_2O$	goethite	$Fe^{3+}O(OH)$
bilinite	$Fe^{2+}Fe^{3+}{}_2(SO_4)_4{\cdot}22H_2O$	hematite	$Fe^{3+}{}_2O_3$
brochantite◊	$Cu_4(SO_4)(OH)_6$	lepidocrocite	$Fe^{3+}O(OH)$
chalcanthite*	$CuSO_4{\cdot}5H_2O$	maghemite	Fe_2O_3
copiapite*	$Fe^{2+}Fe^{3+}{}_4(SO_4)_6(OH)_2{\cdot}20H_2O$	**Other Minerals**	
coquimbite*	$Fe^{3+}{}_2(SO_4)_3{\cdot}9H_2O$	bindheimite	$Pb_2Sb_2O_6(O,OH)$
dietrichite*	$(Zn,Fe^{2+},Mn)Al_2(SO_4)_4{\cdot}22H_2O$	chalcophanite	$(Zn,Fe^{2+},Mn^{2+})Mn^{4+}{}_3O_7{\cdot}3H_2O$
epsomite*	$MgSO_4{\cdot}7H_2O$	chlorargyrite group	Ag(Cl,Br)
ferricopiapite*	$Fe^{3+}{}_{2/3}Fe^{3+}{}_4(SO_4)_6(OH)_2{\cdot}2H_2O$	chrysocolla	$(Cu^{2+},Al)_2H_2Si_2O_5(OH)_4{\cdot}nH_2O$
ferrohexahydrite*	$FeSO_4{\cdot}6H_2O$	cinnabar	HgS
fibroferrite◊	$Fe^{3+}(SO_4)(OH)\cdot5H_2O$	coronadite	$Pb(Mn^{4+},Mn^{2+})_8O_{16}$
goslarite*	$ZnSO_4{\cdot}7H_2O$	ferrimolybdite	$Fe^{3+}{}_2(Mo^{6+}O_4)_3{\cdot}8H_2O$(?)
gunningite*	$ZnSO_4{\cdot}H_2O$	ilsemannite	$Mo_3O_8{\cdot}nH_2O$(?)
gypsum	$CaSO_4{\cdot}2H_2O$	litharge	PbO
hexahydrite*	$MgSO_4{\cdot}6H_2O$	luzonite	Cu_3AsS_4
halothrichite*	$FeAl_2(SO_4)_4{\cdot}22H_2O$	olivenite	$Cu_2(AsO_4)(OH)$
hinsdalite	$(Pb,Sr)Al_3(PO_4)(SO_4)(OH)_6$	psilomelane group	$(Ba,H_2O)_2(Mn^{4+},Mn^{3+})O_{10}$
jarosite◊	$KFe^{3+}{}_3(SO_4)_2(OH)_6$	scorodite	$Fe^{3+}AsO_4{\cdot}2H_2O$
jurbanite	$Al(SO_4)(OH)\cdot5H_2O$		
kornelite	$Fe^{3+}{}_2(SO_4)_3{\cdot}7H_2O$		
leadhillite◊	$Pb_4SO_4(CO_3)_2(OH)_2$		
linarite◊	$PbCu(SO_4)(OH)_2$		
melanterite*	$FeSO_4{\cdot}7H_2O$		
meta-aluminite	$Al_2(SO_4)(OH)_4{\cdot}5H_2O$		
paracoquimbite*	$Fe^{3+}{}_2(SO_4)_3{\cdot}9H_2O$		
pentahydrite	$MgSO_4{\cdot}5H_2O$		
pickeringite*	$MgAl_2(SO_4)_4{\cdot}22H_2O$		
plumbojarosite◊	$PbFe^{3+}{}_6(SO_4)_4(OH)_{12}$		
rhomboclase*	$(H_3O)Fe^{3+}(SO_4)_2{\cdot}3H_2O$		
romerite*	$Fe^{2+}Fe^{3+}{}_2(SO_4)_4{\cdot}14H_2O$		
rozenite*	$FeSO_4{\cdot}4H_2O$		
schwertmannite	$Fe^{3+}{}_8O_8(OH)_6(SO4)..nH_2O$		
serpierite◊	$Ca(Cu,Zn)_4(SO_4)_2(OH)_6{\cdot}3H_2O$		
siderotil*	$Fe^{2+}SO_4{\cdot}5H_2O$		
szomolnokite*	$Fe^{2+}SO_4{\cdot}H_2O$		
voltaite	$K_2Fe^{2+}{}_5Fe^{3+}{}_4(SO_4)_{12}{\cdot}18H_2O$		
woodhouseite	$CaAl_3(PO_4)(SO_4)(OH)_6$		

Appendix C - Statistics Example

Hypothesis statement

$H_0: X - Y = 0$

$H_1: X - Y > 0$

Where X is the concentration of either leach cycle $1, 7$ or 10 and Y the concentration of AMD

Test if the concentration of Al is significantly higher than the concentration of AMD.

The average concentrations for three replicates are given below for AMD and seventh leach cycle. The variance has been calculated with the var.s function in excel. This is the variance based on a sample.

Values for triplicates of 7th leach cycle

	A7	B7	C7	Average	Variance (var.s)
Al (mg/l)	3033	2899	3019	2983.667	5425.33

Values for triplicates of AMD

	AMD10 (1)	AMD 10 (2)	AMD 10 (3)	Average	Variance (var.s)
Al (mg/l)	2744	2713	2812	2756.333	2564.33

$$\mathbf{S_{\overline{X}-\overline{Y}}} = \sqrt{\frac{\mathbf{1}}{\mathbf{n}}\mathbf{S_X^2} + \frac{\mathbf{1}}{\mathbf{m}}\mathbf{S_Y^2}}$$

$\boldsymbol{n = 3\ and\ m = 3}$

$$\boldsymbol{S_{\overline{X}-\overline{Y}}} = \sqrt{\frac{1}{3} \times 2564.333 + \frac{1}{3} \times 5425.333}$$

$\boldsymbol{S_{\overline{X}-\overline{Y}}} = 51.606$

$\boldsymbol{X\ has\ 3\ elments}$

$\boldsymbol{Y\ has\ 3\ elements}$

$$\boldsymbol{t} = \frac{\overline{X} - \overline{Y}}{S_{\overline{X}-\overline{Y}}} \sim t - \text{distribution with } m + n - 2 \text{ degrees of freedom}$$

$$\boldsymbol{t} = \frac{2983.667 - 2756.333}{51.606}$$

$\boldsymbol{t} = 4.405$

The degrees of freedom is 4 (3+3 -2). For a one tailed significance the critical value t-value for 0.05 probability is 2.132.

Thus 4.406 > 2.132 and thus the H_0 hypothesis is rejected which means the Al concentration in the leachate of cycle 7 is significantly greater than the AMD.

The t-value has a corresponding p-value of: 0.0058

Appendix D - Supplementary Data relating to Chapter 1

The d-spacing at 14.932 Å, as shown in Figure 1.15, is attributed to montmorillonite, chlorite or vermiculite (Brindley, 1955). A differentiation should therefore be made between these minerals. The saturation with potassium would result in a collapse of the interlayer spacing of montmorillonite, but not that of chlorite (e.g. Ghosh & Tomar, 1974). It does, however, collapse the d-spacing of vermiculite as well from 14 Å to 10 Å (Schaetzl & Anderson, 2005). The change in montmorillonite d-spacing when changing from Mg-saturation to K-saturation is 14–16 Å to 11–12 Å. The Mg-saturated clay powders in this study were therefore further treated with ethylene glycol (EG) to distinguish between montmorillonite and vermiculite, since the d-spacing of vermiculite stays at 14 Å after saturation with EG, whilst in the case of montmorillonite, the EG moves into the interlayer spaces and increases the d-spacing to 17–18 Å. Figure 1.15 shows the different XRD patterns for the different saturation treatments. The Mg-saturated clay shows a peak at the d-spacing of 14.931 Å and when saturated with potassium the peak shifted to 12.75 Å. The clay sample saturated with EG had a d-spacing of approximately 17.172 Å. The conclusion can be made that the mineral identified in this case was montmorillonite.

Figure D2 shows the XRD pattern of an analyzed ball-milled sample of the highly weathered granite described in section 3.1 of chapter 1.

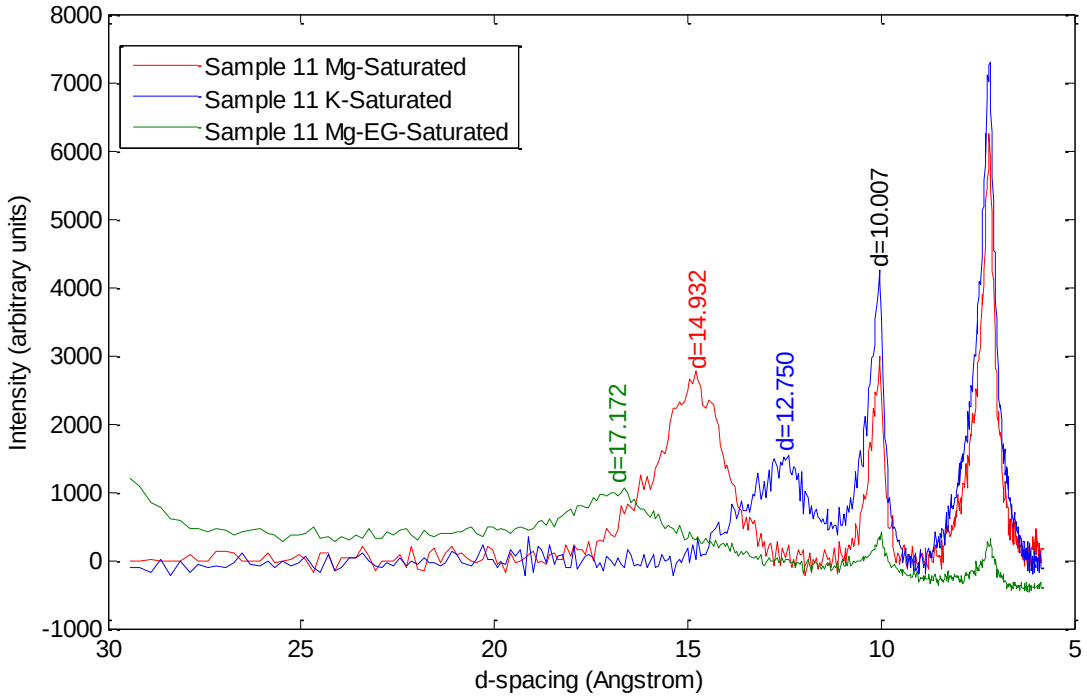

Figure D1: Different saturation conditions for the A-Horizon in pristine soil to determine clay phase.

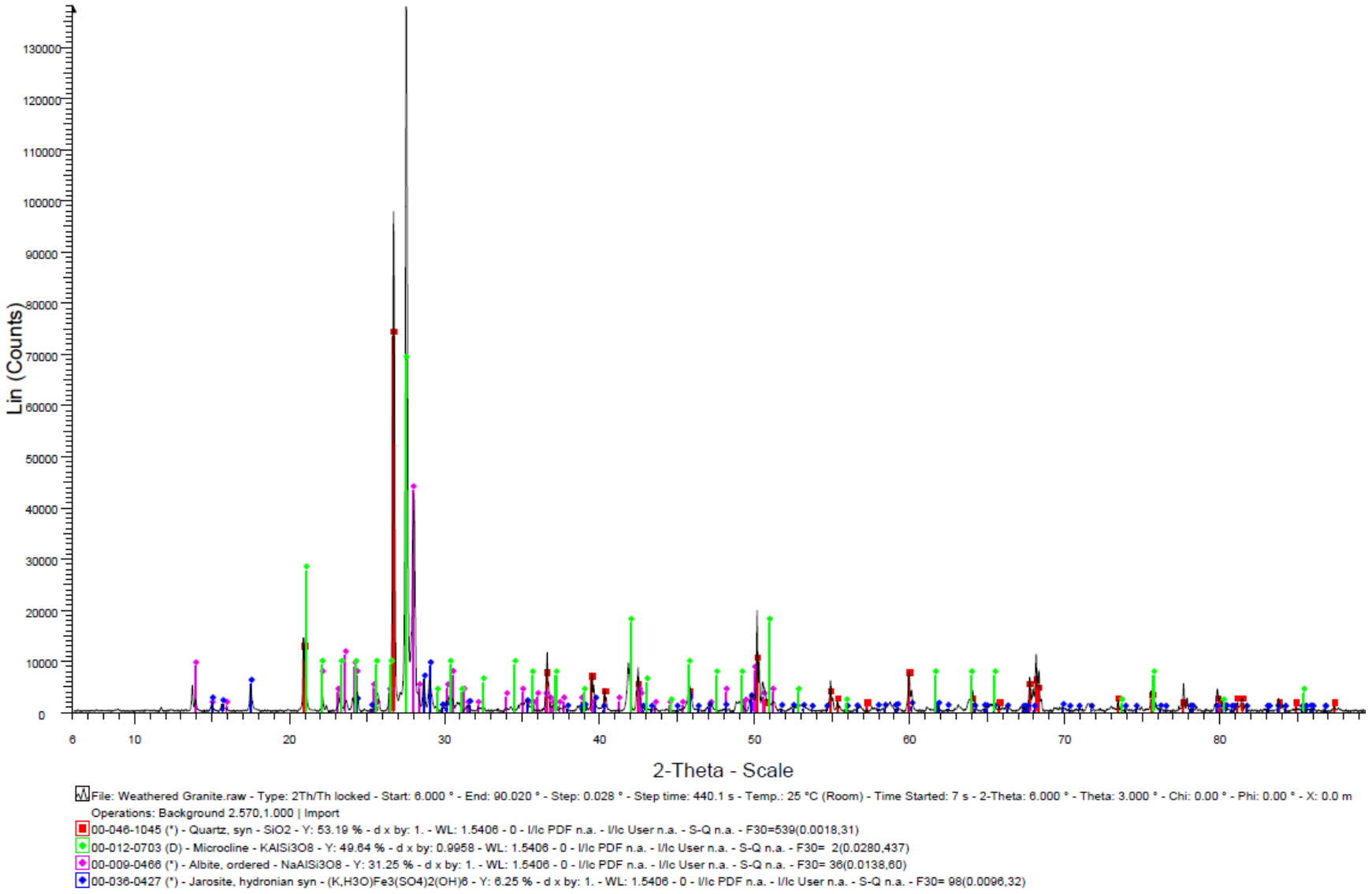

Figure D2: XRD pattern for the ball-milled sample of highly weathered granite described in chapter 1.